AD-A279 116

ESL-TR-92-73
Vol II

STRESS WAVE PROPAGATION IN UNSATURATED SANDS - VOL II FIELD EXPLOSIVE TESTS

E.J. VILLANO; W.A. CHARLIE

COLORADO STATE UNIVERSITY
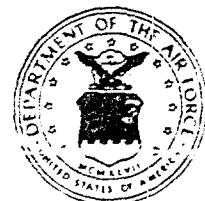## FORT COLLINS CO 80523

APRIL 1993

FINAL REPORT

DTIC
ELECTE
S MAY 1 1 1994
B D

SEPTEMBER 1990 - OCTOBER 1992

DTIC QUALITY INSPECTED 1

ENGINEERING RESEARCH DIVISION
Air Force Civil Engineering Support Agency
Civil Engineering Laboratory
Tyndall Air Force Base, Florida 32403

94 5 09 067

NOTICE

PLEASE DO NOT REQUEST COPIES OF THIS REPORT FROM HQ AFCESA/RA (AIR FORCE CIVIL ENGINEERING SUPPORT AGENCY). ADDITIONAL COPIES MAY BE PURCHASED FROM:

> NATIONAL TECHNICAL INFORMATION SERVICE
> 5285 PORT ROYAL ROAD
> SPRINGFIELD, VIRGINIA 22161

FEDERAL GOVERNMENT AGENCIES AND THEIR CONTRACTORS REGISTERED WITH DEFENSE TECHNICAL INFORMATION CENTER SHOULD DIRECT REQUESTS FOR COPIES OF THIS REPORT TO:

> DEFENSE TECHNICAL INFORMATION CENTER
> CAMERON STATION
> ALEXANDRIA, VIRGINIA 22314

REPORT DOCUMENTATION PAGE

1. AGENCY USE ONLY (Leave blank)	2. REPORT DATE April 1993	3. REPORT TYPE AND DATES COVERED Final Report, Sept. 1990–October 1992	
4. TITLE AND SUBTITLE Stress Wave Propagation in Unsaturated Sands: Vol. 2 Field Explosive Tests			**5. FUNDING NUMBERS** F08635-90-C-0306
6. AUTHOR(S) Edward J. Villano and Wayne A. Charlie (Wayne A. Charlie, P.I.)			
7. PERFORMING ORGANIZATION NAME(S) AND ADDRESS(ES) Colorado State University Fort Collins, CO 80523			**8. PERFORMING ORGANIZATION REPORT NUMBER** TR-92-73-Vol.II
9. SPONSORING / MONITORING AGENCY NAME(S) AND ADDRESS(ES) Air Base Survivability Branch HQ Air Force Civil Engineering Support Agency 139 Barnes Drive Tyndall AFB, FL 32403-5319			**10. SPONSORING / MONITORING AGENCY REPORT NUMBER**

11. SUPPLEMENTARY NOTES

12a. DISTRIBUTION / AVAILABILITY STATEMENT Approved for Public Release Distribution Unlimited	12b. DISTRIBUTION CODE

13. ABSTRACT (Maximum 200 words)

Explosive field tests were conducted in unsaturated Poudre Valley sand for the determination of peak ground shock parameters, propagation velocity and attenuation trends as a function of compactive saturation. The sand was compacted moist to a dry density of 1635 kg/m^3 at compactive saturation levels ranging from 0 to 70 percent. Three explosive masses of 6.22 kg, 7.0 kg and 0.227 kg TNT equivalency were used at a depth of burial of 1.4 meters to provide scaled range ($R/W^{1/3}$) values ranging from 0.32 m/kg$^{1/3}$ to 3.8 m/kg$^{1/3}$. Scaled peak particle acceleration, peak particle velocity, peak stress and propagation velocities are presented as a function of scaled range. Constants (Y-intercept at $R/W^{1/3} = 1$) taken from the developed empirical predictive equations for peak ground shock parameters are generally lower but follow the same trends as those of Tyndall Beach and Ottawa 20-30 sands obtained from centrifuge tests. Slope (-n or -n-1) values taken from the same predictive equations compare closely with centrifuge tests. Peak Particle velocity intercepts are lowests at 0 and 13 percent compactive saturations.

14. SUBJECT TERMS Centrifuge, Centrifuge Modeling, Sand, Unsaturated Sand, Explosive Modeling, Explosives, Moisture			15. NUMBER OF PAGES 157
			16. PRICE CODE
17. SECURITY CLASSIFICATION OF REPORT Unclassified	18. SECURITY CLASSIFICATION OF THIS PAGE Unclassified	19. SECURITY CLASSIFICATION OF ABSTRACT Unclassified	20. LIMITATION OF ABSTRACT UL

EXECUTIVE SUMMARY

STRESS WAVE PROPAGATION IN UNSATURATED SAND: FIELD EXPLOSIVE TESTS

Explosive field tests were conducted in unsaturated Poudre Valley sand for the determination of peak ground shock parameters, propagation velocity and attenuation trends as a function of compactive saturation. The sand was compacted moist to a dry density of 1635 kg/m^3 (relative density of 44 %) at compactive saturation levels ranging from 0 to 70 percent. Three explosive masses of 6.22 kg, 7.0 kg and 0.227 kg TNT equivalency were used at a depth of burial of 1.4 meters to provide scaled range ($R/W^{1/3}$) values ranging from 0.32 m/kg$^{1/3}$ to 3.8 m/kg$^{1/3}$. Scaled peak particle acceleration, peak particle velocity, peak stress and propagation velocities are presented as a function of scaled range. Magnitudes and attenuation trends of peak ground shock parameters and propagation velocities in Poudre Valley sand are analyzed and compared with results obtained by previous researchers. Constants (Y-intercept at $R/W^{1/3} = 1$ m/kg$^{1/3}$) taken from the developed empirical predictive equations for peak ground shock parameters of Poudre Valley sand are generally lower than those of Tyndall Beach and Ottawa 20-30 sands obtained from centrifuge tests conducted by Walsh (1993). Slope (-n or -n-1) values taken from the same predictive equations compare closely in magnitude with those obtained by Walsh. Attenuation trends of slope values show an increase in magnitude from 0 to 20 percent compactive saturations, constancy or decline from 20 to 40 percent and a drop from 40 to 60 percent. These trends are similar to those observed by previous researchers.
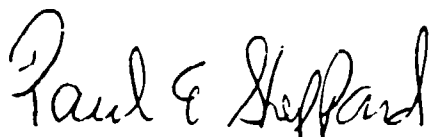
iii

(The reverse of this page is blank.)

PREFACE

This report was prepared by the Department of Civil Engineering, Colorado State University, Fort Collins, Colorado, 80523 under contract Number F08635-90-C-0306 for the Air Force Civil Engineering Support Agency, Air Base Survivability Branch (AFCESA/RACS) 139 Barnes Drive, Tyndall AFB, FL, 32403-5319. The work was initiated in November 1989 and was completed in October 1992.
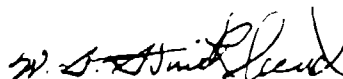
This report is published in two volumes. Volume 1 is written by Mr. Andy J. Walsh and Dr. Wayne A. Charlie and covers centrifuge explosives tests conducted at AFCESA/RACS during the summers of 1990 and 1991. Volume 2 is written by Mr. Edward J. Villano and covers field explosives tests conducted at Colorado State University during the fall of 1991 and spring of 1992. Mr. Andy J. Walsh and Mr. Edward J. Villano worked under the direction of Professor Wayne A. Charlie.

This report has been reviewed by the Public Affairs Office (PA) and is releasable to the National Technical Information Service (NTIS). At NTIS, it is available to the general public, including foreign nationals.

This technical report has been reviewed and is approved for publication.

Paul E. Sheppard, GS-13
Project Officer

W.S. Strickland, GM-14
Chief, Air Base Survivability
Section

Felix T. Uhlik, III, Lt Col, USAF
Chief, Air Base Systems Branch

(The reverse of this page is blank.)

TABLE OF CONTENTS

TABLE OF CONTENTS
(Continued)

TABLE OF CONTENTS
(Concluded)

LIST OF TABLES

LIST OF TABLES
(Concluded)

LIST OF FIGURES

LIST OF FIGURES
(Continued)

LIST OF FIGURES
(Continued)

LIST OF SYMBOLS AND UNITS

AH	Ampere-hour (flow of electric charge per hour)
a_o	peak particle acceleration (m/s^2 or g)
$a_o \cdot W^{1/3}$	scaled peak particle acceleration (g's$\cdot$kg$^{1/3}$)
c	propagation velocity (m/s)
cc	cubic centimeter
$^\circ$C	degree Celsius
C_u	coefficient of uniformity
C_c	coefficient of curvature
cm	centimeter
COE	center of explosion
dB	decibel
D.M.S.	Dense Moist sand
DC	direct current
D_r	relative density (%)
D_{10}	grain diameter corresponding to 10 % finer (mm)
D_{30}	grain diameter corresponding to 30 % finer (mm)
D_{50}	grain diameter corresponding to 50 % finer (mm)
D_{60}	grain diameter corresponding to 60 % finer (mm)
e	void ratio
e_{min}	minimum void ratio
e_{max}	maximum void ratio
E	Young's modulus (kPa)
f	coupling factor for near surface explosions
$^\circ$F	degree Fahrenheit
F.S.O.	full scale output
ft	feet
g	acceleration due to gravity (9.81 m/s^2)
gm	gram
GPH	gallons per hour
G_s	specific gravity of sand particle
HP	horsepower (745.7 watts or 550 ft-lb/s)
Hz	hertz (cycles per second)
kg	kilogram
kHz	kilohertz (1000 hertz)
kPa	kilopascal (1000 x N/m^2)
kw	kilowatt
lb	pound
m	meter
M	modulus of stiffness of soil (kPa)
mA	milliampere (1 X 10^{-3} Ampere)
MHz	megahertz (1 X 10^6 hertz)
mm	millimeter
mg	milligram
MJ	megajoule (1 X 10^6 Newton-meter)
mV	millivolt (1 X 1^{-3} Volt)
n	attenuation coefficient
N	Newton (kg$\cdot$m/s^2)
NDMG	nuclear density/moisture gauge
O.20-30	Ottawa 20-30 sand
PBX	plastic-bonded explosive
pcf	pounds per cubic foot
PETN	pentaerythritol tetranitrate explosive
P_o	peak soil stress (kPa)
psi	pounds per square inch
P.V.S	Poudre Valley sand
r	radius per unit length of explosive charge (m)
R	range, or distance to center of explosion (m)
R^2	statistical coefficient of determination
$R/W^{1/3}$	scaled range (m/kg$^{1/3}$)

LIST OF SYMBOLS AND UNITS
(Concluded)

s	second
S	saturation (%)
SHPB	Split-Hopkinson Pressure Bar
SI	International System of Units
SP	poorly graded sand grain classification
S.R.	scaled range (m/kg$^{1/3}$)
t	time (second)
t_a	pulse arrival time (s)
T.B.S	Tyndall Beach sand
TDR	transient data recorder
t_r	pulse rise time (s)
TNT	trinitrotoluene explosive
V	volt
V_a	air filled void space (m^3)
VDC	direct current voltage
VAC	alternating current voltage
V_o	peak particle velocity (m/s)
V_w	volume of water (m^3)
V_v	volume of voids (m^3)
w	water content (%)
W	explosive charge mass (kg)
X	axis value on plot
Y	ordinate value on plot
α	attenuation coefficient in SHPB tests, m^{-1})
ε	strain (%)
μV	microvolt (1 X 10^{-4} Volt)
ρ	density of soil (kg/m^3)
ρc	acoustic impedance of soil (kg/m^2-s)
ρ_{max}	maximum dry density (mass/volume, kg/m^3)
ρ_{min}	minimum dry density (mass/volume, kg/m^3)
Ω	Ohm
MΩ	megaOhm (1 X 10^6 Ohms)
ρ_d	dry density of soil (mass/volume, kg/m^3)
ρ_{tot}	total density of soil (mass/volume, kg/m^3)
σ	compressive stress (kPa)
$\sigma_{trans.}$	stress in soil from SHPB test (kPa)
$\sigma_{incident}$	stress in striker bar of SHPB apparatus (kPa)
$\sigma_{trans}/\sigma_{inc.}$	transmission ratio
γ_d	dry density (force/volume, N/m^3)

I. INTRODUCTION

A. OBJECTIVE

The general objective of this research is to determine the influence that the degree of saturation during compaction of sand has on blast-induced ground shock and stress wave propagation. Four specific objectives arise out of this general objective.

1. Develop empirical equations from field test results which predict scaled peak particle acceleration, peak particle velocity and peak stress as a function of saturation during compaction.

2. Determine if explosive field testing produces the same trends for stress transmission and propagation velocity versus compactive saturation obtained from Split-Hopkinson Pressure Bar (SHPB) tests conducted by Pierce (1989), Ross (1989), Charlie et al. (1990a) and Veyera and Fitzpatrick (1990).

3. Determine if explosive field testing produces the same magnitudes and trends for peak stress, peak particle velocity, scaled peak particle acceleration and propagation velocity obtained from centrifuge explosive testing of sand compacted moist conducted by Walsh (1993).

4. Compare the developed empirical equations to those given by Drake and Little (1983).

B. BACKGROUND

Since the 1950's, much research has been conducted on stress wave propagation through different soil types of varying saturation. However, until the late 1980's, very little attention has been focused on the behavior of stress wave propagation through partially saturated sands. Recent studies on compacted sands conducted by Pierce (1989), Ross (1989) and Walsh (1993) have shown there to be a direct relationship between stress wave attenuation and saturation at compaction.

Stress wave propagation in partially saturated sands has been of special interest to the United States Air Force since its strategic underground structures are often buried in partially saturated sand. If a penetrating bomb detonated near such an underground strategic structure, considerable damage could be caused by the explosive stress wave travelling through the soil to the structure. To estimate soil-structure response and structural damage from such an event, blast-induced ground motion parameters for a given field condition are required. Among these ground motion parameters are peak particle acceleration and velocity, peak stress, and stress wave attenuation coefficients.

Since it would be impractical to attempt determining these parameters by full-scale explosive testing for each and every proposed strategic site, other means of determination needed to be considered. Centrifuge modeling of full-scale explosions in sand began at Tyndall Air Force Base in the late 1980's. The current research is designed in part to evaluate the accuracy of centrifuge modeling of full-scale explosive events in unsaturated sand. The accuracy of centrifuge modeling will be assessed by analysis and comparison of test results at three evaluated centrifuge g levels (19, 26 and 67 g's) and at 1 g (1 g= 9.81 m/s^2). This report covers the results of the 1 g explosive tests in unsaturated sand. The centrifuge explosive tests conducted at 19, 26 and 67 g's are reported by Brownell (1992a), Dowden (1993) and Walsh (1993). Additionally, the results are compared with the well established trends reported by Drake and Little (1983).

2

C. SCOPE

Explosive field tests were conducted in Poudre Valley sand compacted at a constant dry density of 1635 kg/m³ at saturations of 0 (dry), 13 (natural), 20, 40, 60, and 70 percent. Three explosive sizes of 6.22 kg, 7.0 kg and 0.227 kg (TNT equivalent) buried at a depth of 1.4 m were used to achieve a wide range of stress wave magnitudes at constant distances from the center of explosion (COE). Accelerometers and soil stress gages were utilized to measure particle acceleration and soil stress at established distances from the COE. This instrumentation furnished all the necessary raw data for the determination of peak particle acceleration and velocity, peak soil stress, attenuation coefficients, and propagation velocities.

The data acquisition system consisted of accelerometer signal conditioners, transient data recorders, and computer software designed to handle high frequency transient data. Cube root scaling laws were used in the analysis of the data to simplify comparison of data with test results reported by previous researchers, which were also based on cube root analysis.

The data plots which best represent the influence that the degree of saturation during compaction of sand has on blast-induced ground shock and stress wave propagation, and upon which the bulk of the conclusions will be drawn are: 1) peak particle acceleration, peak particle velocity, peak stress and propagati   . . .   versus scaled range and; 2) constants (Y-intercepts) and slopes (-n-1 and -n, where n is the attenuation coefficient) versus saturation. The constants and slopes will be used to develop predictive equations in the form given by Drake and Little (1983).

(The reverse of this page is blank.)

II. LITERATURE REVIEW

A review of the most pertinent research relating to explosive stress wave propagation in soils is provided in this chapter.

A. GROUND SHOCK FROM PENETRATING CONVENTIONAL WEAPONS

Drake & Little (1983) collected explosive ground shock data from over a 35 year period, and from this data developed empirical equations to predict the magnitudes and attenuation behavior of ground motion parameters for varying soil types and conditions. Drake and Little's equations rewritten in SI units are:

$$a_o \cdot W^{1/3} = f \cdot 126 \cdot c \cdot (2.52)^{-n-1} \cdot \left(\frac{R}{W^{1/3}} \right)^{-n-1} \qquad (2.1)$$

$$V_o = f \cdot 48.8 \cdot (2.52)^{-n} \left(\frac{R}{W^{1/3}} \right)^{-n} \qquad (2.2)$$

$$P_o = f \cdot (\rho c) \cdot \frac{1}{20.5} \cdot (2.52)^{-n} \left(\frac{R}{W^{1/3}} \right)^{-n} \qquad (2.3)$$

where a_o is the peak particle acceleration (g's), V_o is the peak particle velocity (m/s) , P_o is the peak soil stress (kPa), W is the explosive charge mass (kg), f is the coupling factor for near-surface detonations (see Figure 2.1), R is the range or distance to the explosion (m), c is the seismic velocity of the soil (m/s), ρ is the soil's density (kg/m^3), ρc is the acoustic impedance (kg/m^2-s), and n is the attenuation coefficient. The explosive charge mass, W, is proportional to the energy released during detonation. W in Equations (2.1) to (2.3) is the equivalent C4 explosive mass.

5
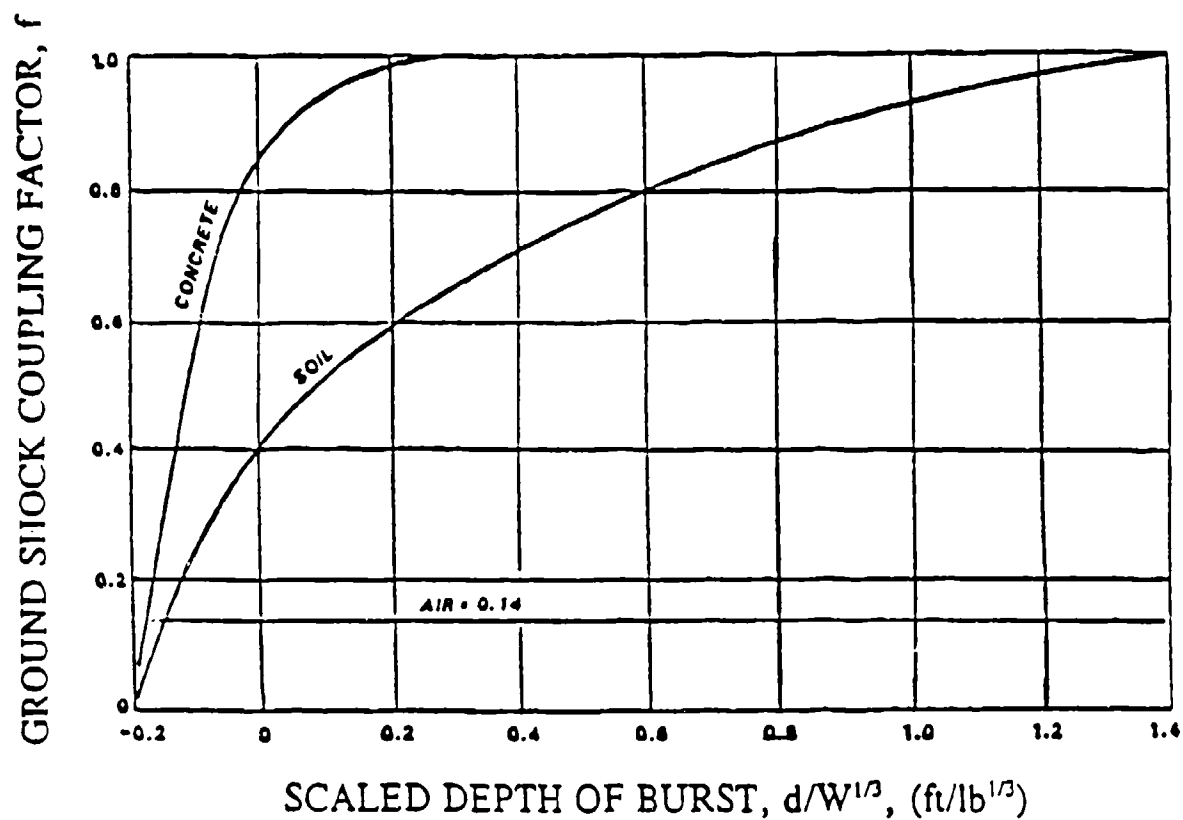
Figure 2.1 Ground Shock Coupling Factor as a Function of Scaled Depth of Burst for Air, Soil and Concrete (Drake and Little, 1983).

6

Other useful relationships presented in Drake and Little's paper are:

$$P_o = \rho c V_o \qquad (2.4)$$

$$t_r \bullet 0.1 t_a \qquad (2.5)$$

$$c = \sqrt{\frac{M}{\rho}} \qquad (2.6)$$

where t_r is the rise time of the stress or particle velocity pulse, t_a is the time of arrival for the stress wave to reach a given instrument, and M is the modulus of the soil.

Equation (2.4) states that peak stress is directly proportional to the peak particle velocity of the soil. Equation (2.5) was derived from the observation that the time it takes for the particle velocity or stress pulse to reach its peak is approximately one tenth the time for the explosive stress wave to reach the location in question. Equation (2.6) states that the propagation velocity for a given soil is a function of its modulus (M) and its mass density (ρ).

Equations (2.1) to (2.3) incorporate the cube root scaling term $(R/W^{1/3})$, which is convenient for comparing explosive data from different tests, where both R and W vary. Amraseys and Hendron (1968), Dowding (1985) and others have validated that there is a consistent relationship between peak particle velocity and scaled range $(R/W^{1/3})$ for a wide range of explosive measurements. Scaled peak particle acceleration $(a_o \bullet W^{1/3})$ and peak stress (P_o) also display a consistent relationship with scaled range.

Cube root scaling is derived from the Buckingham Pi theory of dimensionless analysis (Buckingham, 1915), where the terms V_o/c and $(W \bullet g)/\rho c^2 R^3$ are among the derived dimensionless parameters, and the explosive is considered a point or a sphere. The pi theorem states that any of the parameters may be considered to be a function of another, and that the parameters may be raised to any power. Since ρ and c remain relatively constant when compared with the possible variation in R and $(W \bullet g)$, they are sometimes dropped from the foregoing dimensionless terms.

7

Although the new terms V_o and $(W \cdot g)/R^3$ are no longer dimensionless, they still may be used as if they were dimensionless. Since the parameters may also be raised to any power, V can now be plotted against $(W \cdot g)^{1/3}/R$ or $R/(W \cdot g)^{1/3}$, parameters which were found to produce consistent relationships by Ambraseys and Hendron (1968), Dowding (1985) and others. For spherical charges, the term $W^{1/3}$ is proportional to the charge radius, r. Hence, $R/W^{1/3}$ is essentially proportional to R/r, which is dimensionless.

Figures 2.2 to 2.4 show the relationships between scaled peak particle acceleration, peak particle velocity and peak stress versus scaled range for a variety of soil types and saturations for fully coupled (f=1) detonations (Drake and Little, 1983). Attenuation is greatest for dry loose sand and least for saturated clay/sandy shale. The attenuation curves for dense sands at varying saturation levels would be expected to range between the two aforementioned curves.

Values for the ground shock coupling factor in Equations (2.1) to (2.3) can be determined from Figure 2.1. Typical values for seismic velocity (c), acoustic impedance (ρc), and attenuation coefficient (n) extrapolated from the explosive test data reviewed by Drake and Little are provided in Table 2.1.

The attenuation coefficient (n), is a measure of the soil's ability to diminish explosive energy over distance, and is dependent upon the soil type, density and saturation level of the soil. Since seismic velocity is also directly dependent upon these factors, the attenuation coefficient can also be estimated from the seismic velocity of the uncemented soil as given in Table 2.2.

Figure 2.3 Peak Particle Velocity versus Scaled Range from Explosions in Varying Soil Types (Plotted using Drake and Little's Equations and Design Coefficients, 1983).
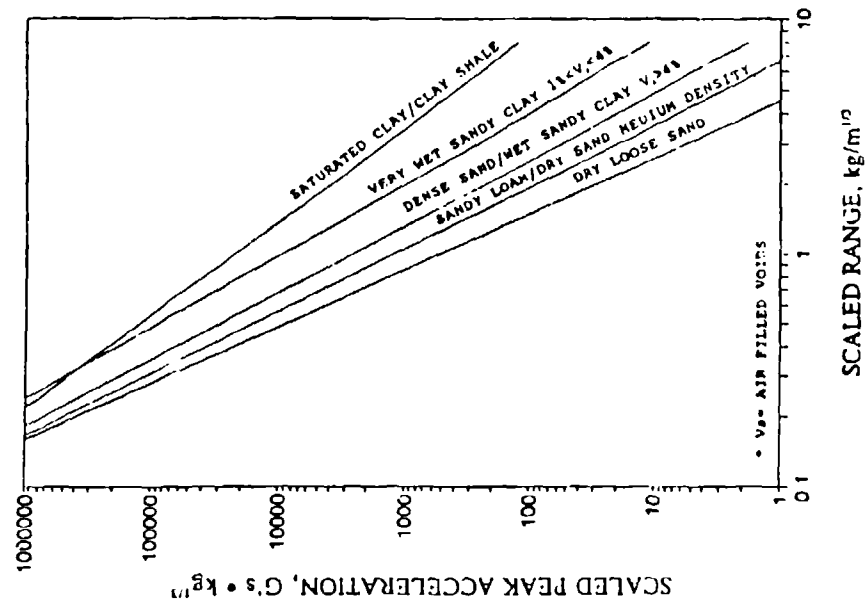
Figure 2.2 Scaled Peak Particle Acceleration versus Scaled Range from Explosions in Varying Soil Types (Plotted using Drake and Little's Equations and Design Coefficients, 1983).
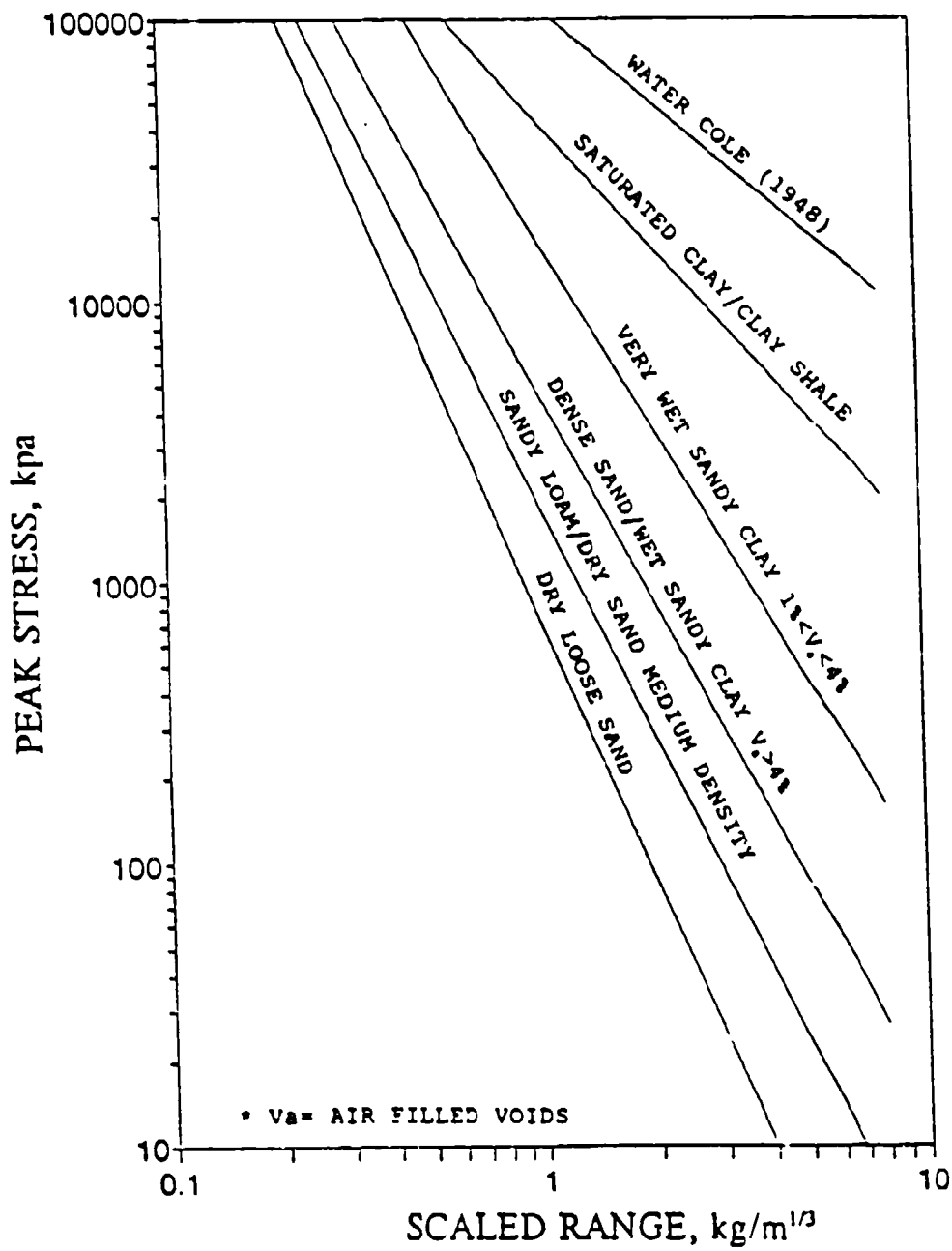
Figure 2.4 Peak Stress versus Scaled Range from Explosions in Varying
Soil Types (Plotted using Drake and Little's Equations and
Design Coefficients, 1983 and Cole's Equation for Water,
1948).

10

TABLE 2.1.   SUGGESTED COEFFICIENTS FOR DESIGN (DRAKE AND LITTLE, 1983).

Material description:	Dry density ρ_{dry} (kg/m³)	Moist density ρ_{wet} (kg/m³)	Seismic velocity c (m/s)	Acoustic impedance (ρc) (kg/m²-s)	Attenuation coefficient (n)	Saturation V_w/V_v (%)
Loose, dry sands and gravels with low relative density	1280	1440	183	272,030	3.0 to 3.25	31
Sandy loam, lcess, dry sands and backfill	1730	1990	305	498,715	2.75	20
Dense sand, with high relative density	1680	1745	488	997,430	2.5	18
Wet sandy clay with air voids (greater than 4 percent)	1520	1960	549	997,430	2.5	95
Saturated sandy clays and sands with small amount of air voids (less than 1 percent)	1425	1875	1676	1,088,100	2.25 to 2.50	97
Heavily saturated clays and shales	1600	2000	1768	3,400,340 to 4,080,410	1.5	100

* All values converted to SI units from English values in Table 1 of Drake and Little (1983)

TABLE 2.2.   SUGGESTED ATTENUATION COEFFICIENTS FOR DESIGN (DRAKE AND LITTLE, 1983).

c (m/s)	n
152 to 183	3.0 to 3.5
229 to 305	3.0
305 to 427	2.75
427 to 548	2.5
>1500	1.5 to 2.25.

B. SPLIT-HOPKINSON PRESSURE BAR TESTING OF UNSATURATED SAND

The Split-Hopkinson Pressure Bar (SHPB) has traditionally been used in determination of stress transmission through solid media. Felice (1986) first used the SHPB apparatus to test dynamic properties of soil. Pierce (1989), Ross (1989) and Charlie et al. (1990a) have recently utilized the SHPB to evaluate the influence of compactive saturation on propagation velocity, stress transmission, and attenuation for compacted sand specimens. A detailed description of the SHPB and its operation is provided by Ross (1989).

Ross (1989) compacted specimens of 50/80 silica sand to a constant dry density of 1600 kg/m^3 at saturations ranging from 0 (dry) to 95 percent, and subsequently subjected them to a compressive stress pulse from the SHPB apparatus. Strain gages attached to the two steel bars on either side of the sand specimen measured the arrival time and magnitude of the compressive stress pulse, σ, before and after travel through the specimen, from which propagation velocity and transmission ratio $(\sigma_{transmitted}/\sigma_{incident})$ could be determined. Test results are reported by Charlie et al. (1990a).

Variation in propagation velocity and transmission ratio with compactive saturation levels is shown in Figure 2.5. Based on their observation of the trends, Charlie et al. (1990a) reports:

> . . . stress wave velocity and transmitted stress increase
> as the saturation increases 0 to 30 to 40 percent for constant
> input stress and constant dry density. At saturation levels
> between 40 to 95 percent, both the wave and the transmitted
> stress decrease with increasing saturation . . . these trends
> may be explained by capillary pressure (Charlie et al., 1990a).

Attenuation of stress versus percent saturation is plotted in Figure 2.6. The highest degree of stress attenuation occurs at 0 and 86 percent saturations, and the lowest at 22 percent saturation. It can be seen that lower attenuation coefficients coincide with higher degrees of stress transmission.
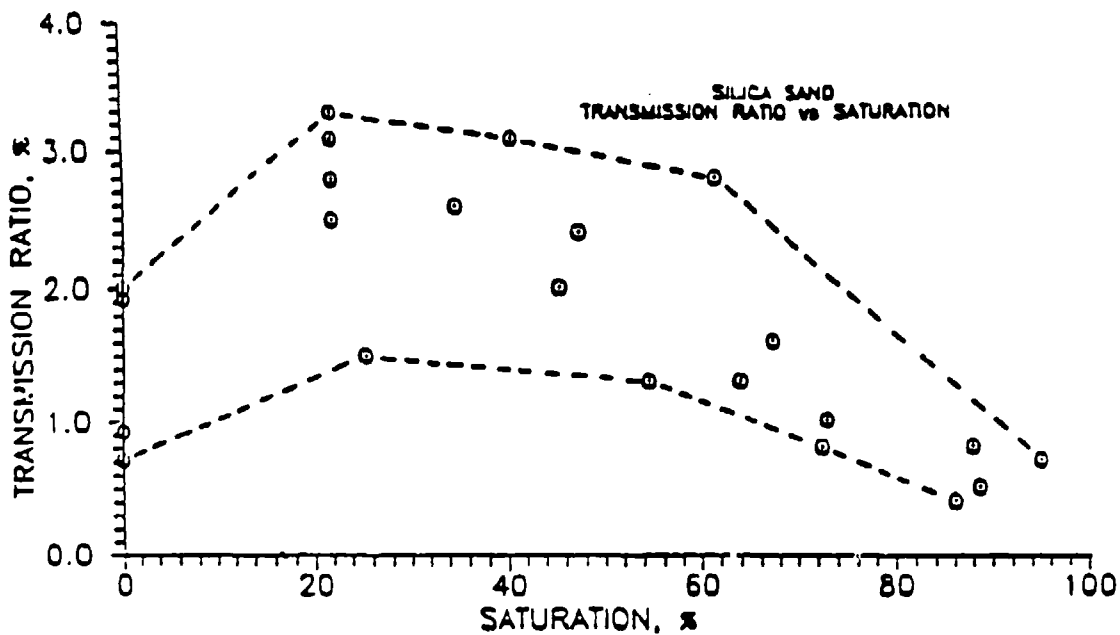
(a)
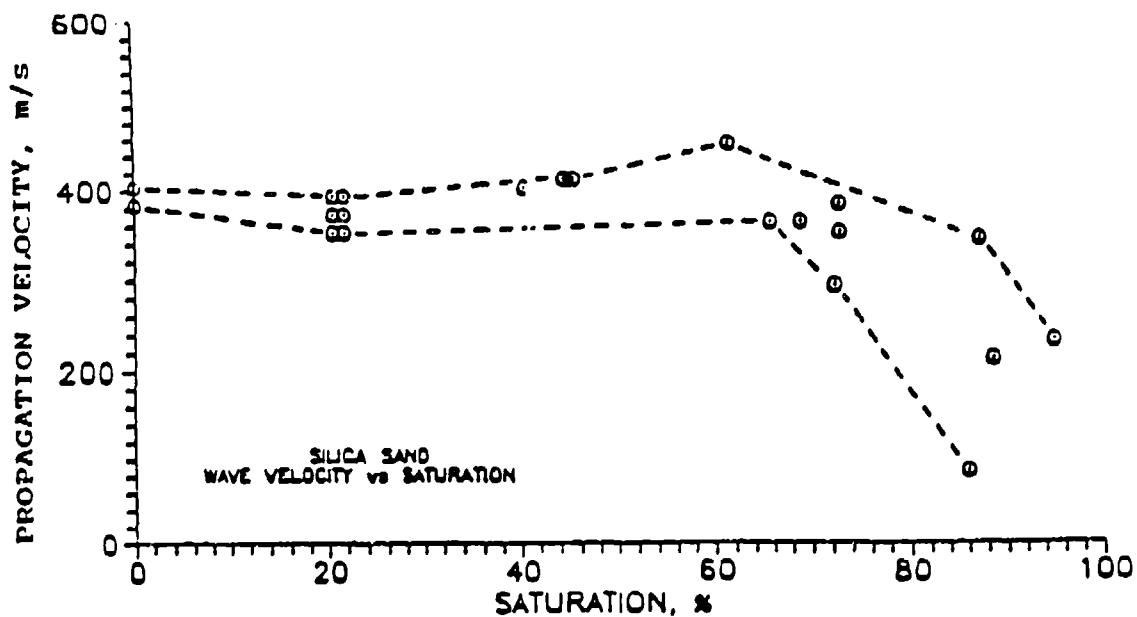
(b)

Figure 2.5 (a) Variation in Transmission Ratio versus Saturation for
50/80 Silica Sand. (b) Variation in Propagation Velocity
versus Saturation for 50/80 Silica Sand. (Charlie et al,
1990a).

13
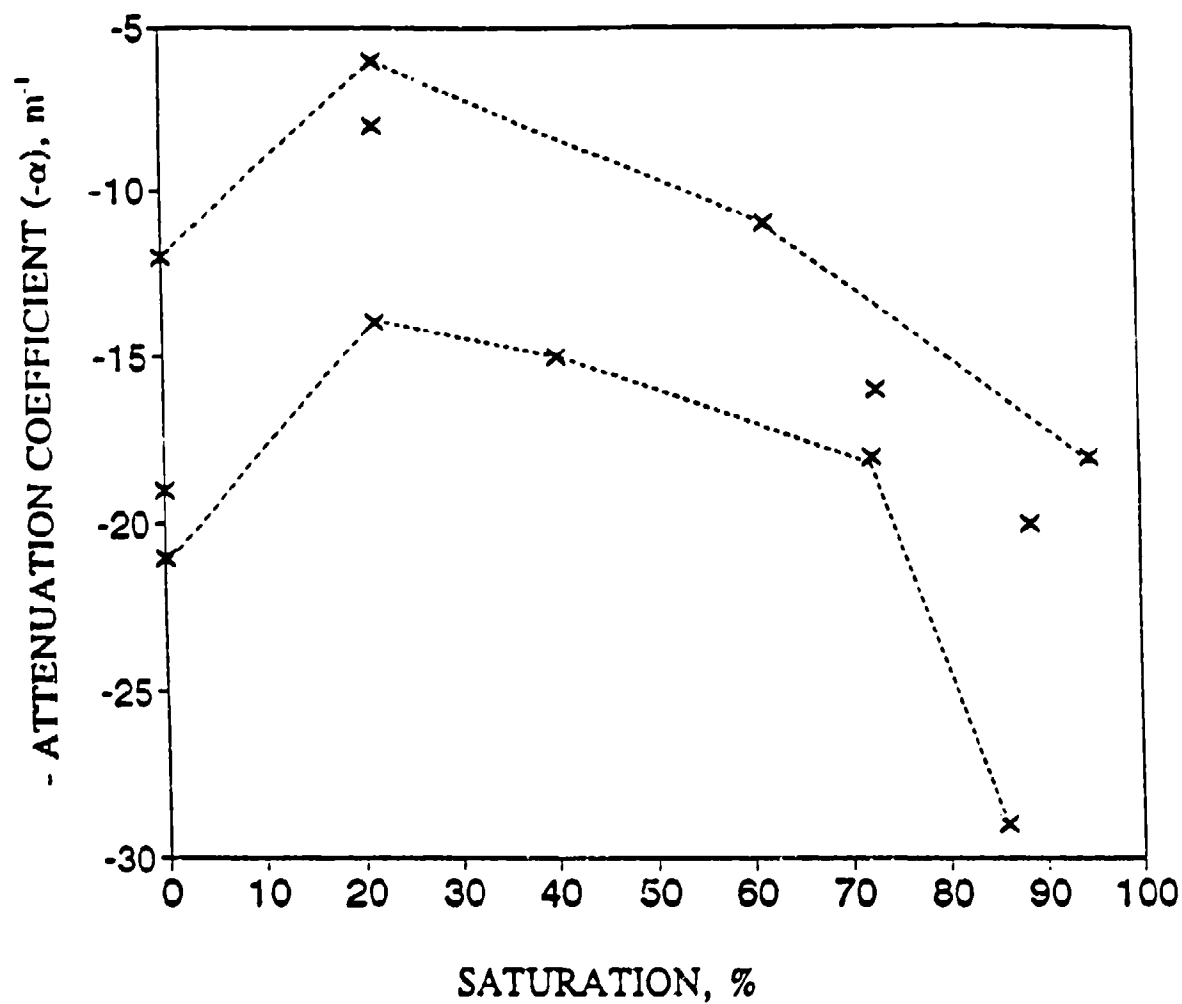
Figure 2.6   Attenuation Coefficient versus Percent Saturation for 50/80
             Silica Sand (Plotted from Test Results from Charlie et al.,
             1990a).

14

According to Charlie et al., attenuation trends may be explained by the capillarity in the soil at the time of compaction. Capillarity, surface tension between sand particles due to the presence of void space water, creates an attraction between particles. Sands with higher capillarity also tend to have higher stiffness. Since propagation velocity, stress transmission and attenuation are functions of a soil's stiffness, a higher capillarity should be evidenced by greater magnitudes of propagation and stress transmission, and by lower attenuation coefficients.

Pierce (1989) compacted samples of dry 20-30 Ottawa and Eglin sands to a constant density, saturating them to prescribed saturation levels subsequent to compaction. The samples were then desaturated and tested on the SHPB apparatus. Test results show that stress transmission and propagation velocity values vary only slightly for the range of saturations tested (Figure 2.7). If capillarity in and of itself affected stress transmission and propagation velocity, significant differences for these values would be seen over the range of saturations tested. Pierce demonstrated that capillarity (~7 kPa) had only a minimal effect in creating soil stiffness when compared with the stress levels associated with SHPB or testing (the lowest peak stress encountered in Pierce's SHPB testing was 1170 kPa).

The degree of saturation during compaction seems to greatly affect a soil's ability to transmit stress. This was particularly demonstrated in Ross's (1989) research, where he first saturated a sand sample to a given saturation, then compacted, then tested it on the SHPB apparatus. Trends obtained from test results (Figure 2.5) differ greatly from Pierce's trends (Figure 2.7). Thus, capillarity, in and of itself, does not significantly increase the stiffness and stress wave energy transmission capabilities of a soil. But, the presence of capillarity at the time of compaction may affect particle arrangement or the magnitude of horizontal stress, which does have an affect on energy transmission. Pierce states:

> . . . compacting samples at different moisture contents may influence the fabric and grain orientation of the sand or change the stress state in the sand (Pierce, 1989, pg. 119).
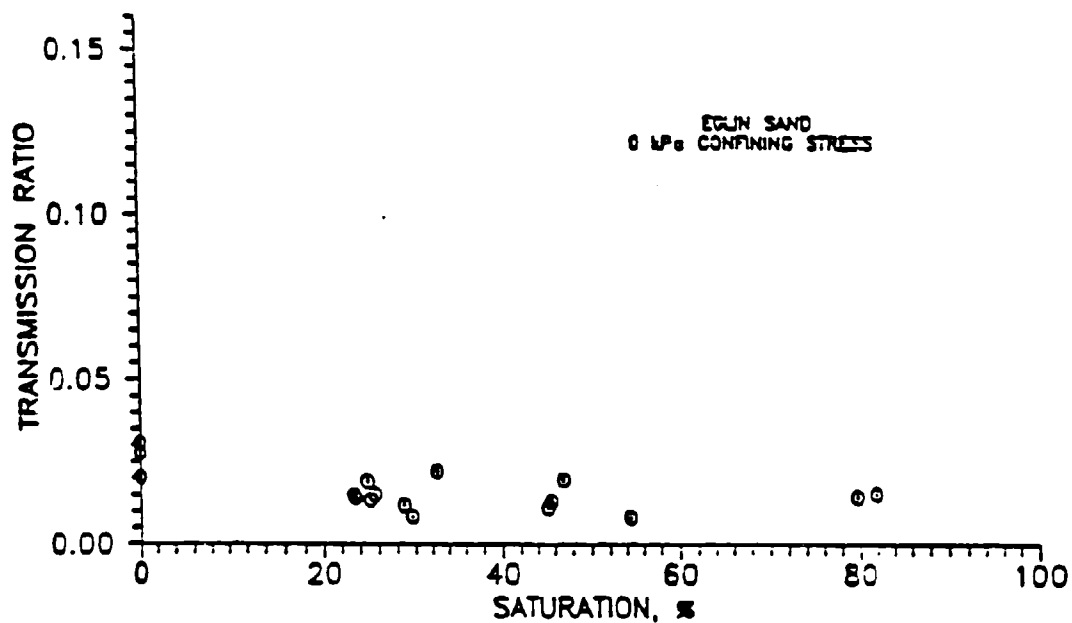
(a)
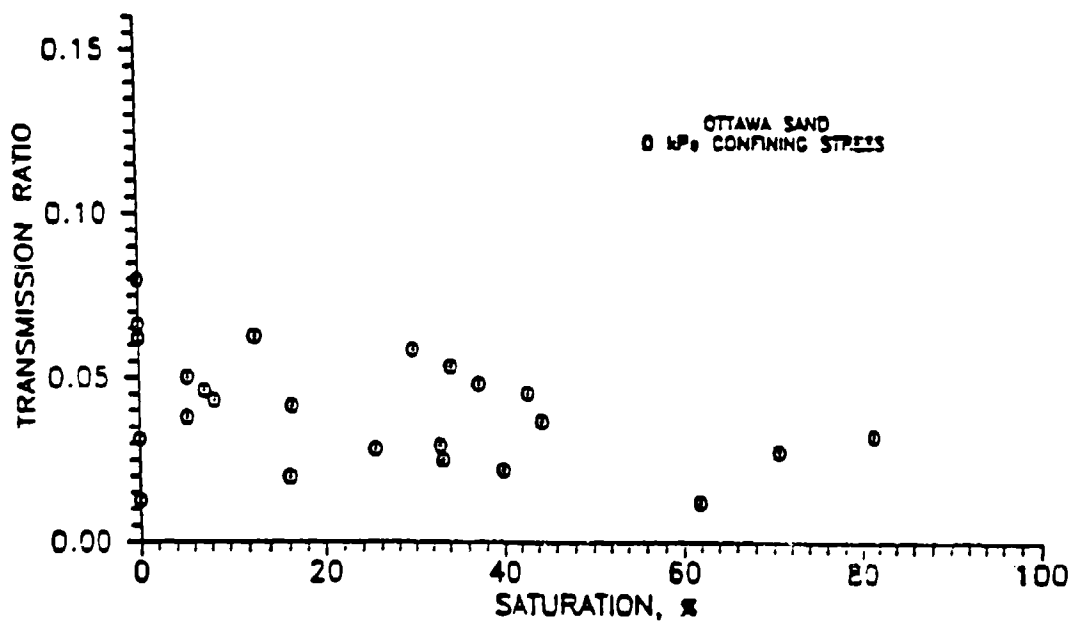
(b)

Figure 2.7 Transmission Ratio versus Saturation for Eglin and Ottawa 20-
30 Sands Under Zero Confining Stress. (a) Eglin Sand (b)
Ottawa 20-30 Sand (Pierce, 1989).

16
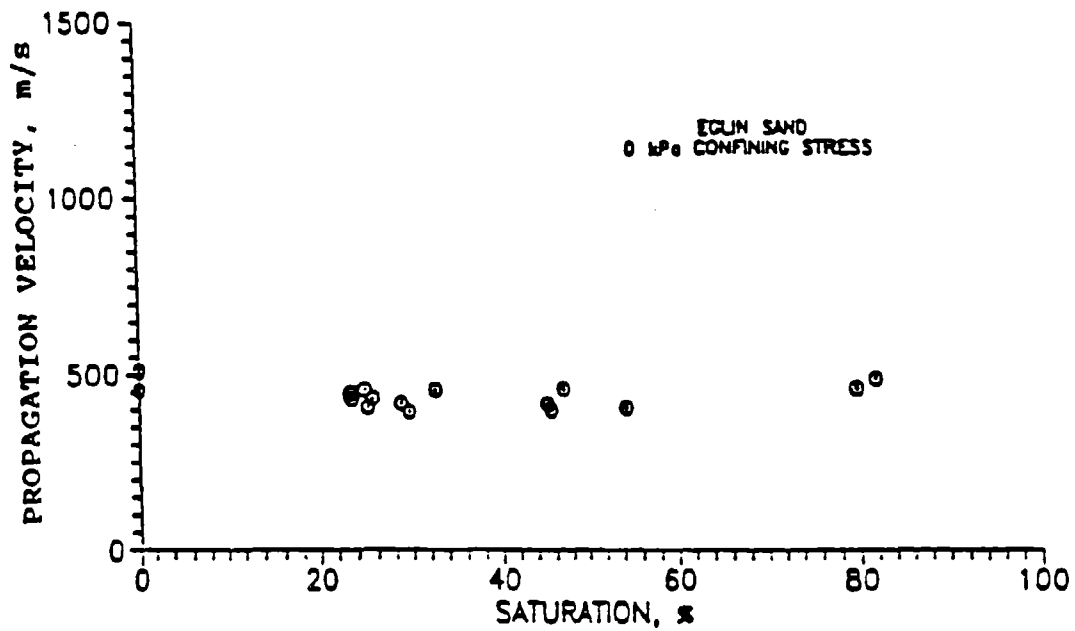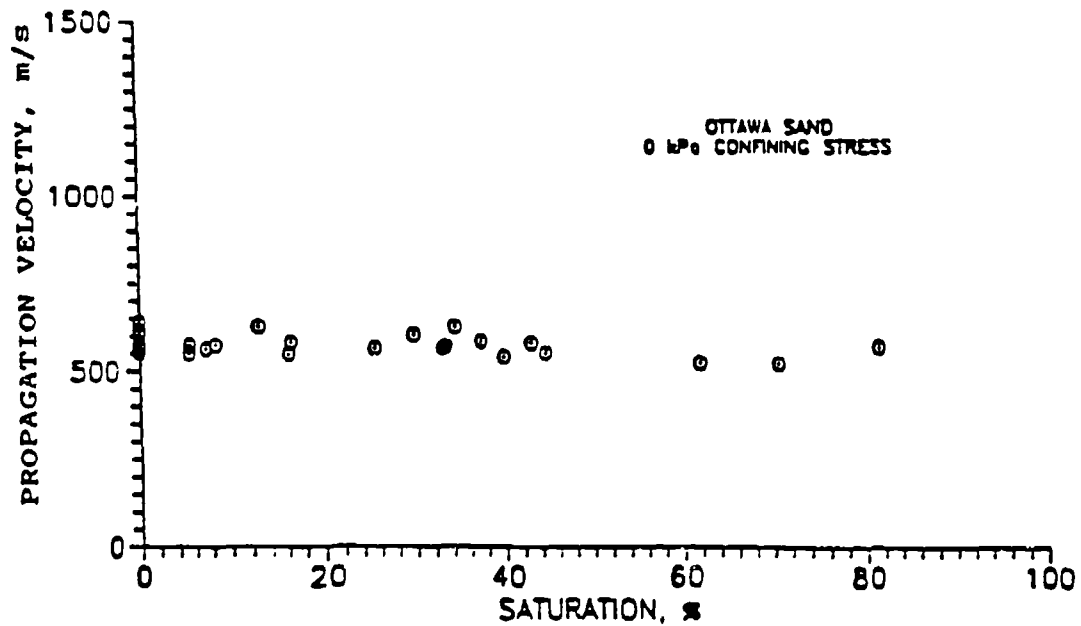
Figure 2.7 (Continued) Propagation Velocity versus Saturation for Eglin and Ottawa 20-30 Sands Under Zero Confining Stress. (c) Eglin Sand (d) Ottawa 20-30 Sand Pierce (1989).

17

C. STRESS TRANSMISSION AND MICROSTRUCTURE IN COMPACTED MOIST SAND

Veyera and Fitzpatrick (1990) extended the work of Pierce (1989), Ross (1989) and Charlie et al. (1990a) by evaluating the influence soil microstructure has on stress transmission behavior of unsaturated soils. They affirm the hypothesis that capillary pressures do not directly affect a granular soil's ability to transmit stress, but they do affect particle packing and orientation during compaction. They state:

> Capillary pressures may strongly influence the soil microstructure during compaction ... which could significantly affect both static and dynamic behavior of soil (Veyera and Fitzpatrick, 1990, pg. 7).

Veyera and Fitzpatrick's work consisted of an attempt to determine the relationship between soil structure at the microscopic level to the dynamic soil properties at the macroscopic level. To isolate the effects that microstructure has on stress transmission and propagation velocities, a series of sand specimens were compacted moist for a range of saturations and tested dry. Removing moisture from the specimen after compaction and prior to testing negated any influence that pore water could have on stress transmission through the compacted microstructure of the sand.

Figures 2.8 and 2.9 compare the trends obtained from samples compacted moist and tested dry with trends obtained from samples compacted moist and tested moist. The trends are essentially the same, and are similar to the results of Ross's (1989) tests. Test results suggest:

> . . . soil microstructure characteristics developed during compaction which influence transmission ratio and wave speed, remain intact even after the moisture in the pores has been removed (Veyera and Fitzpatrick, 1990, pg. 51).

Thus, the degree of saturation during compaction, not after, affects soil microstructure characteristics, which in turn affect stress transmission and propagation velocity. Figure 2.10 shows that compactive saturation levels also influence the compactive effort required to reach a constant density.

18
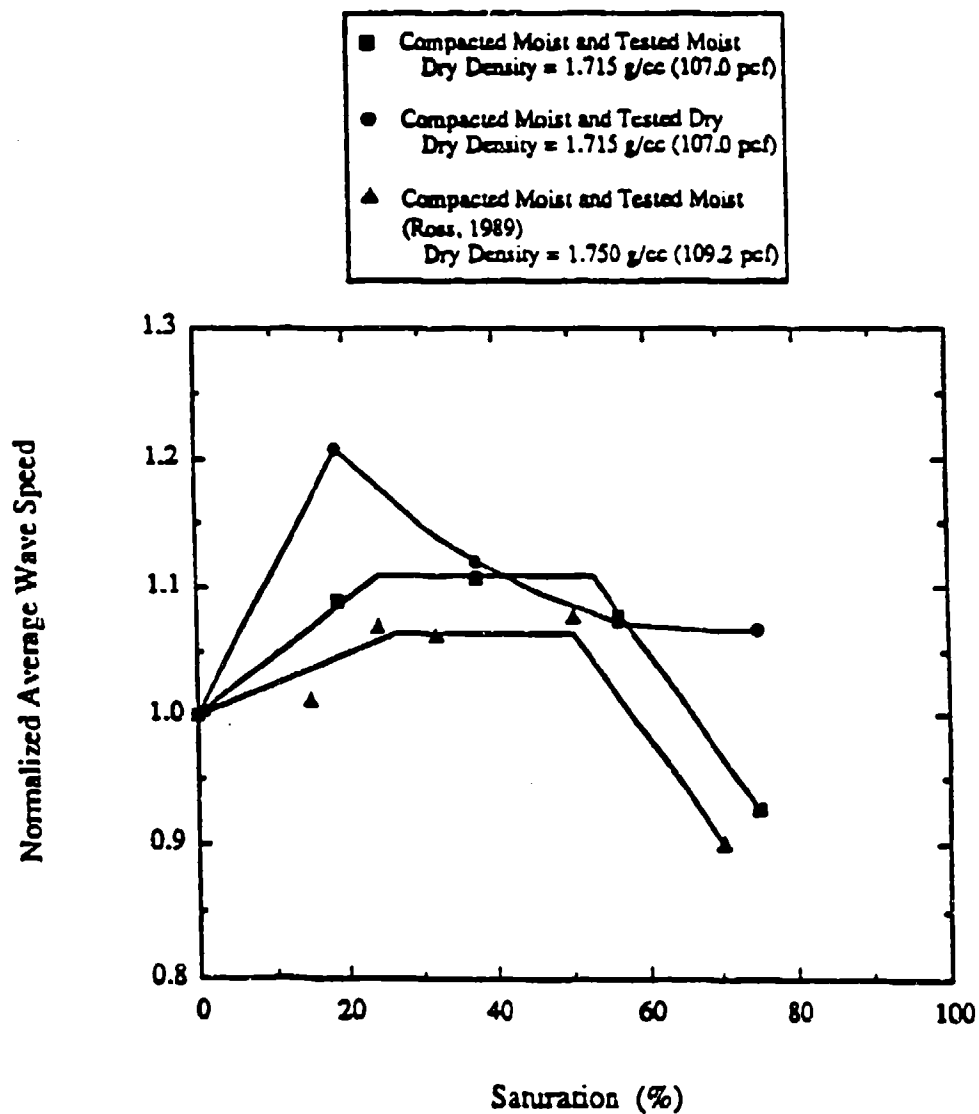
Figure 2.8   Normalized Average Wave Speed as a Function of Saturation for Ottawa 20-30 Sand (Veyera and Fitzpatrick, 1990).

19
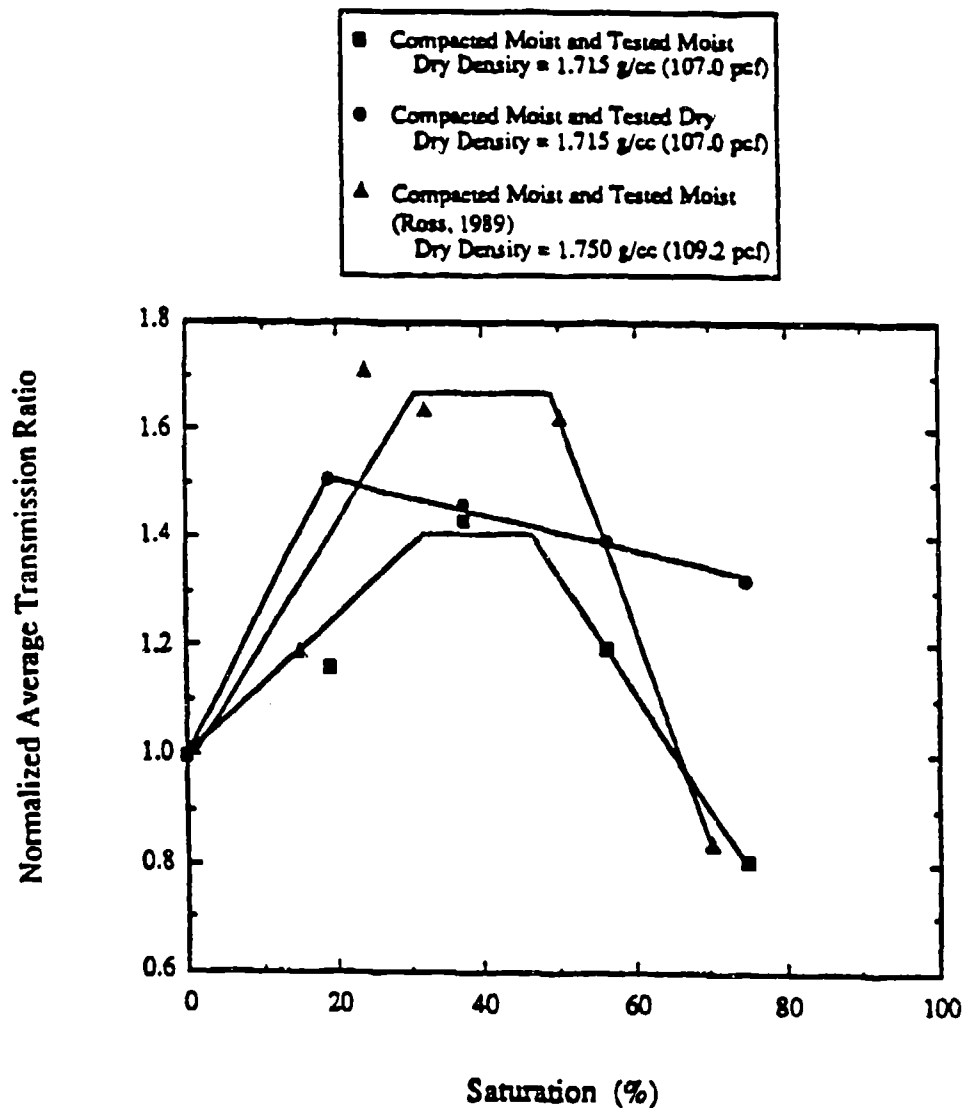
Figure 2.9   Normalized Average Transmission Ratio as a Function of Saturation for Ottawa 20-30 Sand (Veyera and Fitzpatrick, 1990).

Tube Wall Thickness = 2.54 cm (1.0 inches)
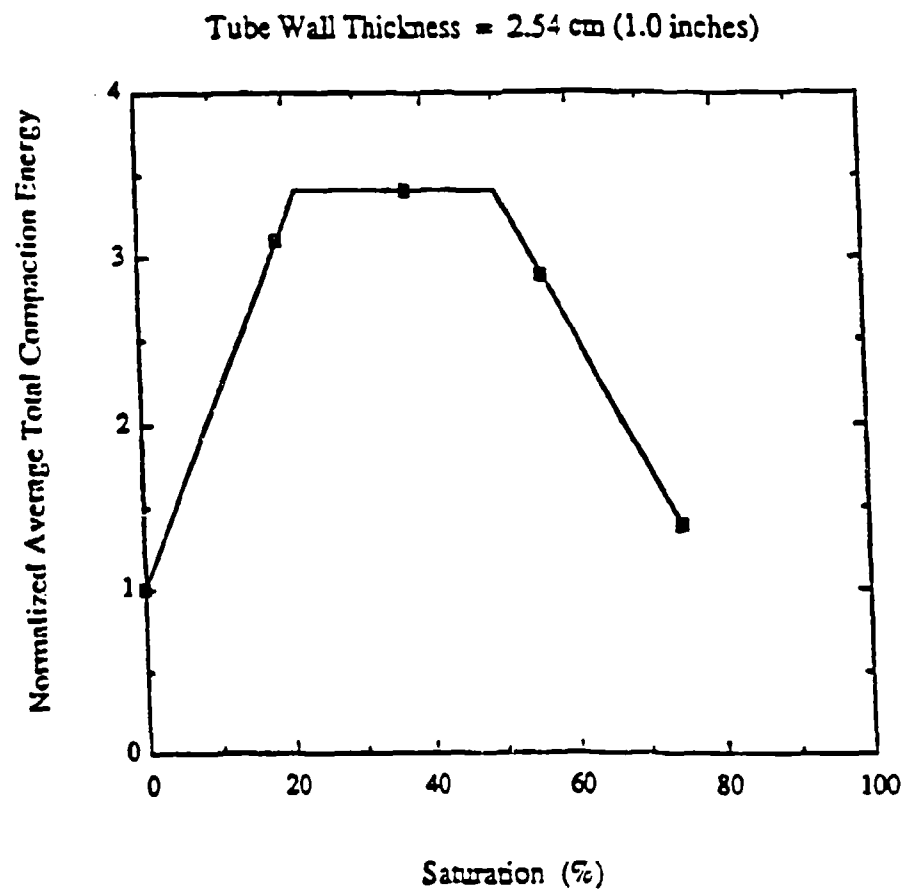
Figure 2.10 Normalized Average Total Compactive Energy for Ottawa 20-30 Sand Compacted to a Dry Density of 1715 kg/m³ (Veyera and Fitzpatrick, 1990).

21

D. CENTRIFUGE MODELING OF EXPLOSIVE-INDUCED STRESS WAVE PROPAGATION IN UNSATURATED SAND

Walsh (1993) conducted centrifuge modeling of explosive detonations in unsaturated sands. The tests were conducted at Tyndall Air Force Base using Ottawa 20-30 and Tyndall Beach sands compacted to a dry density of 1612 kg/m^3 (DR= 35%) and 1521 kg/m^3 (DR= 42%), respectively. The purpose of the tests was to assess if centrifuge modeling could accurately predict stress transmission behavior for full-scale explosive events in unsaturated sands. Scaling relations used to relate centrifuge test parameters to prototype test parameters are given in Table 2.3. Details on the operation of the centrifuge, scaling relations and other related information are provided by Walsh (1993).

In order to simulate a wide range of full-scale test conditions, centrifuge tests by Walsh (1993) were conducted at three different g levels (19, 26, and 67), using two explosive charge weights (350 and 1031 mgs of PBX 9407) over saturation levels ranging from 0 percent to 70 percent. Specimens were compacted moist and tested moist. The 19-g and 26-g tests conducted in Tyndall Beach sand modeled 7.8 kg and 7.3 kg TNT equivalent detonations in the field, and the 67-g test conducted in Ottawa 20-30 sand modeled a 118 kg TNT equivalent detonation in the field.

Centrifuge test results showing peak ground motion parameters and attenuation trends are presented in Figures 2.11 and 2.12. In Figure 2.11, intercept values are plotted versus saturation for peak stress, scaled peak particle acceleration, and peak particle velocity. Intercept values were taken from peak parameter (stress, scaled acceleration, velocity) versus scaled range (R/W$^{1/3}$) plots, at a scaled range of one (R/W$^{1/3}$ = m/kg$^{1/3}$ = 1). In all three plots for Tyndall Beach sand, energy transmission is lowest at 0 percent and 50 to 70 percent, and is highest at 20 to 40 percent saturation. The trends shown in these figures are very similar to those of Charlie et al. (1990a) (Figure 2.5), Pierce (1989) (Figure 2.7) and Veyera and Fitzpatrick (1990) (Figures 2.8 and 2.9).

TABLE 2.3. STANDARD SCALING RELATIONS (FROM BRADLEY ET Al., 1984).

$$N = \frac{acceleration\ of\ model}{acceleration\ of\ prototype}$$

Parameter	Prototype	Model
Linear Dimension	1	$1/N$
Gravity (g)	1	N
Area	1	$1/N^2$
Volume	1	$1/N^3$
Dynamic time	1	$1/N$
Velocity (Distance/Time)	1	1
Acceleration (Distance/Time^2)	1	N
Density (Mass/Volume)	1	1
Unit Weight (Force/Unit Volume)	1	N
Force	1	$1/N^2$
Stress (Force/Area)	1	1
Mass	1	$1/N^3$
Energy	1	$1/N^3$
Strain (Displacement/Unit Length)	1	1
Hydrodynamic Time	1	$1/N^2$
Impulse	1	$1/N^3$
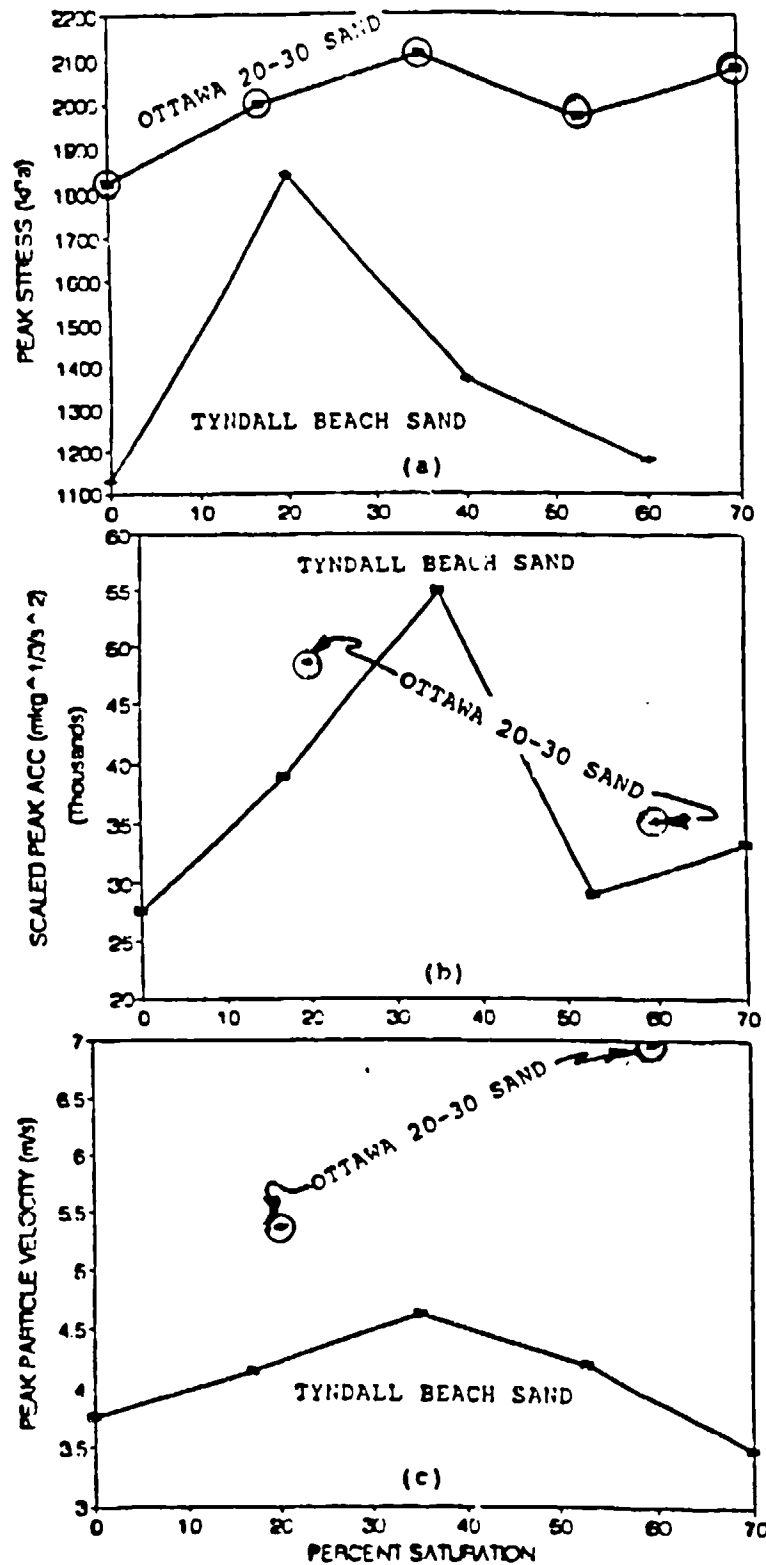
Figure 2.11 Intercept Values for Tyndall Beach and Ottawa 20-30 Sands.
(a) Peak Stress. (b) Scaled Peak Particle Acceleration. (c)
Peak Particle Velocity. (Walsh, 1993).

24
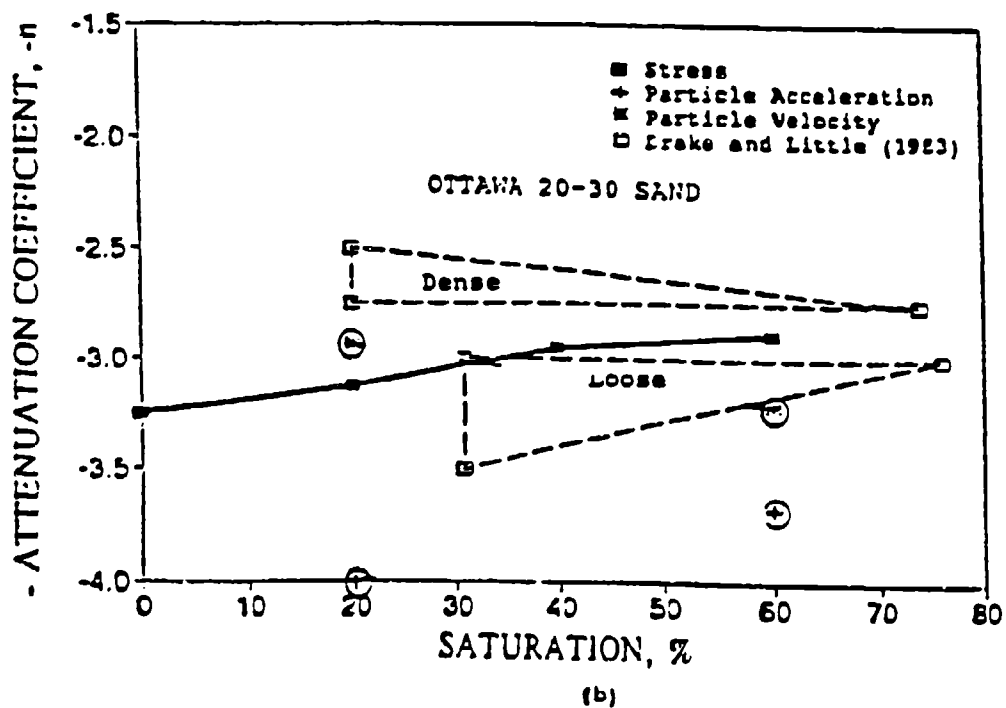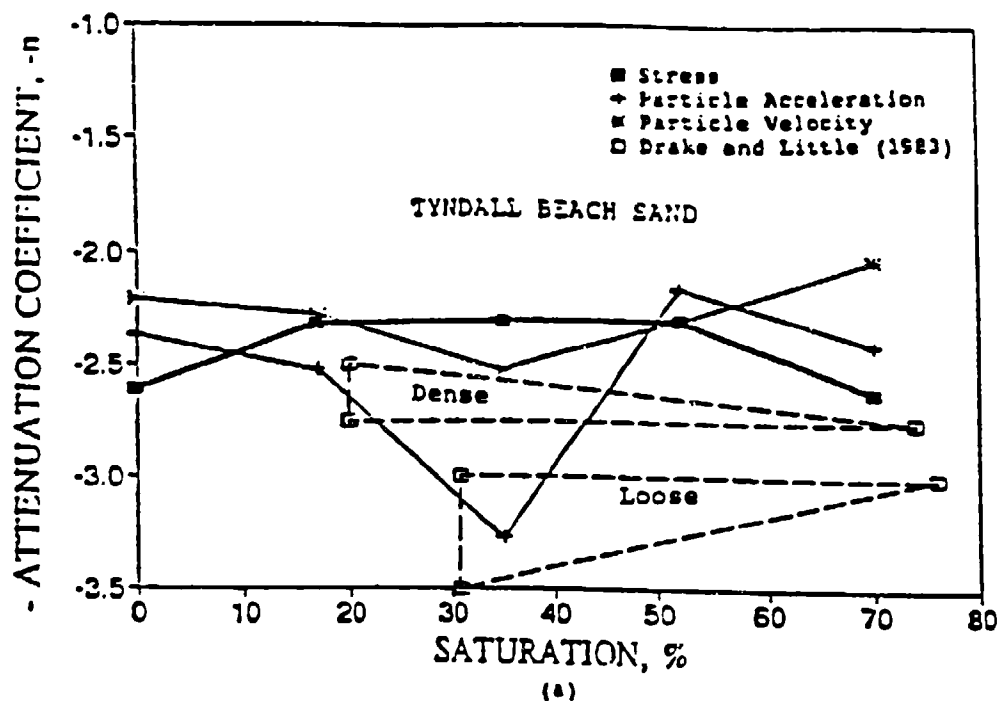
Figure 2.12 Attenuation Coefficients as a Function of Saturation from Regressions of Peak Ground Shock Parameters and from Drake and Little (1983). (a) Tyndall Beach Sand. (b) Ottawa 20-30 Sand (Walsh, 1993).

In Figure 2.10a (Tyndall Beach sand), attenuation of the stress wave over distance is greatest at 20 to 50 percent saturation and least at 0 and 70 percent saturation. In Figure 2.10b (Ottawa 20-30 sand), attenuation rises steadily from 0 to 60 percent saturation. It is uncertain why the attenuation is greatest at 60 percent saturation for Ottawa 20-30 sand. This behavior has not been observed in any of the other tests.

Figure 2.13 shows measured propagation velocity versus saturation from centrifuge test data. Seismic velocities suggested by Drake and Little for dense and loose sands are included for comparison. An envelope encloses the range of suggested seismic velocity values for dense and loose sands. Attenuation trends in Figure 2.13a for Tyndall Beach sand are similar to those observed in Figures 2.5, 2.7, 2.8, 2.11 and 2.12.

E. SOIL MECHANICS PRINCIPLES THAT EMBRACE UNSATURATED SOILS

Fredlund (1985) synthesized the equations surrounding the behavior of saturated and dry soils, and developed equations for the behavior of unsaturated soils. Pierce (1989) reported:

> The theory presented by Fredlund accurately predicted that the capillary pressures developed in the sands which were compacted dry, then saturated, then desaturated would have little influence on the stiffness (Pierce, 1989, pg. 121).

Walsh (1993) determined that Fredlund's theory was not particularly useful in predicting blast-induced soil parameters in sands compacted moist.
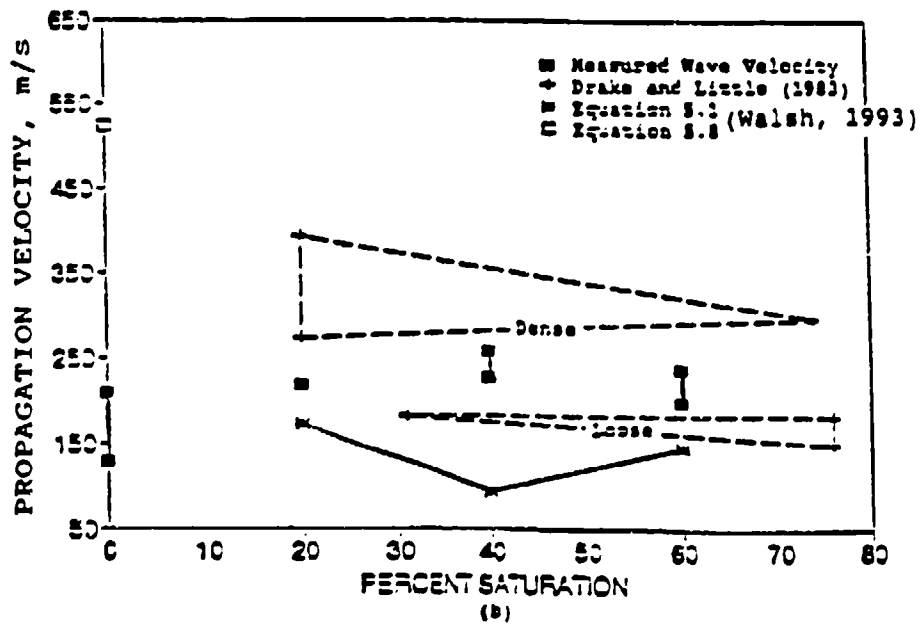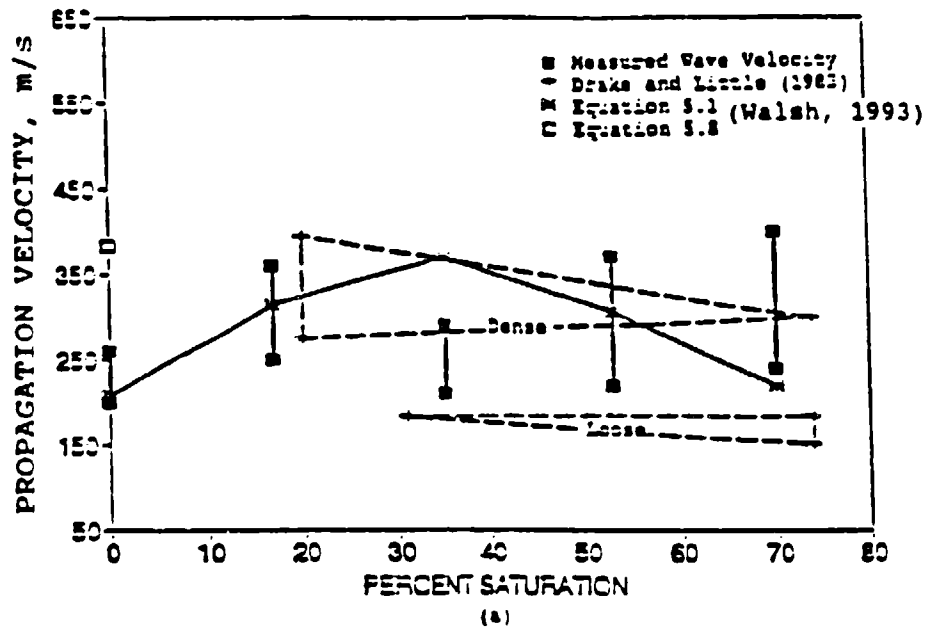
Figure 2.13 Measured Propagation Velocities from Centrifuge Data at a Scaled Range of 2.9 m/kg$^{1/3}$, and Seismic Velocities from Drake and Little (1983), and Computed from Equations 5.1 and 5.8 (a) Tyndall Beach Sand. (b) Ottawa 20-30 Sand (Walsh, 1993).

F. SUMMARY OF PREVIOUS RESEARCH

Drake and Little (1983) developed empirical equations to predict blast-induced peak ground motion parameters for a wide range of soil types and conditions. Cube root scaling laws were used in the analysis.

Pierce (1989), Ross (1989) and Charlie et al. (1990a) conducted SHPB tests on unsaturated sand specimens, and determined that the saturation level at compaction influences stress transmission and attenuation behavior. Stress transmission was greatest at 20 to 60 percent saturation and least at less than 20 and greater than 60 percent saturations. They hypothesized that capillarity, in and of itself, does not directly influence the stiffness of sands compacted moist.

Veyera and Fitzpatrick (1990), while attempting to determine the relationship between soil microstructure and dynamic soil parameters on the SHPB apparatus, validated the trends of Ross (1989) and Charlie et al. (1990a). The degree of saturation at the time of compaction largely determines particle orientation and packing and possibly horizontal stress, which directly influences stress transmission. Samples compacted moist and tested dry showed essentially the same trends as samples compacted moist and tested moist, which affirms that the presence of capillarity after compaction does not alter the stress transmission characteristic of soils.

Walsh's (1993) centrifuge test results showed the same trends for stress transmission, propagation velocity, and attenuation (except for Ottawa 20-30 sand) as the trends reported by Pierce (1989), Ross (1989) Charlie et al. (1990), and Veyera and Fitzpatrick (1990).

The physical properties of 50/80 silica sand tested by Pierce (1989), Ross (1989) and Charlie et al. (1990a); for Ottawa 20-30 sand tested by Veyera and Fitzpatrick (1990) and Walsh (1993); for Eglin sand tested by Pierce (1989) and for Tyndall Beach sand tested by Walsh (1993) are given in Table 2.3.

TABLE 2.4. PHYSICAL PROPERTIES OF 50/80 SILICA, OTTAWA 20-30, EGLIN AND TYNDALL BEACH SANDS.

Sand property or categorization	Sand type			
	50/80 silica	Ottawa 20-30	Eglin	Tyndall Beach
Specific gravity, G_s	2.65	2.65	2.65	2.65
Max. dry density, ρ_{max}, kg/m³	1685	1720	1670	1630
Min. dry density, ρ_{min}, kg/m³	1475	1560	1450	1450
e_{max}	0.796	0.705	0.817	0.817
e_{min}	0.572	0.545	0.590	0.621
Test dry density, ρ_d, kg/m³	1600[3]	1760[1]; 1750[2]; 1715[4]; 1714[5]; 1612[6]	1760[1]; 1754[5]	1601[5]; 1521[6]
Test relative density, DR, %	63[3]	122[1]; 117[2]; 97[4]; 97[5]; 35[6]	134[1]; 132[5]	85[5]; 42[6]
D_{50}, mm	0.25	0.70	0.26	0.19[5]; 0.25[6]
Percent passing #200 sieve	< 5 %	0	7	0
C_u	2.16	1.16[1]; 1.40[2,4,5,6]	3.4	1.18[5]; 1.67[6]
C_c	1.12	1.04[1]; 1.03[2,4,5,6]	1.29	0.95[5]; 1.07[6]
Classification (ASTM D2487)	SP	SP	SP-SM	SP
Grain shape	subrounded	subrounded to rounded	subangular to subrounded	subrounded to subangular
Residual saturation, %	9	5	16	11

[1] Reported by Pierce (1989)
[2] Reported by Ross (1989)
[3] Reported by Charlie et al. (1990a)
[4] Reported by Veyera (1990)
[5] Reported by Veyera (1992)
[6] Reported by Walsh (1993)
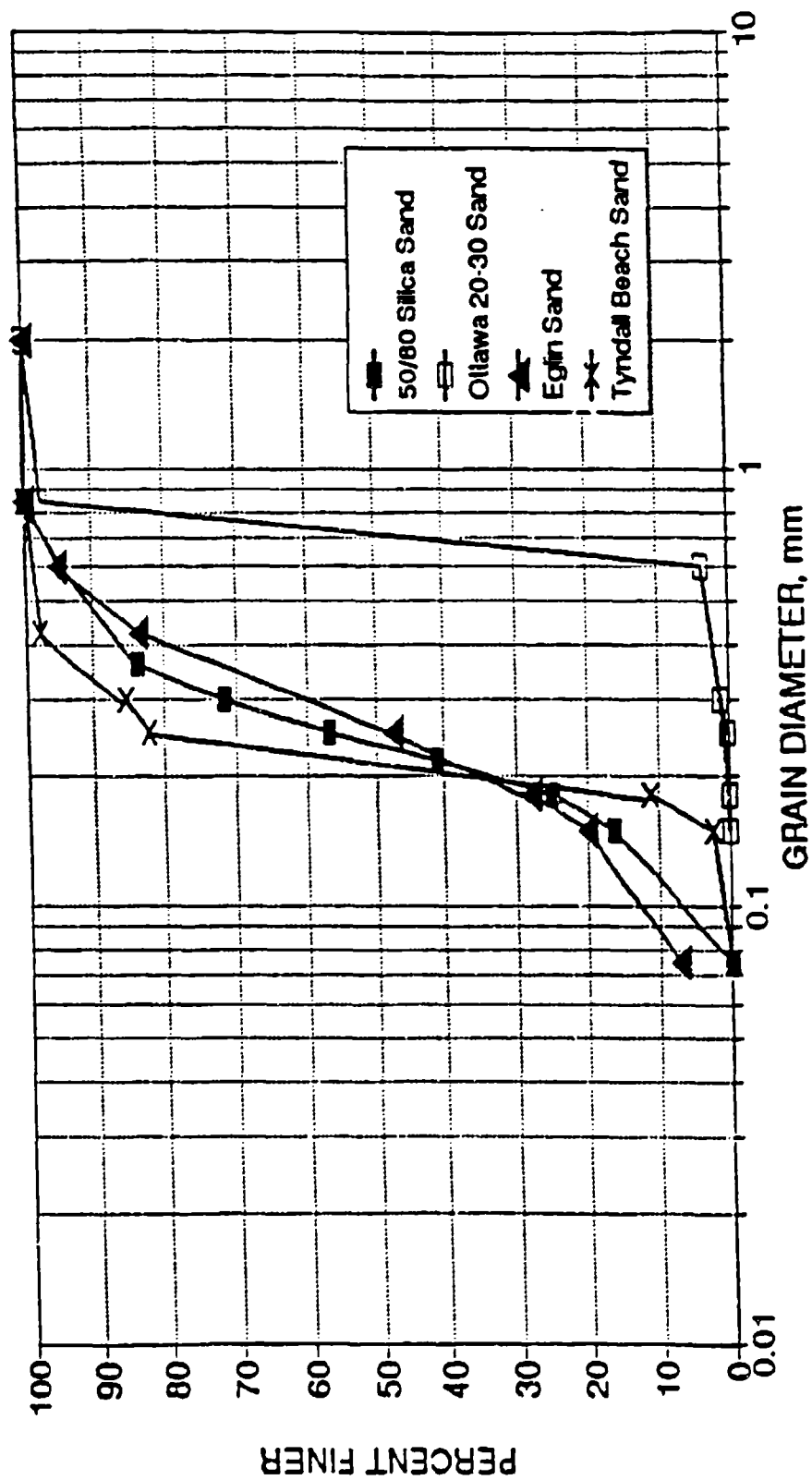
Figure 2.14 Grain Size Distribution for 50/80 Silica, Ottawa 20-30, Eglin and Tyndall Beach Sands.

III. EXPERIMENTAL PROCEDURE

A. LOCATION AND DESCRIPTION OF TEST SITE

The test site is located in a valley south of the Colorado State University Engineering Research Center in Fort Collins, Colorado. The site was originally designed and constructed in 1985 for explosive liquefaction studies funded by the Air Force Office of Scientific Research (Bretz, 1989; Schure, 1990; Hassan, 1993). A schematic plan view of the test site is displayed in Figure 3.1.

Explosive tests on unsaturated sand were conducted in an existing, buried, open-ended steel tank, labeled as item 13 in Figure 3.1. The top of the tank is open to the atmosphere and coincident with ground level. At the bottom of the tank are successive layers of gravel and bentonite clay, which allow drainage within the tank and prevent significant upward seepage of groundwater. Tank dimensions are 4.27 m (diameter) by 2.74 m (depth). Photographs of the test site and partially filled tank are displayed in Figures 3.2 and 3.3, respectively.

Other items utilized on the test site were the instrument relay shack (Figure 3.1, item 10 and Figure 3.4), the command center (Figure 3.1, item 1 and Figure 3.5), and the 20,000 liter water tank (Figure 3.1, item 11). The instrumentation shack housed the power supplies and signal conditioners for the instruments. Data acquisition equipment and computers were located in the command center, which served as the center for system control.

31

North
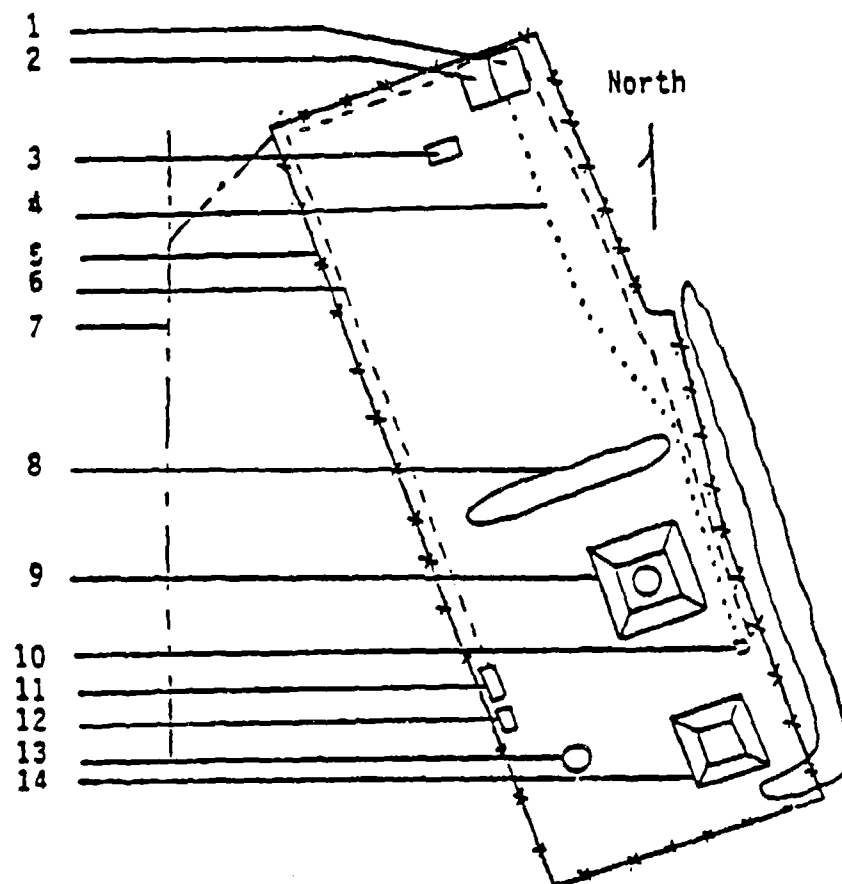
1 Command Center
2 Garage
3 Storage Building
4 Cable Trench   Scale 1:1200
5 Fence
6 Buried Powerline
7 Overhead Powerline
8 Berm
9 Liquefaction Testing Pit
10 Instrumentation Shack
11 Water Tank
12 Storage Shed
13 Shock Wave Propagation Testing Tank
14 Liquefaction Testing Pit

0 10 20
meters

Figure 3.1 Plan View of Test Site (Bretz, 1989).

32

Figure 3.2   Test Site.
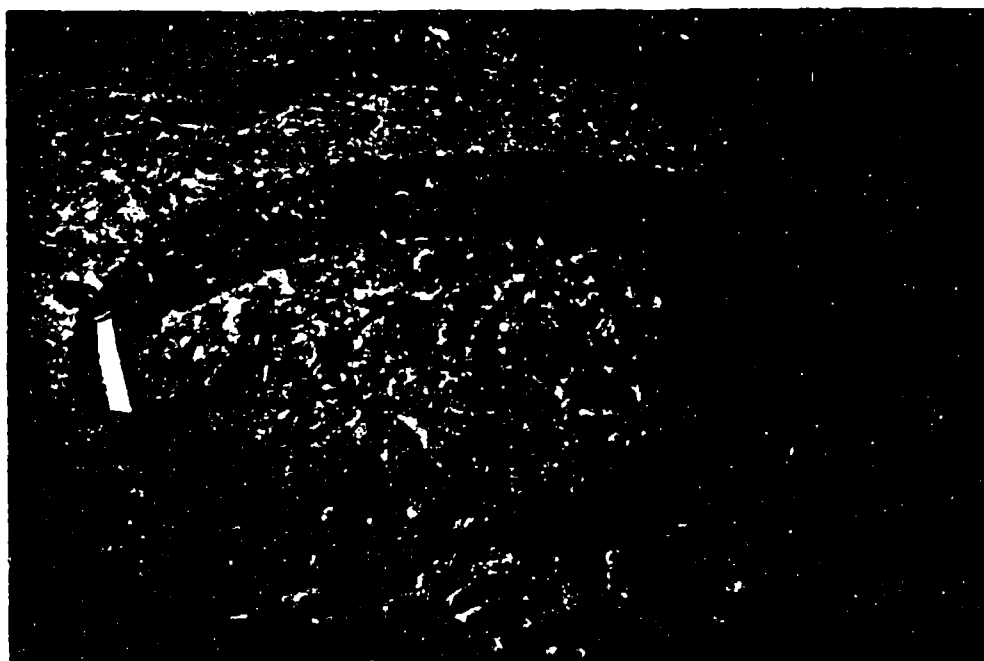
Figure 3.3   Partially Filled Test Tank.

33

Figure 3.4   Instrument Relay Shack.
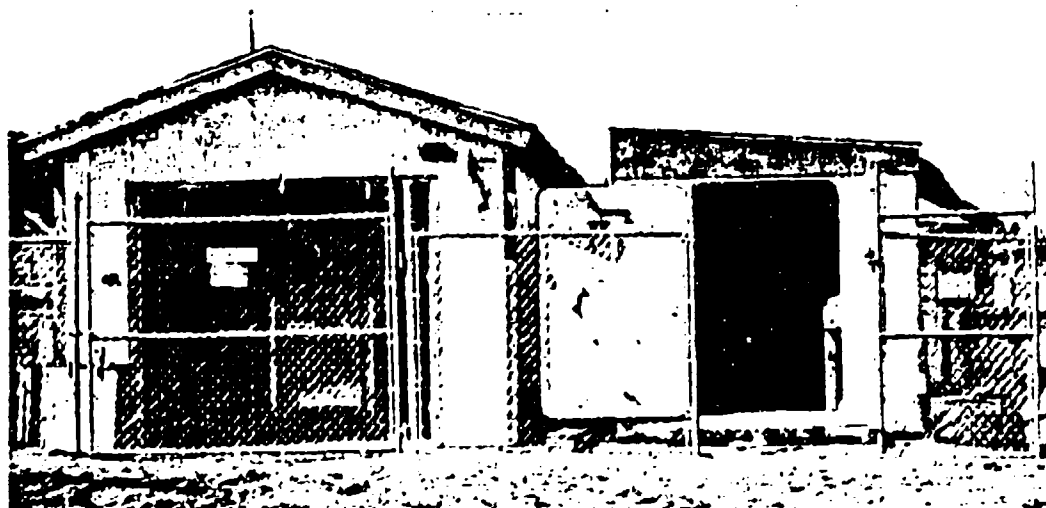
Figure 3.5   Garage and Command Center (Bretz 1989).

B.   EQUIPMENT AND APPARATUS

1.   Field Equipment

Table 3.1 lists the field equipment used in the process of sand placement, saturation, mixing, compaction, density/moisture control and removal.

TABLE 3.1.   EQUIPMENT USED IN FIELD PROCEDURE.

Placement/ Removal:	John D ere JD 300 backhoe
	Outdoor/indoor portable aggregate conveyor belt
	Shovels and rakes.
Saturation:	Teel self-priming centrifugal pump; model 3P601A, 6 kw (8 HP), 7.62 cm (3 inch) inlet/outlet diameter, -76,000 liter/hour (20,000 GPH)
	Teel convertible jet pump; model 9K630, 746 watts
	Teel submersible sump pump; model 3P635, 250 watts
	20,000 liter (5000 gallon) water storage tank
	Three 208 liter (55 gallon) barrels
	7.62 cm hose, garden hose, various spray nozzles.
Mixing:	Sears-Craftsman tiller; model 917.298350, 3.7 kw (5HP), 61 cm (24 inch) tine width, 28 cm (11 inch) tine depth
	Shovels and rakes.
Compaction:	Wacker vibratory soil compactor; model VPG 1550A, 2.6 kw (3.5 HP), 85 Hz exciter frequency, 88 kg.
Density/ Moisture Control:	CPN-1DR-122 Nuclear Density/Moisture gauge; radioactive sources- Cesium 137 and Americium 241/Beryllium, multi-depth probe 30 cm max.

2.   Instrumentation

Blast-induced particle acceleration was measured with Endevco Model 7270A 20,000-g and 6,000-g piezoresistive accelerometers (Figure 3.6). Detailed specifications and calibration data are provided in Appendix A. These accelerometers were ideal for the tests because of their small size (1.4 x .7 x .95 cm), low mass, high resonant frequency and zero damping, features which give reliable response to the fast rise times and short pulse duration associated with transient shock waves.

Input excitation voltage and output signal amplification for the accelerometers were provided by an Endevco Universal Signal Conditioning system, Series 4470 (Figure 3.7). Individual signal conditioners were mounted in Endevco's Model 4942 Rack adapter. Mode cards were inserted into each signal conditioner and calibrated for the specific sensitivity and range of each accelerometer. Detailed specifications for the signal conditioners are given in Appendix B.

Peak soil stress was measured with Kulite LQ-080U soil stress gages (Figure 3.6) developed especially for accurate measurements of blast-induced soil reactions. Detailed specifications are provided in Appendix B. A 12 volt 4.5 AH battery provided the input excitation voltage for each gage. No amplification of the soil stress gages output signal was provided.

Input and output signals were transmitted from the instrumentation relay shack to the instruments in the sand and back through approximately 40 meters of shielded 2 Pair, 22 gage cable. Output signals from the instrument shack were then transmitted through approximately 100 meters of RG 58, 50 Ohm coaxial cable to the transient data recorders in the command center. Both sets of cables were laid on the ground surface.
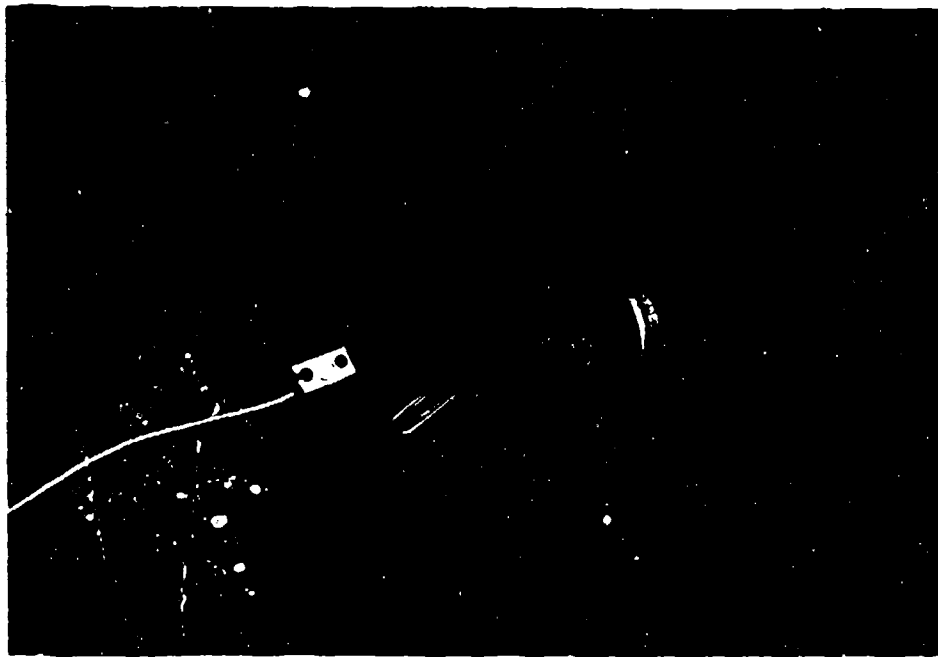
Figure 3.6 Endevco 20,000 g Accelerometer (left) and Kulite LQ 080U Soil
Stress Gage (right).
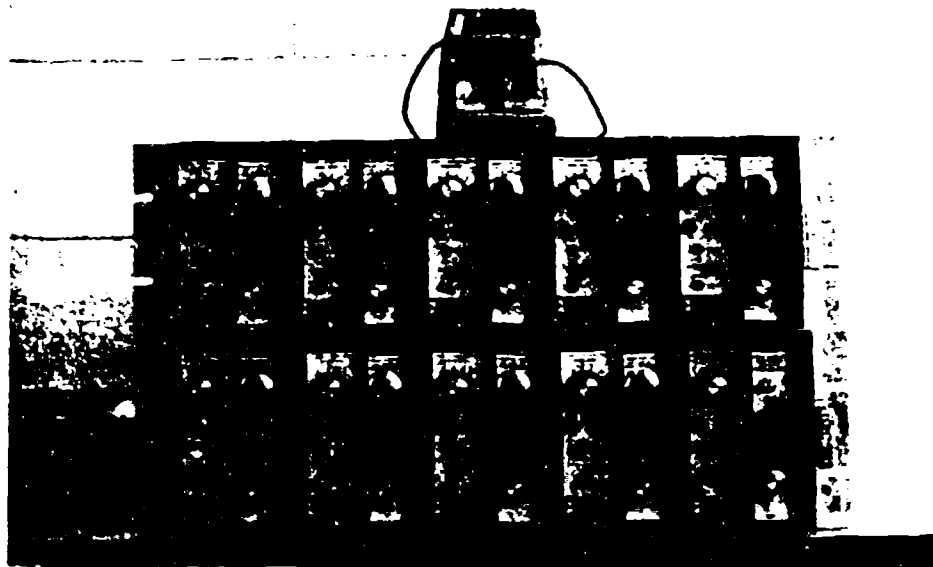
Figure 3.7 Endevco Signal Conditioners.

3. Data Acquisition/Storage/Analysis

a. Transient Data Recorders

Pacific Instruments Model 9820 transient data recorders (TDR's) were used to record the dynamic test data from the accelerometers and soil stress gages. Two racks with 10 modules each were located in the command center. A total of twenty data channels were available for use. The TDRs were triggered and began recording data the instant that voltage from the detonation circuitry was sensed. Incoming analog signals were first digitized at a programmable rate of up to 500,000 samples per second, then stored in the data recorder's memory. Data were then manually transferred to permanent storage on the Compaq 386 hard drive and high-capacity Bernoulli disks. The TDRs are displayed in Figure 3.8. Detailed information on the TDRs is provided by Charlie, et al. (1987).

b. Computer Hardware and Software

Computer hardware consisted of the following devices:

- Compaq Deskpro 386/20e personal computer; 25 MHz, 4 megabytes of RAM, 110 megabyte hard drive, math coprocessor, expanded memory (Figure 3.9)

- Compaq 286 portable field computer (Figure 3.9)

- IBM compatible 386 personal computer

- Bernoulli portable 44 megabyte hard drive (Figure 3.9)

- Hewlett Packard Laserjet III printer.
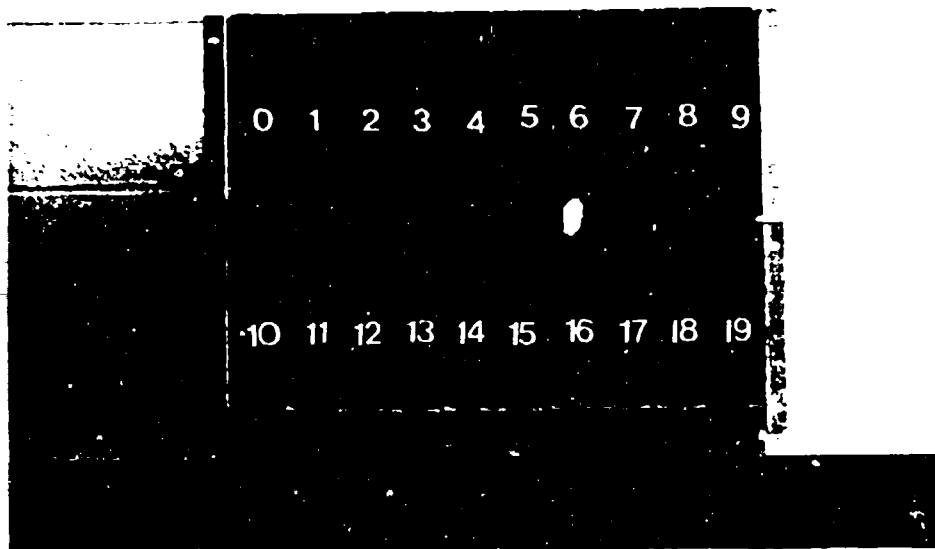
Figure 3.8   Transient Data Recorders.
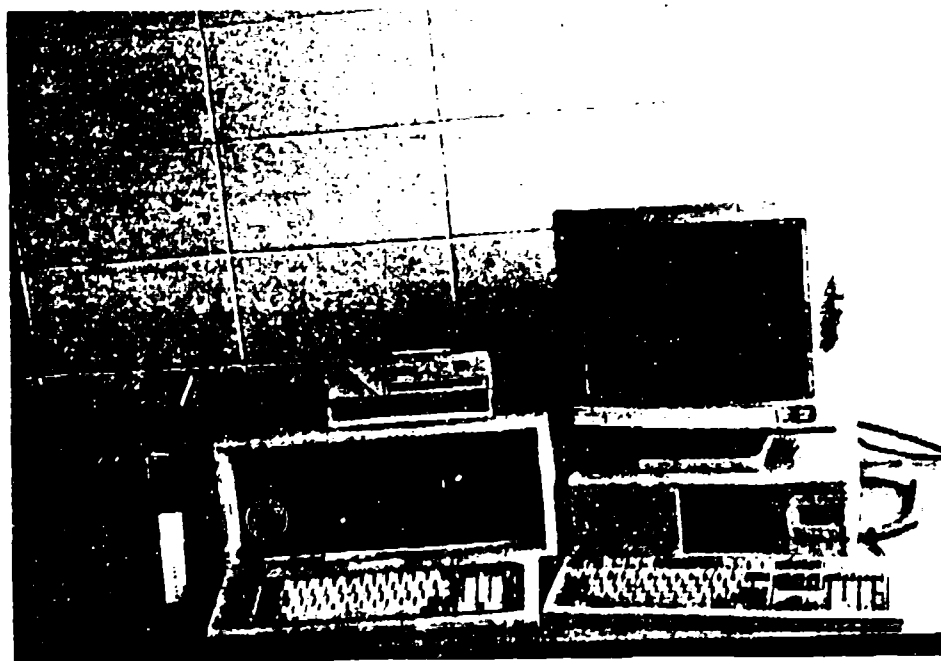
Figure 3.9   Compaq 286 and 386 Computers, Bernoulli Disk Drive.

Both Compaq computers, along with the data acquisition software, were used prior to testing for system control-- channel configuration, calibration of signal voltages, channel monitoring, and initiation of the firing sequence. Subsequent to firing, data from the TDRs was stored on the computer hard drives and the Bernoulli disk drive. The Compaq 386, along with another 386 personal computer, were used for data analysis and preparation of this manual.

Pacific Data Acquisition software provided system control during testing. Other software packages used subsequent to testing for data analysis and manual preparation were Asyst Scientific software 3.1, Quattro Pro 3.0, and Word Perfect 5.1.

4. Miscellaneous Equipment

- Fennel Kassel level, tripod, philadelphia rod
- Fluke 806A multimeter
- Nimbus Instruments Model HVB-1 High Voltage Detonator
- Wiring equipment- Ungar 1095 heat gun, Ungar UTC-300 soldering station

C. FIELD PROCEDURE

1. Sand Placement, Saturation, Mixing and Compaction

a. General Overview of Procedure

Initially, 90,000 kg (100 tons) of Poudre Valley sand was ordered from Mobile Western company of Fort Collins and stockpiled next to the tank for the Fall 1991 tests. The first test was conducted on sand compacted at a saturation of 13 percent (at the natural water content, w, of the sand of 3.1 percent). Subsequent tests were conducted at saturations of 20, 40, 60 and 70 percent. A dry density of approximately 1635 kg/m^3 (102 pcf) was achieved for all tests.

A second batch of sand (65,000 kg or 70 tons), originating from the same source, was ordered for the Spring of 1992 tests. Prior to delivery, the sand was dried to a water content of zero in a dryer drum belonging to a local asphalt company. The first Spring test was conducted dry, and subsequent tests were conducted at the same saturations and dry densities as the Fall tests.

The sand remaining in the tank after detonation was re-used for each test according to the following sequence: (1) removal of sand with backhoe subsequent to testing; (2) replacement of loose sand into the tank for the next test; (2) saturation of sand to the desired percent saturation; (4) compaction of sand in .305 m (1 foot) lifts; 5) explosive testing of sand.

b.   Sand Placement

Sand was placed manually into the tank with shovels (Figure 3.10) in .305 m lifts, often with the aid of a mobile conveyor belt. Lines were painted on the inside of the tank in .305 m increments to aid in determining when enough sand had been placed. Approximately 56,000 kg (62 tons) of sand were required to fill the tank to ground surface level. The lift thickness was chosen according to the 2:1 ratio of stress distribution for rectangular surface loads. It was assumed that vibrations from the soil compactor (.75 m x .45 m) would be distributed over depth according to the same ratio. At a depth of .305 meters then, the intensity of the vibrations are decreased by one-half. Any greater degree of vibration attenuation could have lead to excessive undercompaction of the lower portion of the lift.

41

c.   Sand Saturation and Mixing

Water was added to each lift to reach the target saturation and then mixed in place by means of manual spraying and roto-tilling.   Before addition of water, an average in-situ water content for each lift was measured using the Nuclear Density/ Moisture gage (NDMG).   An HP-41 program calculated the amount of water needed to obtain the desired saturation, given the in-situ and target water contents and densities.

Water was transferred from the 20,000-liter storage tank into 208-liter barrels so that a known volume of water could be obtained from the barrels. The desired volume of water was then pumped from the barrels and distributed evenly onto the surface of the lift using a garden hose and spray nozzle (Figure 3.11).

Lifts were mixed with a tiller immediately after saturation (Figure 3.12) to prevent excessive drainage and drying. Several passes were made with the tiller to ensure even distribution of moisture throughout the lift thickness.

Excessive drainage into lower layers was encountered during saturation for tests conducted at 60 and 70 percent saturation.   Drainage was minimized in this case by using the Teel high-capacity centrifugal pump (1200 liters/minute) to saturate the lift in a matter of minutes (Figure 3.13).

d.   Sand Compaction

Each layer was compacted to a target dry density of 1635 kg/m^3 using the Wacker vibratory compactor (Figure 3.14).   The compactive effort (number of passes) required to reach the target density was determined by trial and error. Compaction control was accomplished by measuring the dry density and moisture content of the lift with the Nuclear Moisture/Density Gauge (NDMG) shown in Figure 3.15, and making additional passes or loosening the sand and re-compacting as necessary. Periodically, moisture contents given by the NDMG were verified by performing the Standard Test

42

for Moisture Content Determination (ASTM D2216) on a sand sample (a microwave oven was used in place of the standard drying oven). When the target saturation and density for a layer had been reached, the same procedure was followed for the next layer.

e.   Moisture and Density Quality Control

Density and moisture measurements using the nuclear density/moisture gauge were taken at four to five locations over the area of each lift at depths of 10 cm and 20 cm. A backscatter reading was also taken at each location. Average values of dry density and saturation were calculated and compared with the target dry density and saturation. The sand's density and saturation were modified as needed to match target values.

f.   Removal of Sand

Upon completion of a test (Figure 3.16), crater dimension measurements were taken, and all layers were removed with a backhoe and stockpiled next to the tank for the next test (Figure 3.17). Following the dry test, crushed sand located near the CEO was removed and not reused.

Figure 3.10   Placement of Lifts into the Tank.

Figure 3.11   Addition of Water to Lifts to Reach Target Saturation.

44

Figure 3.12 Mixing of Lifts.

Figure 3.13 Addition of Water to Lifts for Tests Conducted at 60 and 70 Percent Compactive Saturations.

Figure 3.14   Vibratory Compaction of Lifts

Figure 3.15 Density Measurement with Nuclear Density Gauge.
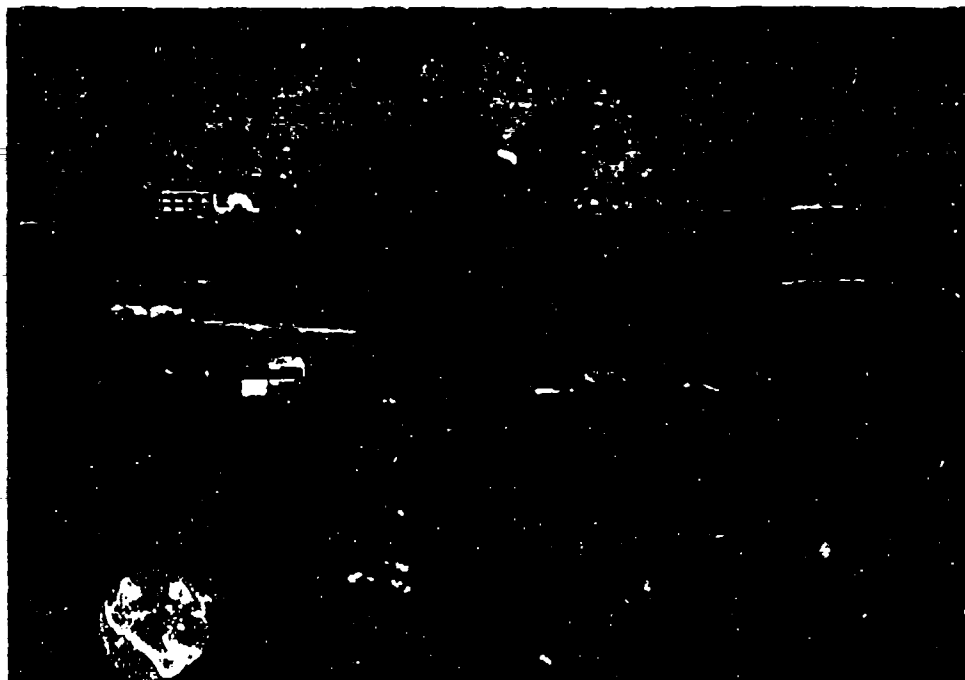
Figure 3.16 Typical 7.0 kg Blast.

Figure 3.17 Removal of Sand with Backhoe.

2. Instrumentation Preparation and Placement

a. Instrument Preparation

All instruments were factory calibrated and sealed against moisture by the manufacturer. Instrument preparation for field tests consisted of wire splicing, waterproofing, testing continuity for proper connections, and testing wheatstone bridge circuitry.

Wire leads from the accelerometers and soil stress gages were soldered to shielded 2-pair 22-gage cable, which transmitted input and output voltages from the instrument relay shack and back. A multimeter was used to check for continuity across the wires and for balance in the wheatstone bridge circuitry of the instrument. All junctions where wires had been spliced were sealed against moisture by sheathing the wires with multiple layers of dielectric grease and electric shrink wrap.

Five-pin connectors were attached at the end of the accelerometer cables and plugged into the signal conditioner. The input leads of the soil stress gage cables were attached to the positive and negative posts of 12 volt batteries, and the output leads were connected directly to RG 58 coaxial cable. A common system ground was provided by the TDRs.

b. Instrument Placement

The instrument layer was located on the surface of the third layer from the bottom of the tank (see Figure 3.18). After all layers had been placed, a surcharge of 1.4 meters of compacted sand covered the instrument layer, which corresponds to a scaled depth of burst of 1.88 m/kg$^{1/3}$ and coupling factor of 1 (Figure 2.1). The center of explosion, which coincided with the instrument layer, was covered with enough surcharge such that it received the full energy from the burst.

The center of the tank (also the CEO) was established by finding the intersection of two perpendicular chords (ropes stretched across the rim of the tank). Markings were then painted at appropriate locations on the

rim and inside tank wall so that the center of tank could easily be re-established.

Instruments were placed along radial lines originating from the center of the tank at distances of .91, 1.07, 1.37 and 1.98 meters (3, 3.5, 4.5, 6.5 feet) for Fall 1991 tests (Figure 3.19). Additional instruments were placed at 1.69 m and 1.83 m (5.5 ft and 6.0 ft) for Spring 1992 tests conducted at 0, 13, and 20 percent saturations (Figure 3.20). Spring tests conducted at 40 and 60 percent saturations employed an instrument placement scheme which allowed for greater scaled ranges (Figure 3.21). Instruments placed closer than approximately .91 meters from the COE were destroyed by the blast. Instrument locations were chosen such that the distance interval between each successive instrument from the COE doubled, a feature which facilitates data spread on a log-log plots.

Soil stress gages were placed along a radial line excending from the COE to the edge of the tank and slightly offset in order to minimize disruption of the stress field. Offsetting was not necessary for the accelerometers, since their size and mass were virtually identical to larger grain sizes.

Each instrument was placed with its face perpendicular to the COE for tests conducted in the Fall of 1991 (Figure 3.19). However, a different instrument orientation and placement scheme was necessary for tests conducted during the Spring of 1992. For Spring tests conducted at 0, 13 and 20 percent saturations, charge masses were placed .61 meters apart and fired separately (see Sec. V for discussion). Instrument faces were accordingly aligned perpendicular to the bisector of the two charges to minimize the effects of a-perpendicularity on stress measurement (Figure 3.20). When an instrument had been placed and oriented, presaturated sand was carefully placed over the instrument and hand tamped until firm. After all instruments had been placed and covered, pre-saturated sand was backfilled so as not to disturb the zones where the instruments had been placed. The layer was then compacted with the vibratory compactor as with the other layers.

3. Explosive Procedure

Seven kg charges (TNT equivalent) were used for Fall 1991 tests.
Seven kg charges and .227 kg charges were used for Spring 1992 tests
conducted at 13 and 20 percent saturations. The dry test (saturation of
zero percent) conducted in Spring 1992 utilized 6.22 and 0.227 kg charges.
Charges of 0.227 kg were used for Spring tests conducted at 40 and 60
percent saturations. The buried charge masses were cylindrical in shape,
with the explosive center of mass located on the same plane as the
instrument level (see Figure 3.18). The smaller .227 kg charge was offset
.61 meters from the 7 kg charge (see Figure 3.20).

When the top sand layer had been compacted, a 10 cm auger was used to
bore a hole deep enough such that the center of mass of the placed
explosive corresponded with the instrument layer (Figure 3.22). Holes
could not be bored for tests conducted in dry sand, so the explosives were
lowered into a 10 cm I.D PCV pipe (wall thickness of 5 mm) positioned in
the tank before sand placement. The explosives were then packed inside
the hole to eliminate air gap voids between the explosive and soil or PCV
pipe. Sand was then placed over the explosive and recompacted.

Instrument location:	Distance from center of 6.22 & 7.0 charge meters	feet	Distance from center of 0.227 kg charge meters	row	feet
A	0.91	3.0	1.34	a	4.40
			1.43	b	4.69
B	1.07	3.5	1.48	a	4.87
			1.58	b	5.17
C	1.37	4.5	1.77	a	5.81
			1.87	b	6.15
D	1.68	5.5	2.07	a	6.78
			2.17	b	7.12
E	1.83	6.0	2.21	a	7.26
			2.32	b	7.61
F	1.98	6.5	2.36	a	7.75
			2.47	b	8.10

Figure 3.18   Cross Section of Tank Showing Instrument Layer and Explosive Placement.

51
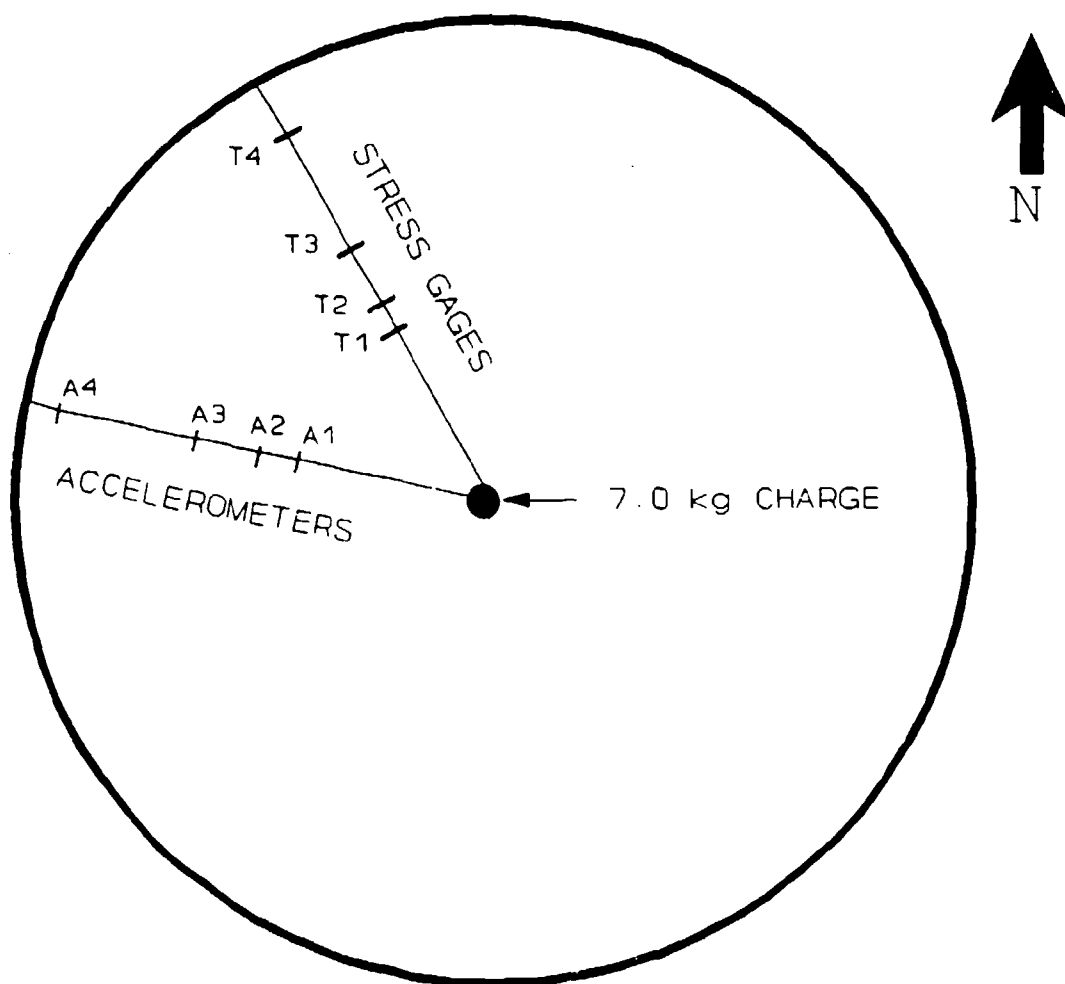
Instrument location:	Distance from center of 7.0 kg charge	
	meters	feet
A1,T1	0.91	3.0
A2,T2	1.07	3.5
A3,T3	1.37	4.5
A4,T4	1.98	6.5

Figure 3.19 Plan View of Instrument Layer Showing Instrument and Explosive Locations for Fall 1991 Tests.
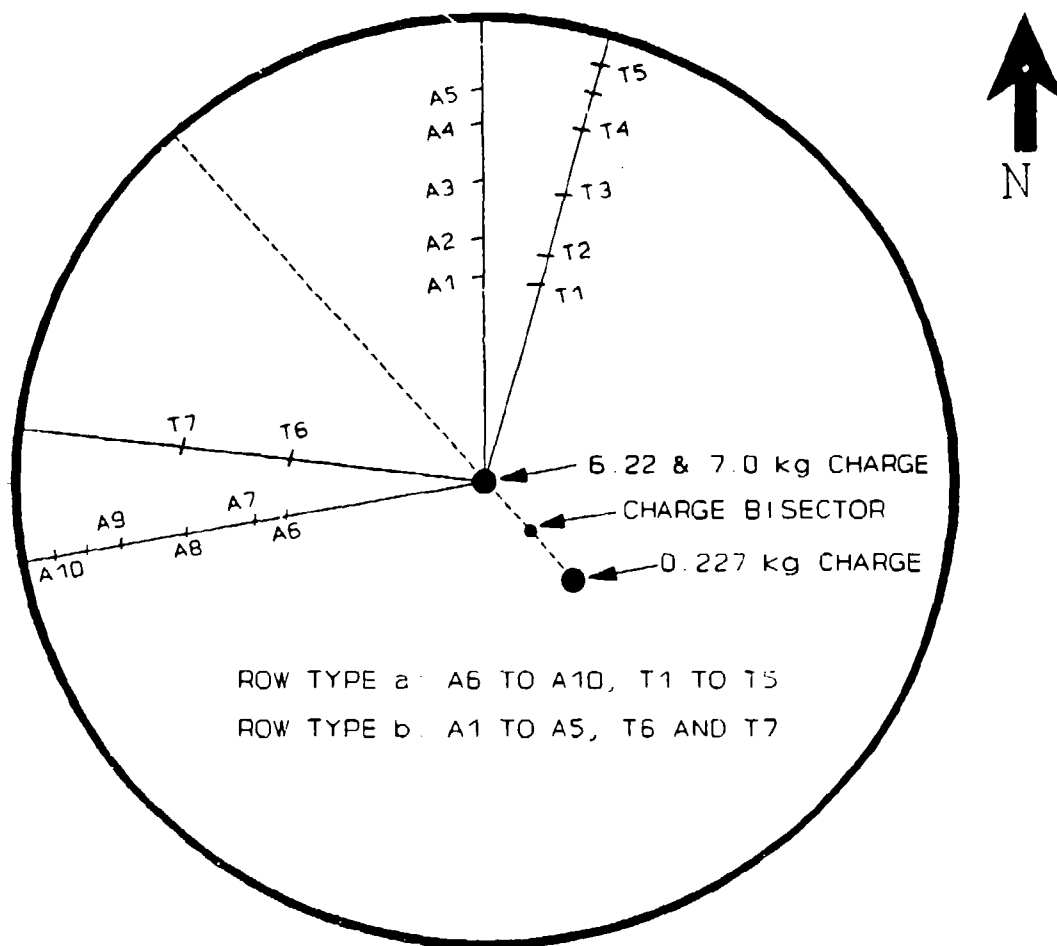
| | ROW TYPE a: A6 TO A10, T1 TO T5 |
| | ROW TYPE b: A1 TO A5, T6 AND T7 |

Instrument location:	Distance from center of 6.22 & 7.0 kg charge meters	feet	Distance from center of 0.227 kg charge meters	row	feet
A6,T1	0.91	3.0	1.34	a	4.40
A1,T6			1.43	b	4.69
A7,T2	1.07	3.5	1.48	a	4.87
A2			1.58	b	5.17
A8,T3	1.37	4.5	1.77	a	5.81
A3,T7			1.87	b	6.15
A9,T4	1.68	5.5	2.07	a	6.78
A4			2.17	b	7.12
----	1.83	6.0	2.21	a	7.26
A5			2.32	b	7.61
A10,T5	1.98	6.5	2.36	a	7.75
------			2.47	b	8.10

Figure 3.20 Plan View of Instrument Layer Showing Instrument and Explosive Locations for Spring 1992 Tests Conducted at 0, 13 and 20 Percent Saturations.
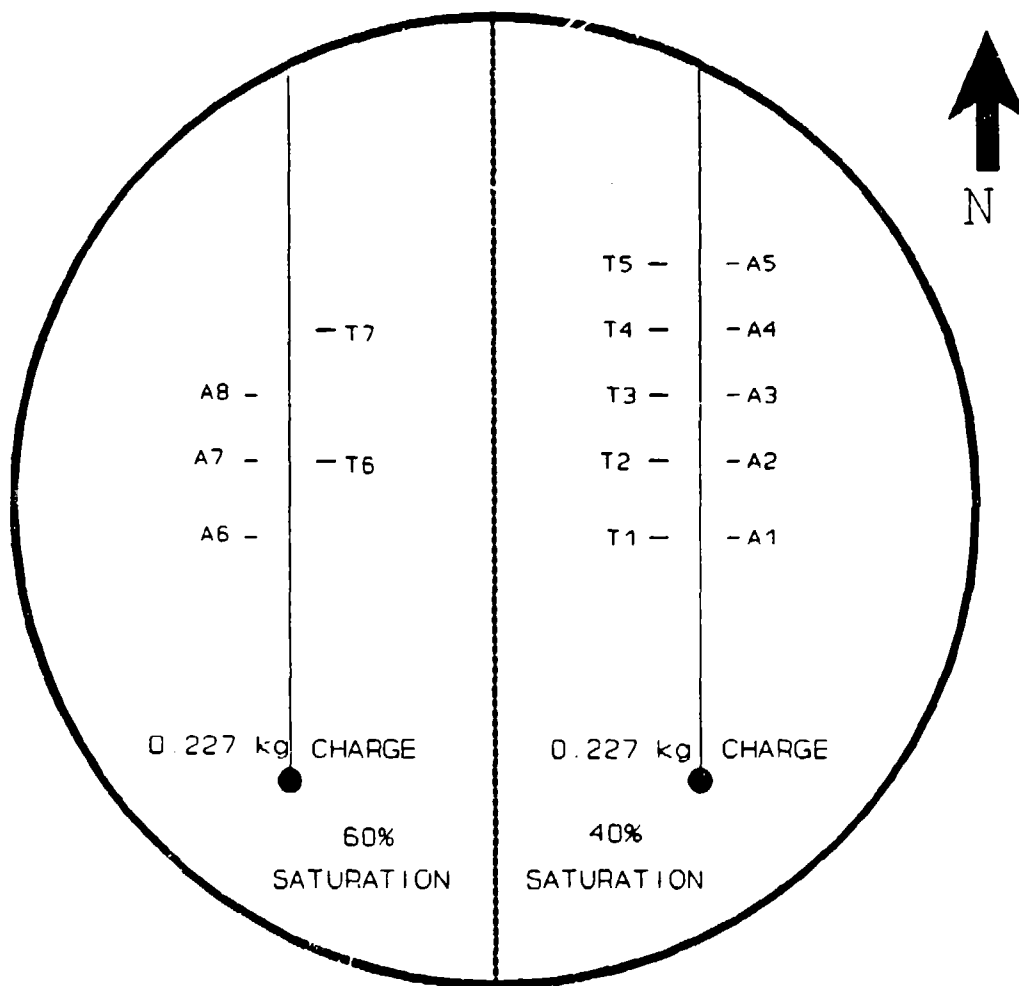
Instrument location:	Distance from center of 0.227 kg charge	
	Meters	Feet
A1,T1,A6	1.09	3.58
A2,T2,A7,T6	1.44	4.71
A3,T3,A8	1.74	5.70
A4,T4,T7	2.02	6.63
A5,T5	2.31	7.58

Figure 3.21 Plan View of Instrument Layer Showing Instrument and Explosive Locations for Spring 1992 Tests Conducted at 40 and 60 Percent Saturations.

Three types of explosives were used in the field tests: instantaneous blasting caps, Primacord[R], and Powermite[R] high explosive gel sticks. Explosive properties are given in Section IV. All three were used simultaneously to create the burst for the 7 kg and 0.227 kg TNT equivalent detonations. Nine .94 kg sticks of Powermite[R] were placed into the hole in bundles of three. 1.75 meters of 4.68 mm Primacord[R] was interlaced between the mass of Powermite[R] sticks and strung to the surface, where it was connected to a Dupont CWAS blasting cap. The blast was initiated by electrically detonating the blasting cap, which detonated the detonation cord, which in turn detonated the buried explosive mass. Figure 3.23 show the three explosive types used.

Safety precautions were taken for the explosive procedure according to the Explosives Procedure Manual of Colorado State University (Charlie et al., 1990b).

4. Data Acquisition and Computer Procedure

All data acquisition equipment was turned on at least one half hour before the blast to allow instruments and equipment to warm up and reach a state of system equilibrium. Individual accelerometer sensitivities were entered into the signal conditioner channel, and channels were balanced and "zeroed".

Data channels were also configured for both instrument types using Pacific Monitor software. Channel configuration included setting the number of pre and post trigger time segments, duration of data recording and trigger voltages. When the system had been configured, calibrated, and balanced, several mock firings were conducted to verify that the system was operational. Data were then downloaded from the TDRs after a successful test.

Figure 3.22 Boring the Explosive Hole with a 10 cm Auger.
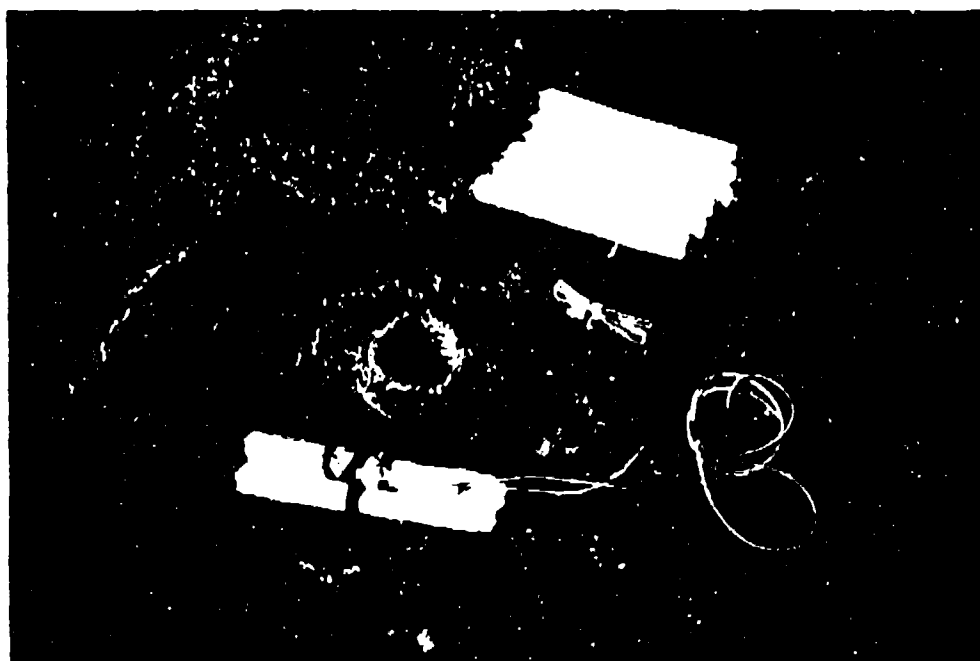
Figure 3.23 Powermite^R Explosive Gel Sticks.

IV. EXPERIMENTAL RESULTS

A. INTRODUCTION

This chapter presents the results from sand property tests, compaction procedures, explosive property investigation, and explosive test results.

B. POUDRE VALLEY SAND

The sand utilized in the test program was Poudre Valley sand, a crushed gravel obtained from the Poudre River Valley. The supplier was Western Mobile Northern of Fort Collins, Colorado. Poudre Valley sand is classified as a poorly graded sand (SP) under the Unified Soil Classification System as set forth in ASTM D2487 (ASTM, 1987). Its particles are angular to subangular in shape, being composed mainly of feldspar and quartz. Important physical properties of the sand are given in Table 4.1.

Physical property tests were conducted in accordance with ASTM D854 (Specific Gravity), ASTM D422 (Particle Size Analysis), ASTM D558 (Moisture-Density Relationship), ASTM D4253 & D4254 (Maximum and Minimum Index Density) and ASTM D2325 (Capillary-Moisture Relationships). The minimum and maximum dry density tests were performed by the Bureau of Reclamation Soil Mechanics Laboratory in Denver, Colorado. The target dry density of 1635 kg/m^3 represents a relative density of 44 percent.

Figures 4.1 to 4.6 display the results of physical property tests conducted on Poudre Valley sand. The grain size distribution for Poudre Valley sand is given in Figure 4.1. Comparison with grain size distribution curves in Figure 2.14 for 50/80 silica, Ottawa 20-30, Eglin, and Tyndall Beach sands reveals that Poudre Valley sand has the widest grain size distribution (C_u= 4.05) and the second to largest mean grain size (D_{50}= 0.65 mm). Grain sizes as large as 4.75 mm are seen in Figure 4.1 for Poudre Valley sand. The grain size distribution for Poudre Valley

sand is replotted in Figure D.2 for comparison with grain size
distribution curves for 50/80 silica, Ottawa 20-30, Eglin and Tyndall
Beach sands. Figure 4.2 shows dry density plotted as a function of water
content and saturation. The lowest dry density occurs at a water content
of approximately 7.5 percent (or S = 35 percent). This correlates to a
large compactive effort necessary to reach a constant dry density between
35 and 45 percent saturations in Figure 4.3. Veyera and Fitzpatrick
(1990) observed that the largest compactive effort required to reach a
constant dry density of 1715 kg/m^3 in Ottawa 20-30 sand occurred at 40
percent saturation (Figure 2.10). Conversely, the largest dry density in
Poudre Valley sand occurs at 0 percent water content and saturation, which
corresponds to the lowest compactive effort to reach a constant dry
density in Figure 4.3. Figure 4.4 shows the water retention curve for
Poudre Valley sand. The residual saturation occurs at approximately 3
percent. Figure 4.5 shows stress-strain relationships for dry Poudre
Valley sand at 100 percent and 63 percent relative densities, obtained
from static one-dimensional, confined compression tests conducted by Bretz
(1989). In Figure 4.6, relative density and void ratio are plotted
against corresponding values of dry density.

TABLE 4.1.   POUDRE VALLEY SAND PROPERTIES.

Sand Property or Categorization	Poudre Valley Sand
Specific Gravity, G_s	2.65
Maximum Dry Density, ρ_{max}, kg/m^3	1860
Minimum Dry Density, ρ_{min}, kg/m^3	1490
$e_{maximum}$	0.740
$e_{minimum}$	0.424
Test Dry Density, ρ_{test}, kg/m^3	1635
Test Relative Density, DR, %	44
D_{50}, mm	0.65
Percent Passing # 200 seive	0.75%
C_u	4.05
C_c	0.99
Classification (ASTM D2487)	SP
Grain Shape	angular to subangular
Residual Saturation, %	3
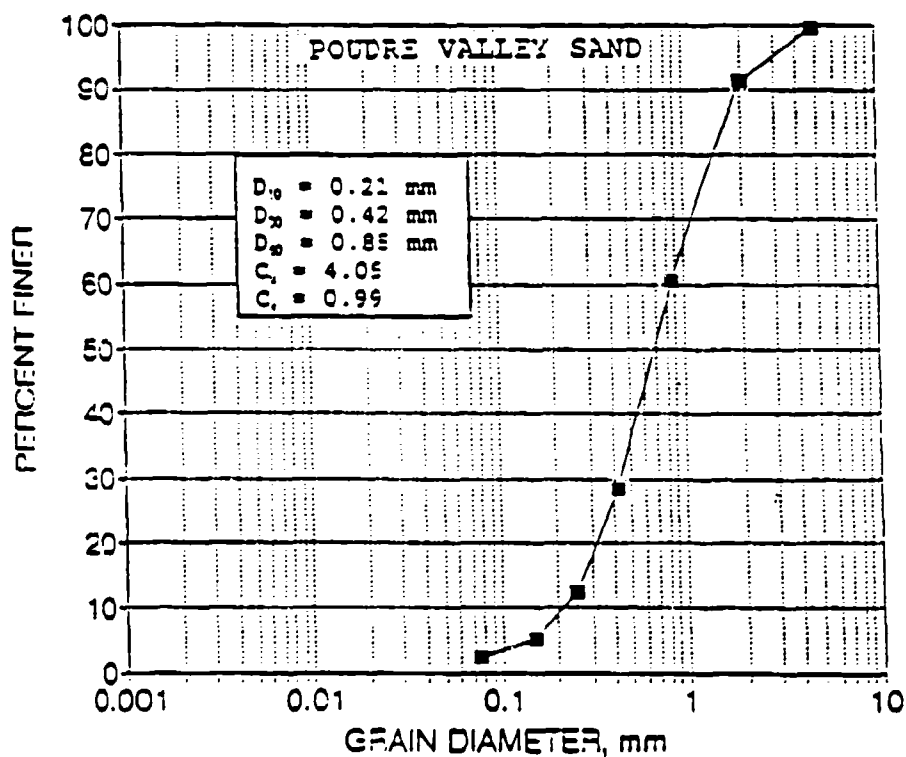
Figure 4.1 Grain Size Distribution for Poudre Valley Sand.
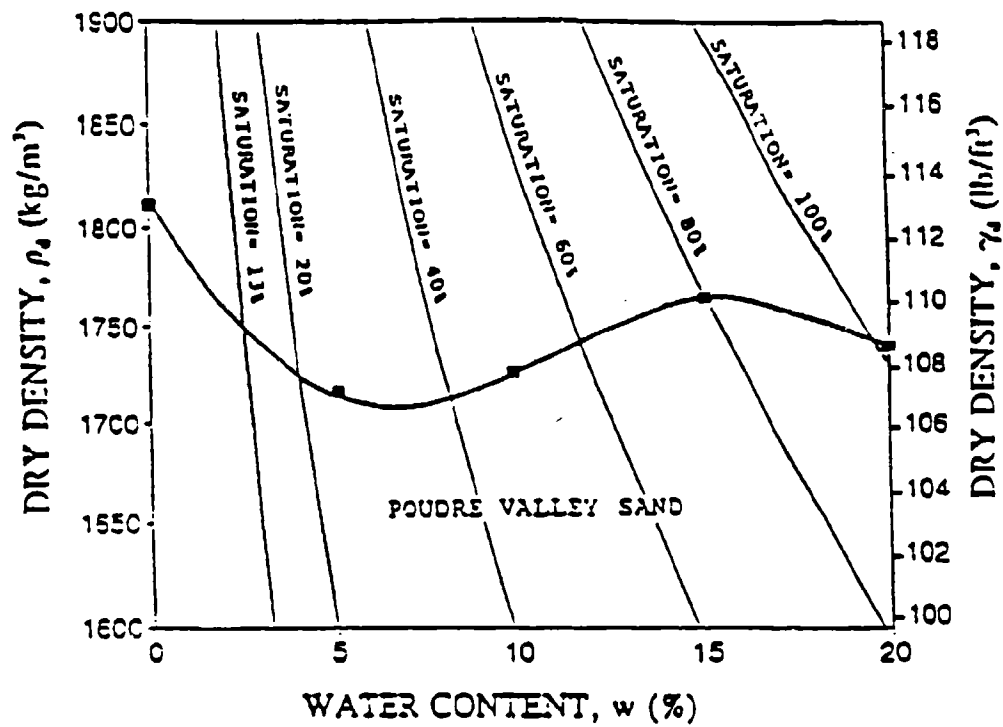
Figure 4.2 Dry Density Versus Water Content for Poudre Valley Sand (Standard Proctor Test; ASTM D698 Method A, ASTM, 1987).
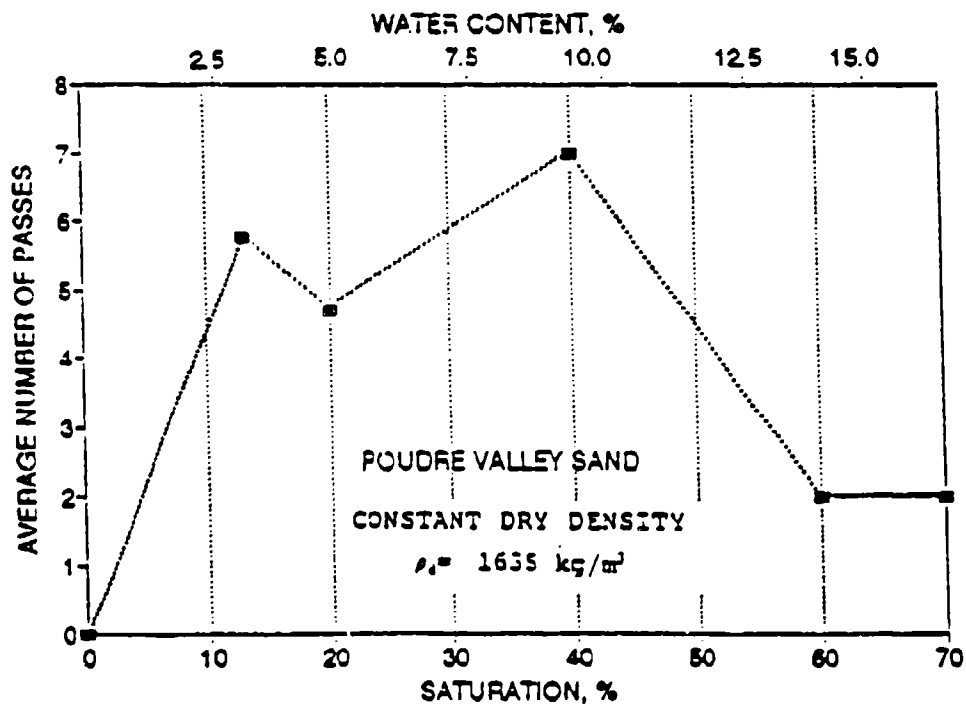
Figure 4.3 Compactive Effort (Number of Passes with Vibratory Compactor) versus Percent Saturation to Reach a Constant Dry Density of 1635 kg/m³ for Poudre Valley Sand.
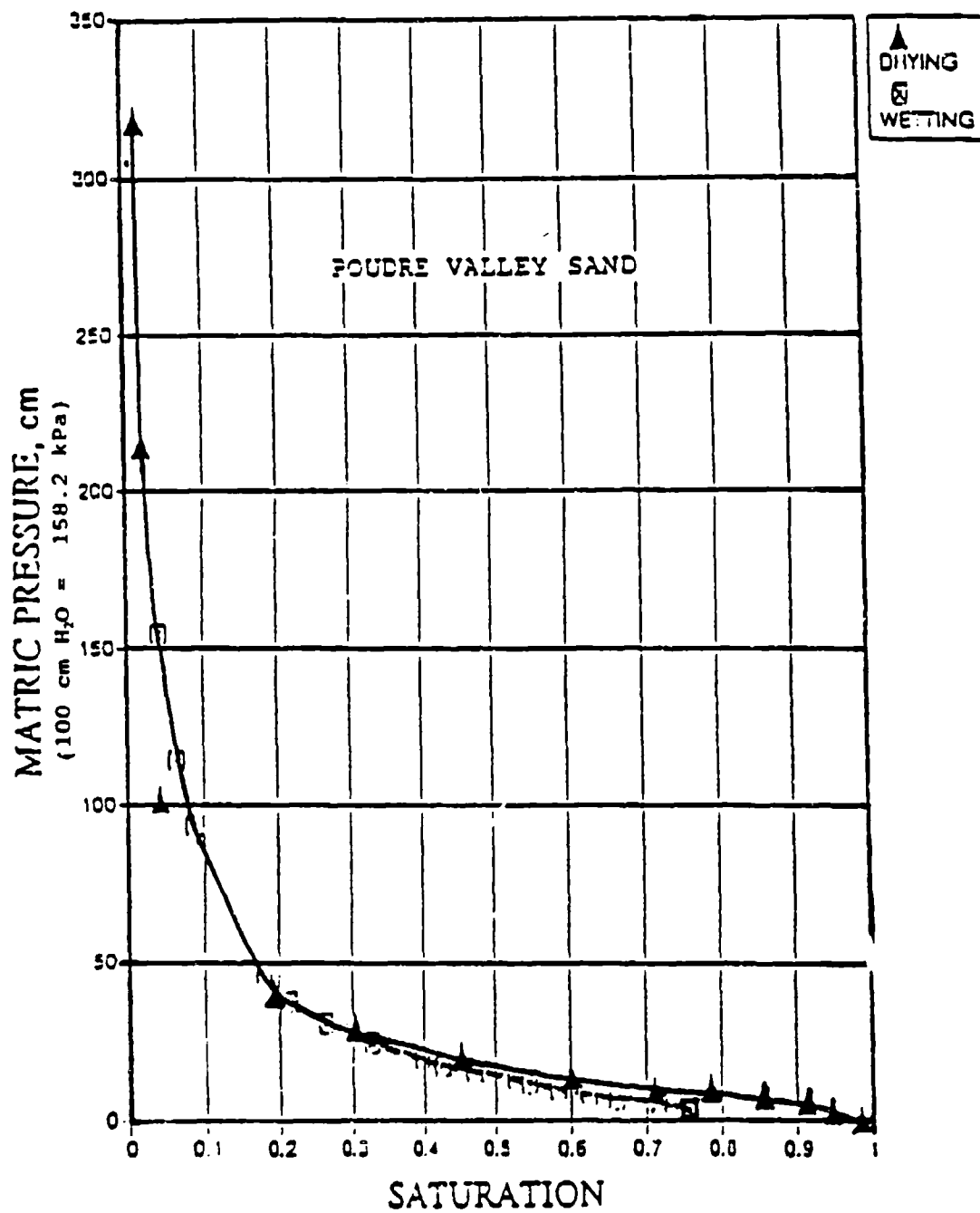
Figure 4.4 Water Retention Curve for Poudre Valley Sand.
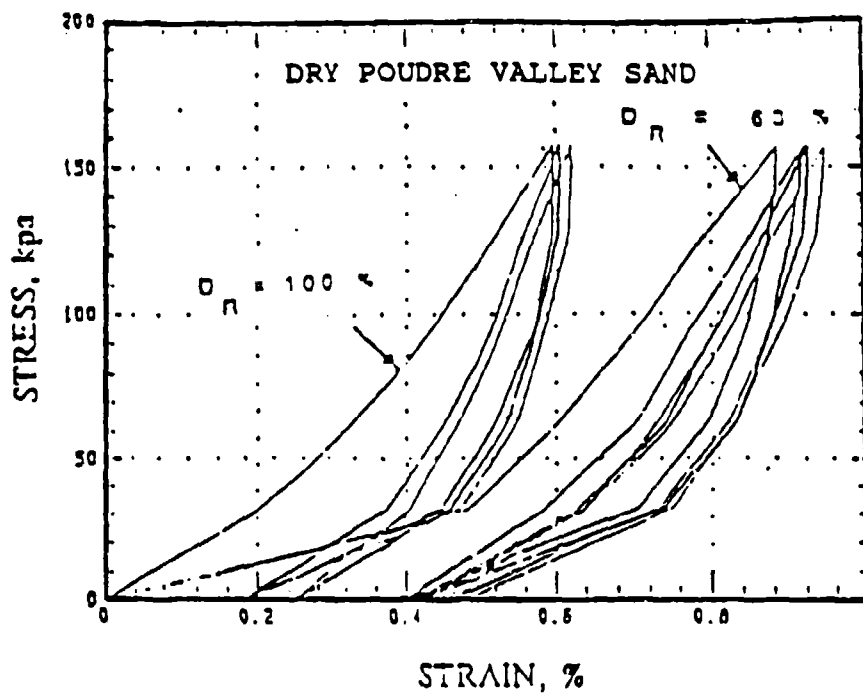
Figure 4.5 Stress-Strain Relationship for Poudre Valley Sand (Bretz, 1989).
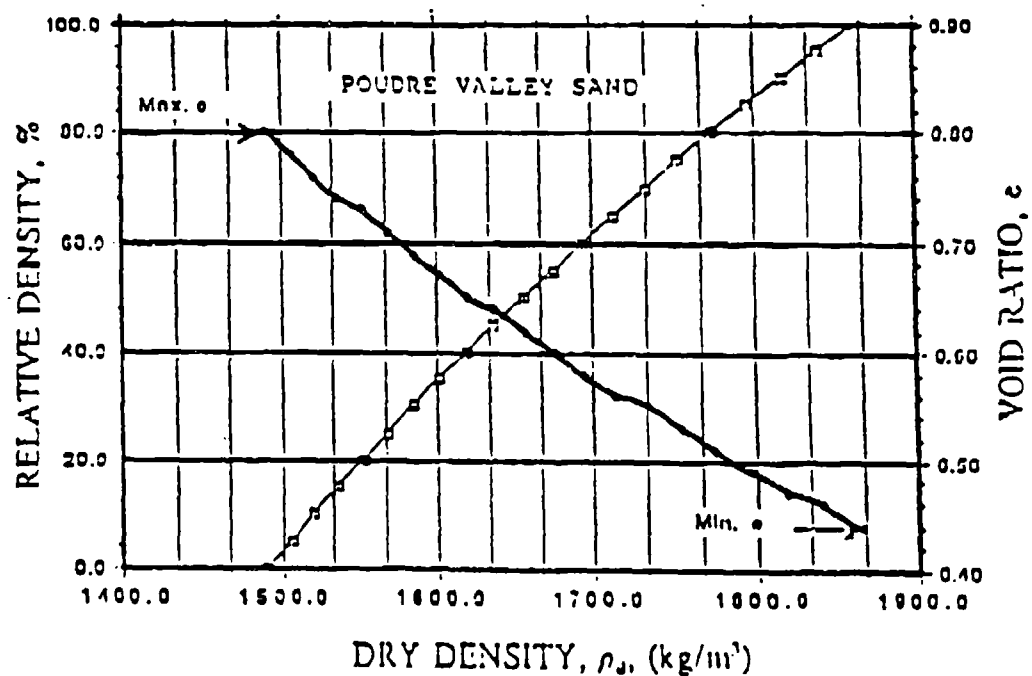
Figure 4.6 Relative Density and Void Ratio versus Dry Density for Poudre Valley Sand (Bureau of Reclamation Soil Mechanics Laboratory-- Denver, Colorado).

C. EXPLOSIVE PROPERTIES

Physical properties for the three explosive types used in the field tests are provided in this subsection. The instantaneous CWAS electric blasting caps, manufactured by Dupont, are Number 8 strength cylindrical aluminum shells encasing Pentaerythritol Tetranitrate (PETN) explosive powder. Two 3-meter long plastic insulated copper wires are joined inside the cap by a high-resistant bridge wire embedded in the cap ignition mixture. When high voltage is supplied across the two leads, the ignition mixture detonates and triggers the explosive powder.

Primacord[R], a detonating cord manufactured by the Ensign-Bickford Company, is rated at 10.66 grams of PETN per meter. The explosive is encased by polypropylene yarn, plastic tape, and textile yarn counterings. Primacord[R] is relatively insensitive to premature or accidental ignition due to heat, impact, friction, static stray current and lightning (Ensign-Bickford Co., 1984), which makes it ideal for use in the field.

Powermite[R], a high explosive water gel, is manufactured by IRECO Company of Salt Lake City, Utah. The explosive gel is packaged in cylindrical sticks 40 cm long and 5 cm in diameter enclosed by a thin plastic film which can easily be cut for obtaining smaller charge weights. Powermite[R] yields approximately 80 percent of the energy released by TNT. It is also relatively insensitive to premature or accidental ignition due to the factors mentioned above.

Specific properties for each of the explosives described above and of TNT and C4 for comparison are provided in Table 4.2.

TABLE 4.2. PHYSICAL PROPERTIES OF EXPLOSIVES.*

Explosive type	Density (kg/m³)	Propagation velocity (m/s)	Heat of detonation (MJ/kg)	TNT equivalent weight based on heat of Det.
PETN[1] • Blasting cap • Primacord[R]	1600	8300	6.29	1.47
Powermite[R,2]	1180	5200	3.35	0.78
TNT[3]	1550	6900	4.27	1.00
C4[3]	1720	8040	5.87	1.37

* Values obtained from [1]Bretz (1989), [2]IRECO Company, and [3]Military Explosives (1984). CWAS Blasting caps manufactured by Dupont Co. Primacord[R] manufactured by Ensign-Bickford Co. of Simsbury, Connecticut Powermite[R] manufactured by IRECO Co. of Salt Lake City, Utah.

D.   FIELD TEST RESULTS

This section presents the results from field data reduction, and describes how these results were obtained.   Output voltages from accelerometers and soil stress gages were sampled at a rate of 500,000 samples per second and stored in TDR data arrays.   These voltage-time history arrays were then converted to particle acceleration and stress time histories using a conversion formula which takes into account individual instrument sensitivities, voltage amplification and desired units.   Particle acceleration-time histories were integrated to obtain particle velocity-time histories.   Figures 4.7 to 4.9 show representative particle acceleration, particle velocity and stress time histories. Figure 4.10 shows a typical stress time history from the Fall of 1991 tests, where cross talk was experienced due to stress gages being hooked to a common power source.   This plot shows the signal from one stress gage superimposed over the signal from another gage.

Useful information extracted from the time histories were peak values, pulse arrival time and rise time.   Interval propagation velocities were calculated by dividing the interval distance between two consecutive instruments by the travel time between them.   Average propagation velocities were calculated by dividing the distance between the center of explosive and instrument by the time of travel to the instrument.   Scaled range and scaled acceleration were obtained by dividing the distance and multiplying the acceleration by a factor of $W^{1/3}$, respectively.

Tabulations of test results for compactive saturations of 0 to 70 percent are given in Tables B.1 to B.6 in Appendix B.   Table 4.3 provides a listing of parameters for tests conducted in Fall of 1991 and Spring of 1992.

TABLE 4.3. FIELD TEST PARAMETERS.

Test #	Date	Saturation (%)	Mean dry density γ_d (kg/m³)	Mean relative density, DR (%)	Explosive mass (Powermite®) (kg)	TNT Equivalent (kg)	Number of accelerometer channels*	Number of stress gage channels*
1	9/19/91	13	1613	38	8.5	7.0	2	2
2	9/28/91	20	1621	41	8.5	7.0	4	3
3	10/4/91	40	1627	42	8.5	7.0	4	4
4	10/17/91	60	1631	43	8.5	7.0	4	4
5	11/14/91	70	1653	50	8.5	7.0	4	4
6	4/9/92	0	1639	46	7.56 / 0.276	6.22 / 0.227	9	6
7	4/22/92	13	1637	45	8.5 / 0.276	7.0 / 0.227	8	6
8	4/25/92	20	1648	48	8.5 / 0.276	7.0 / 0.227	8	2
9	5/7/92	40	1656	50	0.276	0.227	5	0
10	5/7/92	60	1643	47	0.276	0.227	4	0

* Data yielding channels
Mean dry density for all tests = 1637 kg/m³ (Standard Deviation = 13.2 kg/m³)
Mean relative density for all tests = 45 percent (Standard Deviation = 3.8 percent)
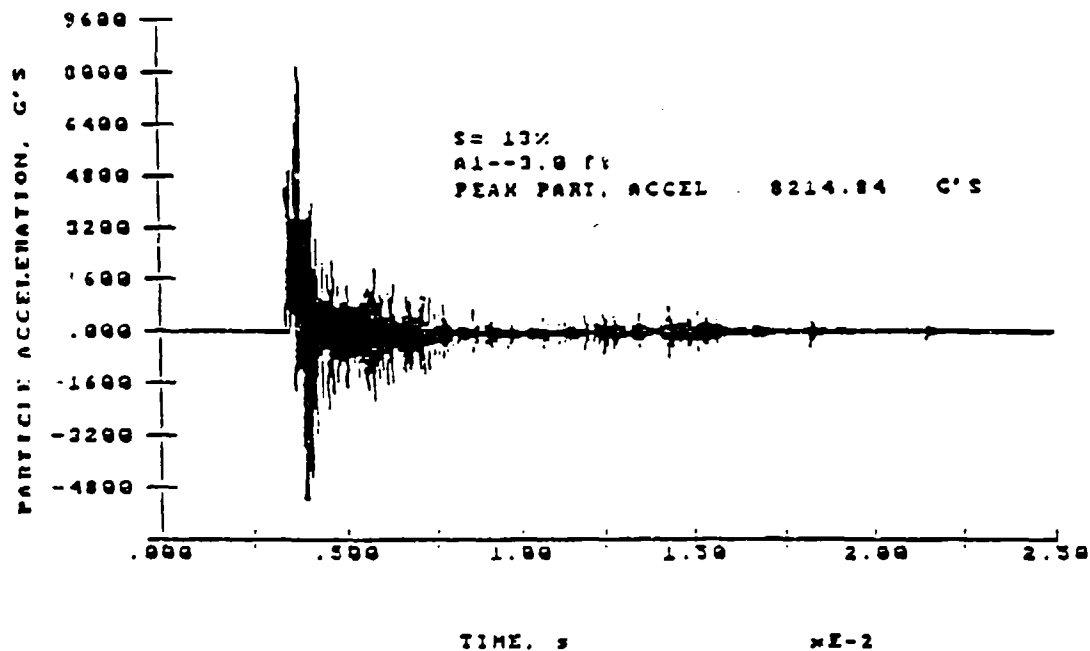
Figure 4.7   Representative Particle-Acceleration Time History.
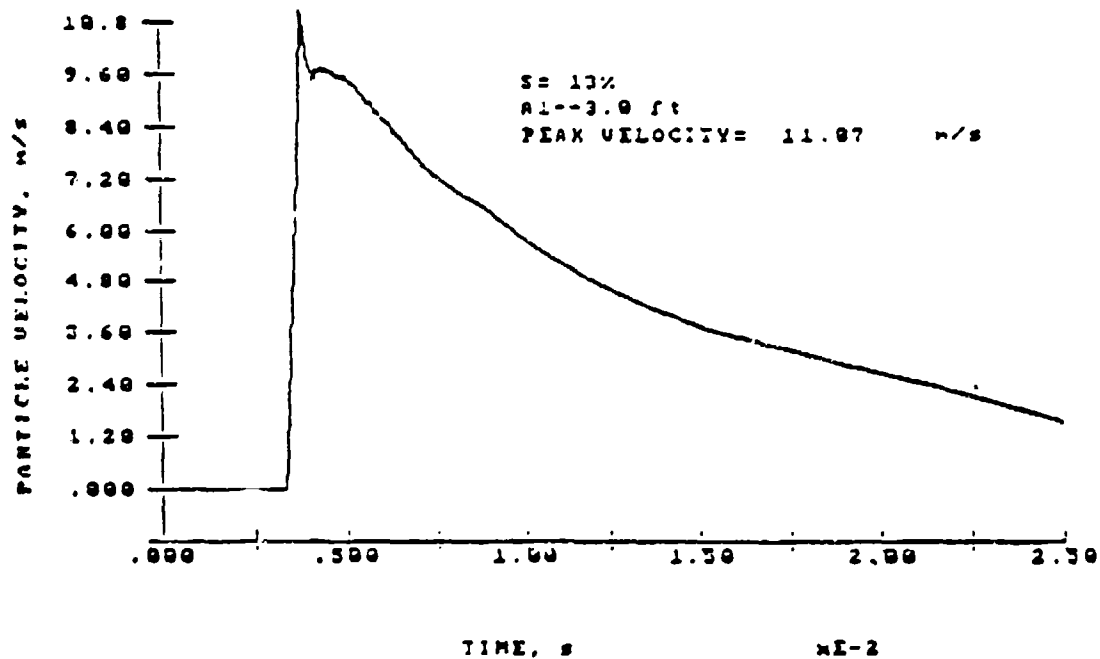
Figure 4.8   Representative Particle Velocity-Time History.

68

S= 13%
T1--3.0 ft
PEAK STRESS=   402.17   psi
(2773 kpa)

STRESS, psi

TIME, s   xE-2
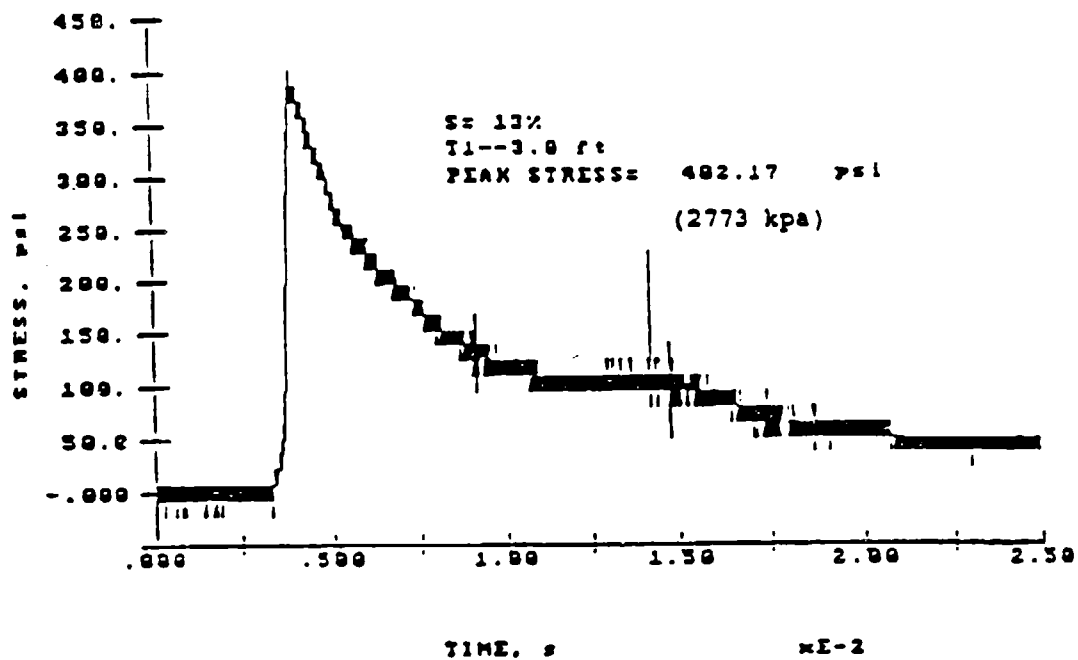
Figure 4.9   Representative Soil Stress-Time History.

TEST 20-1
TSG3; DIST= 3.0 FT
PEAK STRESS=   427.0   PSI
(2950 kpa)

STRESS (PSI)

TIME (SECONDS)   xE-3
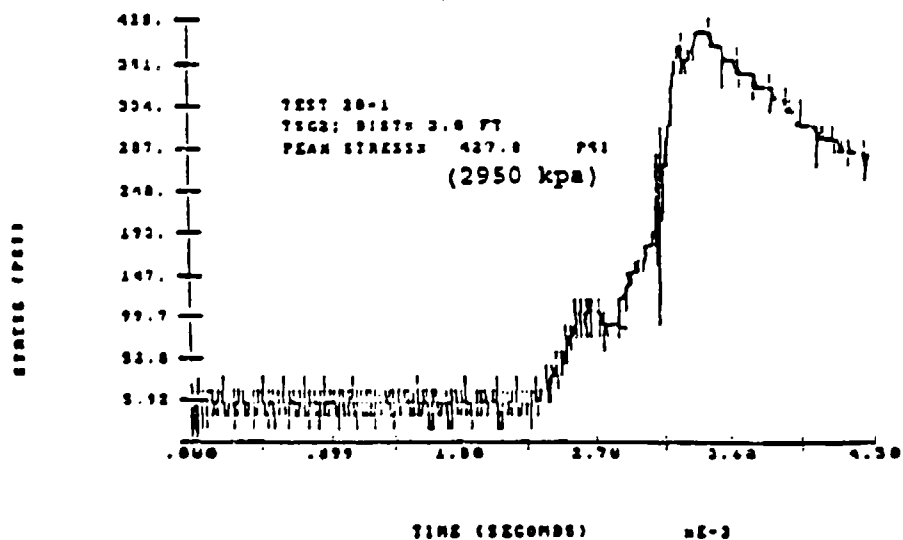
Figure 4.10   Representative Stress-Time History Showing Cross Talk.

69

Scaled peak particle acceleration, peak particl velocity and peak soil stress versus scaled range curves for each satuya ion are plotted in Figures 4.11, 4.12 and 4.13 respectively. In these figures, two clusters of data can be seen. They represent data from the large (6.22 kg and 7.0 kg) tests and small (0.227 kg) tests. A regression analysis was run on the data, and a best-fit line was constructed through the points on a log-log scale. The slope of this best-fit line is displayed on the graph. Plots of average and interval propagation velocity versus scaled range with best-fit lines are displayed in Figures 4.14 and 4.15. Plots of peak stress versus peak particle velocity with slopes indicating acoustic impedance values are shown in Figure 4.16. A summary of regression data is provided in the next section.

Other supplemental plots of test data are provided in Appendix C. These plots are listed in Table 4.4.

TABLE 4.4.   SUPPLEMENTAL PLOTS O; TEST DATA iN APPENDIX C.

Plot	Figure No.
Interval propagation velocity versus distance, 6.22 kg and 7.0 kj shots.	C.1
Interval propagation velocity versus distance, 0.227 kg shot.	C.2
Interval propagation velocity versus peak particle velocity, 6.22 and 7.0 kg shots.	C.3
Interval propagation velocity versus peak particle velocity, 0.227 kg shot.	C.4
Interval propagation velocity versus peak stress, 6.22 and 7.0 kg shots.	C.5
Pulse time of arrival versus distance, 6.22 and 7.0 kg shots.	C.6
Pulse time of arrival versus distance, 0.227 kg shot.	C.7
Pulse rise time versus time of arrival, 6.22 and 7.0 kg shots.	C.8
Pulse rise time versus time of arrival, 0.227 kg shot.	C.9
Scaled peak particle acceleration vs. scaled range; comparison of Poudre Valley, Tyndall, Ottawa and sands of varying density.	C.10
Peak particle velocity versus scaled range; comparison of Poudre Valley, Tyndall, Ottawa and sands of varying density.	C.11
Peak stress versus scaled range; comparison of Poudre Valley, Tyndall, Ottawa and sands of varying density.	C.12
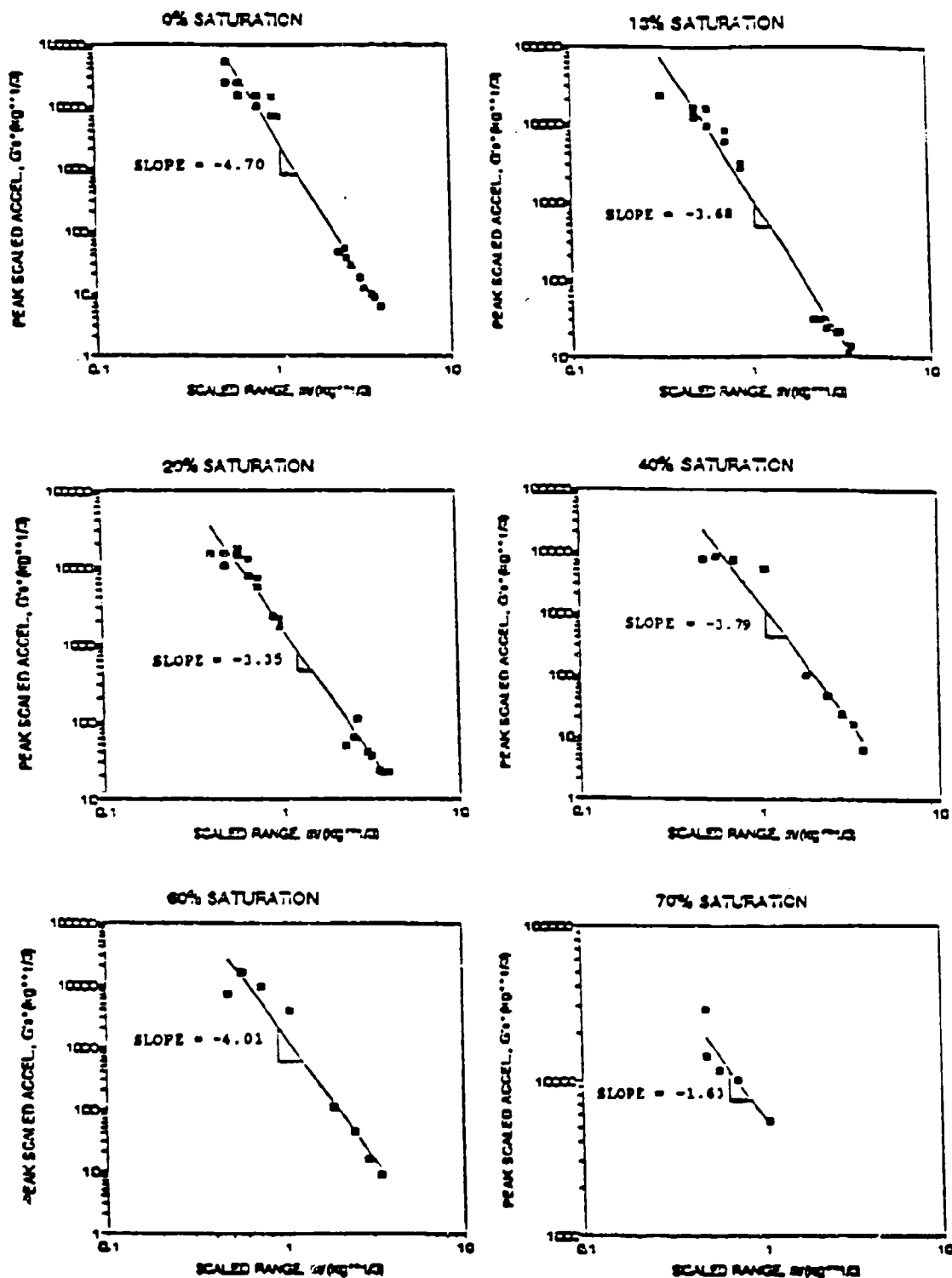
Figure 4.11 Scaled Peak Particle Acceleration versus Scaled Range for Tests Conducted at 0, 13, 20, 40, 60 and 70 Percent Compactive Saturations.

71
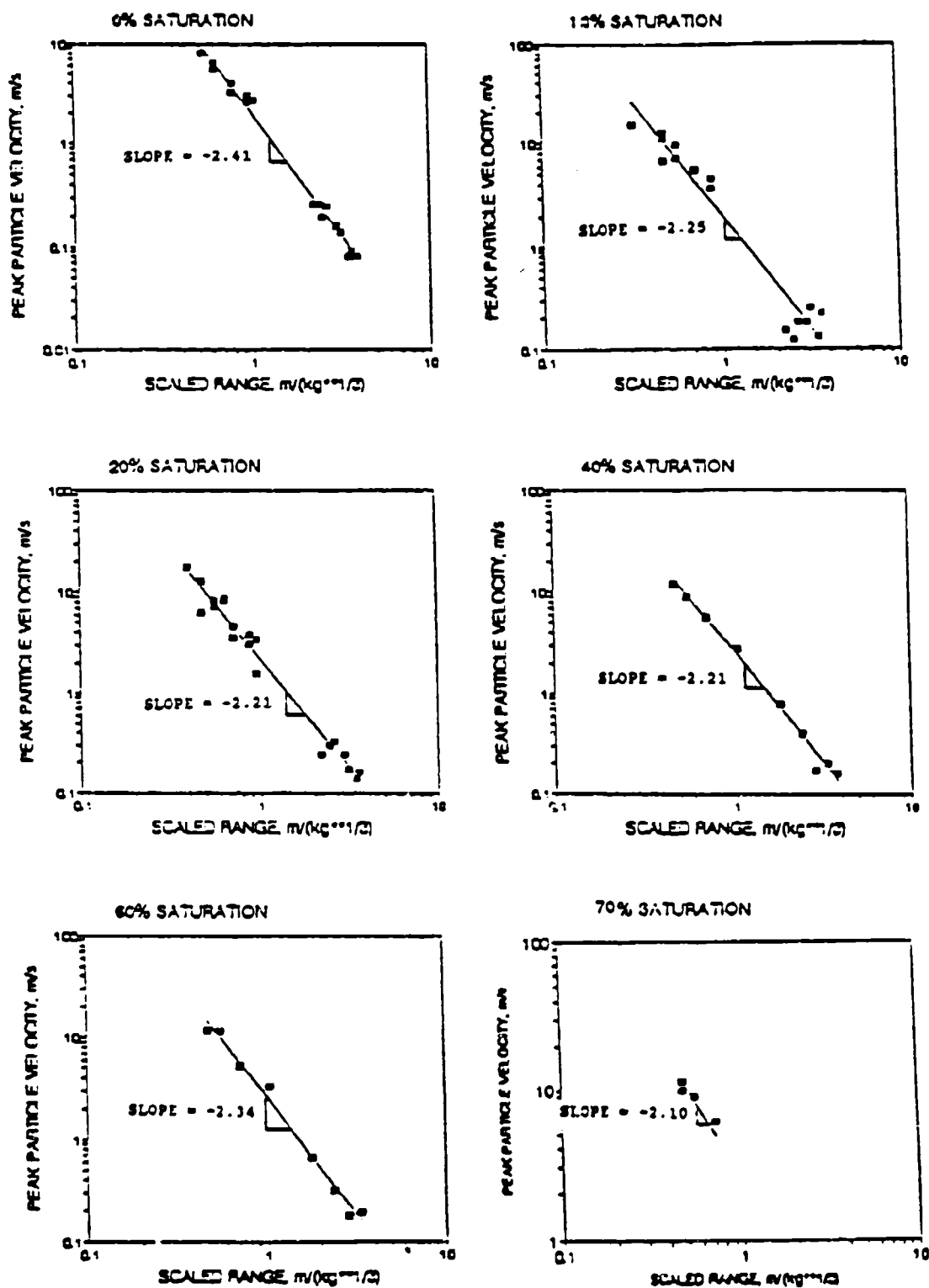
Figure 4.12 Peak Particle Velocity versus Scaled Range for Tests Conducted at 0, 13, 20, 40, 60 and 70 Percent Compactive Saturations.
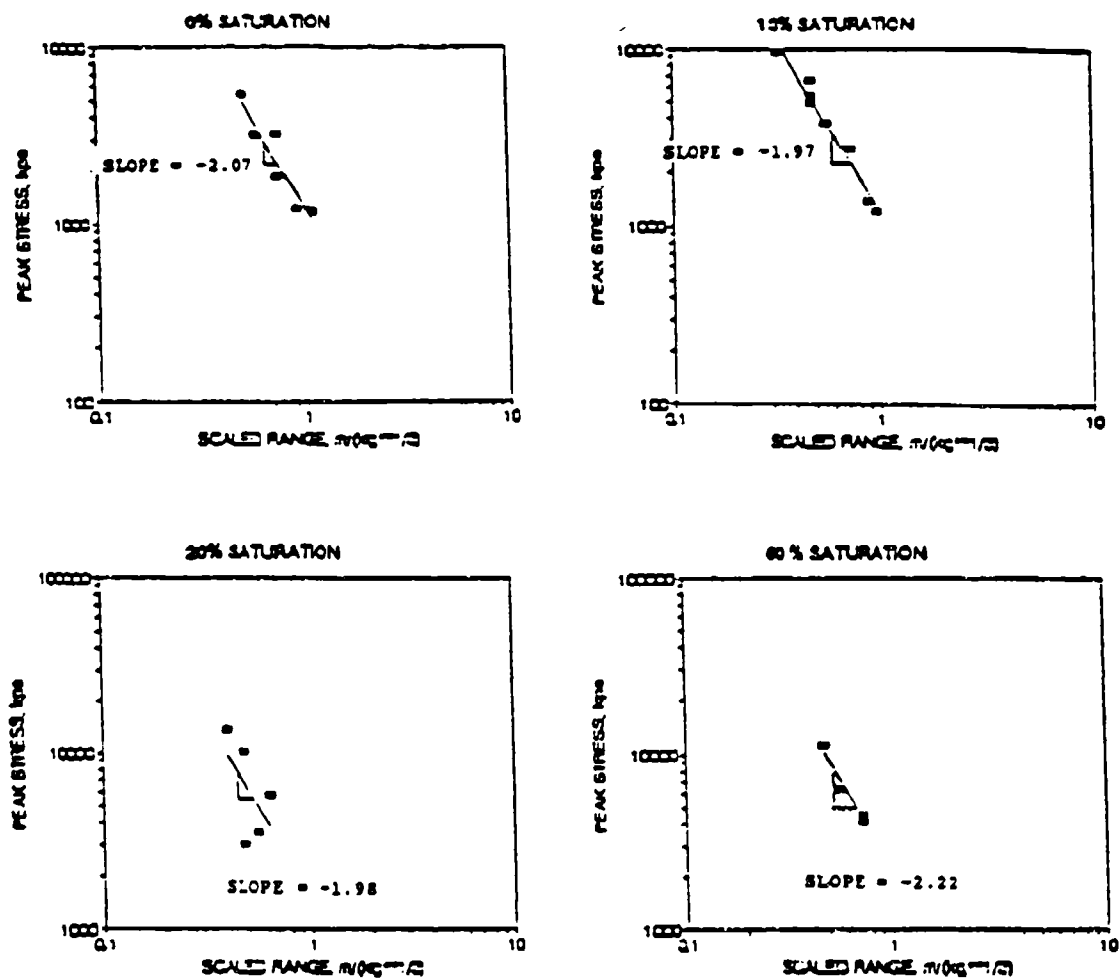
Figure 4.13 Peak Stress versus Scaled Range for Tests Conducted at 0, 13, 20, and 60 Percent Compactive Saturations.
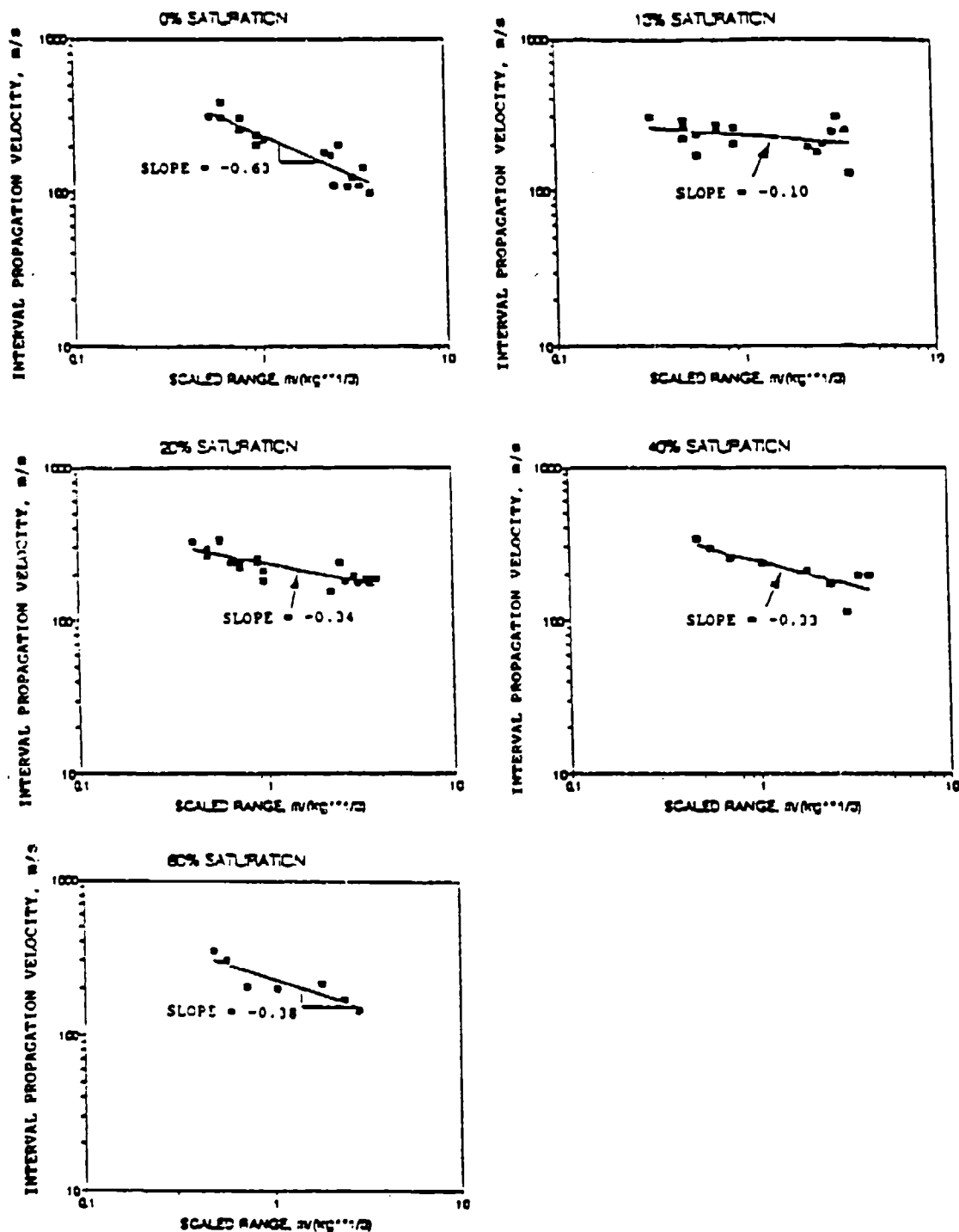
Figure 4.14 Interval Propagation Velocity versus Scaled Range for Tests Conducted at 0, 13, 20, 40 and 60 Percent Compactive Saturations.
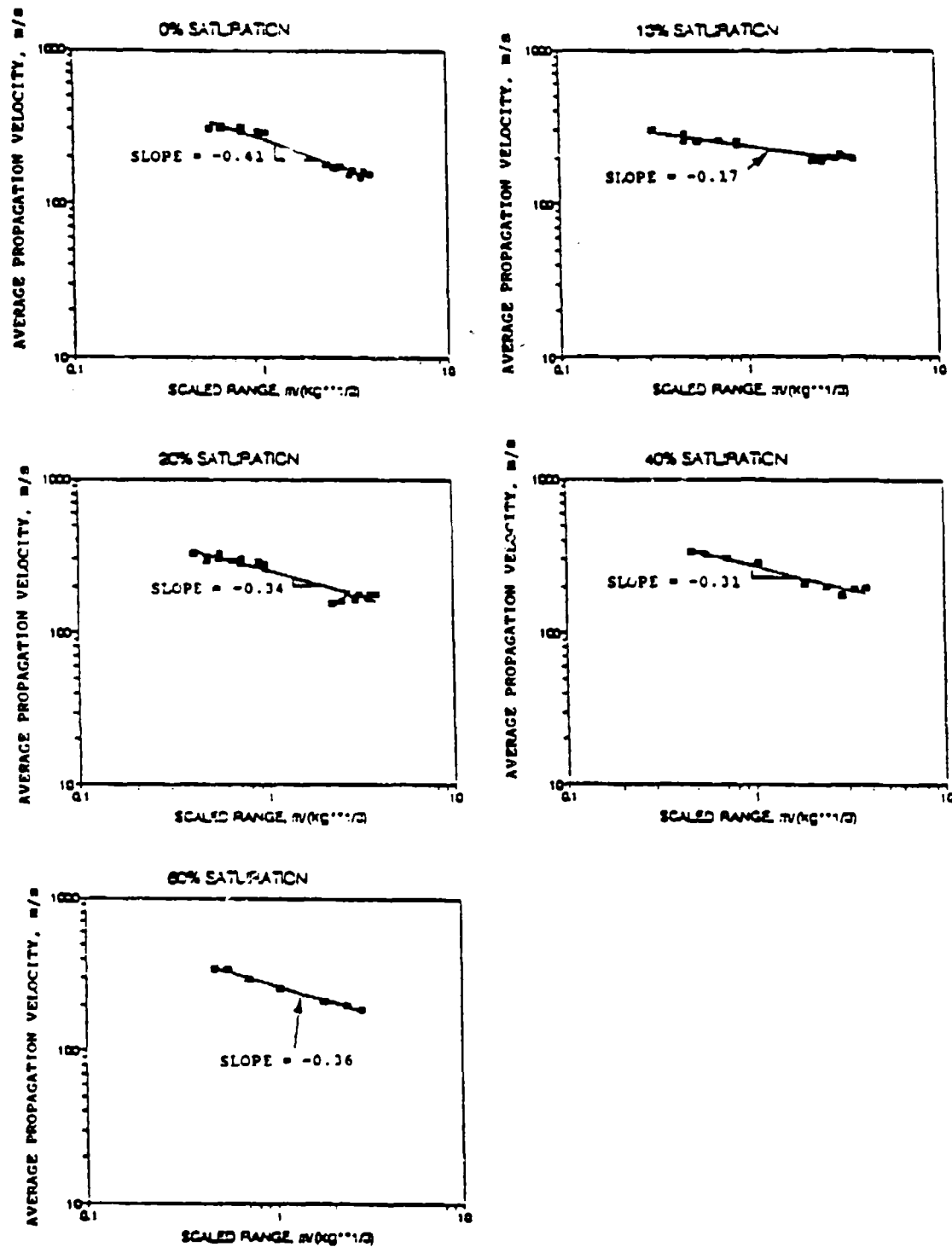
Figure 4.15 Average Propagation Velocity versus Scaled Range for Tests Conducted at 0, 13, 20, 40 and 60 Percent Compactive Saturations.
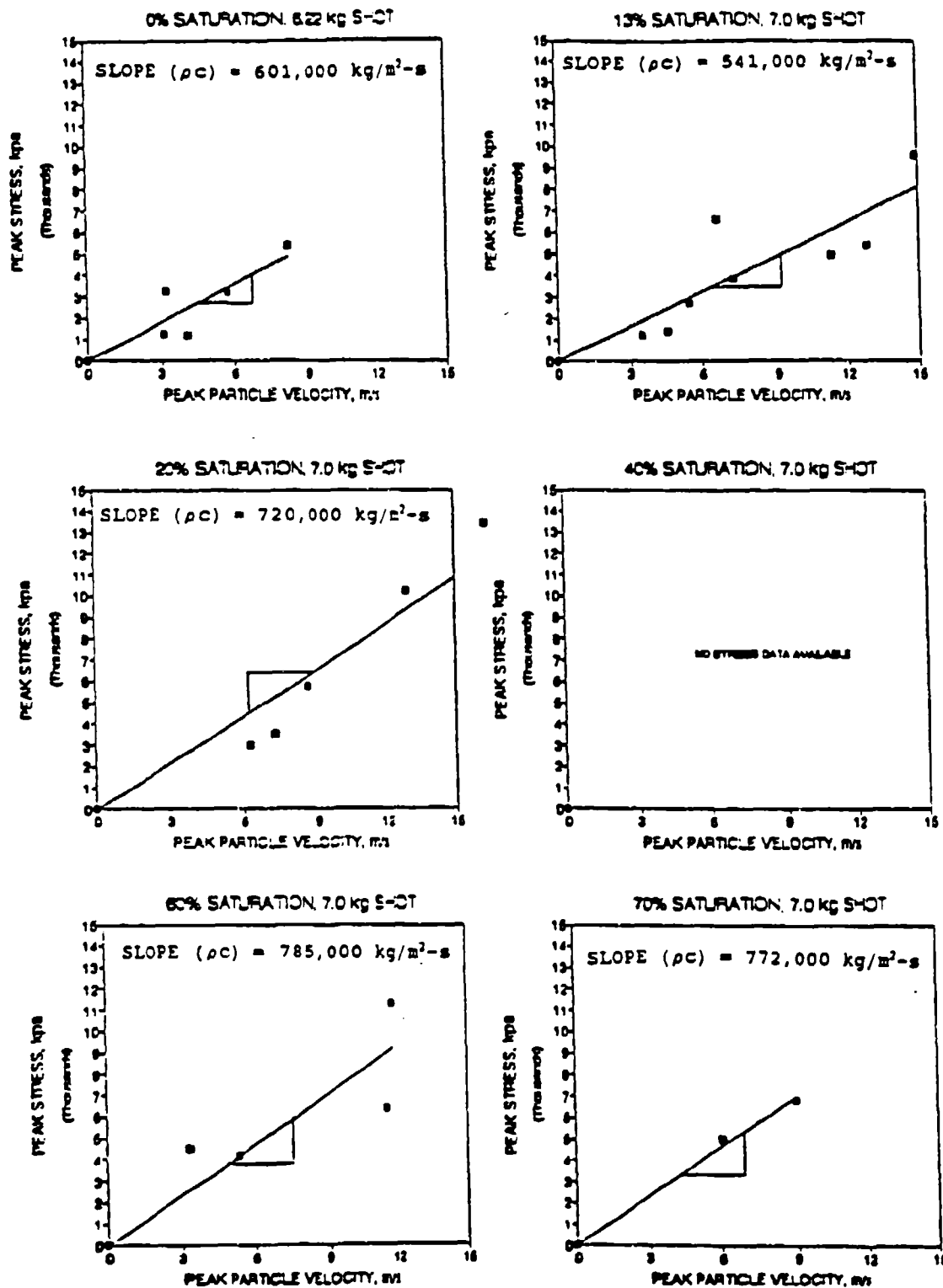
Figure 4.16 Peak Stress versus Peak Particle Velocity for Tests Conducted at 0, 13, 20, 40, 60 and 70 Percent Saturations in Poudre Valley Sand Using a 7.0 kg Charge Mass.

V. ANALYSIS OF RESULTS

A. INTRODUCTION

Analysis and discussion of test results is provided in this section. Peak ground motion parameter prediction equations are developed from the results of a regression analysis run on soil response data, plotted in Figures 4.11 to 4.13. The constants and slopes of these equations are analyzed and compared with those of Drake and Little (1983) and Walsh (1993). Propagation velocity, attenuation and stress transmission trends over a range of compactive saturations are also analyzed and compared with those of Drake and Little (1983), Charlie et al. (1990a) and Walsh (1993). Acoustic impedance values obtained from testing are analyzed and compared with those reported by Walsh (1993). Lastly, effective stress increases are analyzed as a function of saturation and capillarity.

B. PREDICTION EQUATIONS FOR PEAK PARTICLE ACCELERATION, PEAK PARTICLE VELOCITY AND PEAK SOIL STRESS

Empirical equations developed by Drake and Little (1983) for the prediction of blast-induced scaled peak particle acceleration, peak particle velocity, and peak stress in soil were presented in Section 2 (Equations (2.1) to (2.3)). Table 2.1 lists suggested design coefficients for use in these equations depending on the soil type, density and seismic velocity. These coefficients were derived from the peak parameter ($a_o \cdot W^{1/3}$, V_o and P_o) versus scaled range plots shown in Figures 2.2 to 2.4.

Similarly, predictive equations for Poudre Valley sand are developed from the peak parameter versus scaled range plots shown in Figures 4.11 to 4.13. The general form of these equations is,

$$Y = Constant\left(\frac{R}{W^{1/3}}\right)^{slope} \qquad (5.1)$$

where the constant is the Y-intercept taken at a scaled range of 1 $m/kg^{1/3}$ ($R/W^{1/3}=1$), and the slope is taken from the best-fit regression line through the data points. Tables 5.1 to 5.3 present these equations along with the regression data from which they were derived. Also included for comparison are ranges of slopes and constants from prediction equations developed by Walsh (1993) and suggested by Drake & Little (1983). Empirical constant and slope values as well as constant and slope attenuation trends will be compared.

1. Predictive Equations for Scaled Peak Particle Acceleration

Equations are presented in Table 5.1 for each test saturation, 0 to 60 percent, along with corresponding regression values. The coefficients of determination, R^2, are all 0.95 or greater for scaled peak particle acceleration.

The range of constants and slopes for Poudre Valley sand compare closely with those given by Equation (2.1) and Tables 2.1 and 2.2 (Drake and Little, 1983) for dense moist sands with the exception of the results of the 0 percent test. The constant from Equation (2.1) was determined by plugging a range of attenuation coefficients (n= 2.5 and 2.75) and seismic velocities (c= 396 m/s and 274 m/s) suggested for dense moist sands into the term $f \cdot 126 \cdot c \cdot (2.52)^{-n}$.

78

There are several possibilities why the constant term in Table 5.1 of 3040 g·kg$^{1/3}$ for the test conducted dry is high. The most likely explanation is related to the confinement of the explosive in PVC pipe rated at 1100 kPa. The stress wave associated with a confined explosion typically causes shorter duration pulses with smaller rise times and higher peak magnitudes. Acceleration-Time histories for the 0 percent test displayed these features, which suggests that confinement had some effect on wave propagation.

Another possible explanation for the high constant value may be related to over-densification of the sand during placement. Repeated loads of sand were dropped from a height of up to two meters onto layers of uncompacted dry sand. The sand's dry density may have reached levels greater than the target density of 1635 kg/m^3 since there was no repulsive capillary forces to keep sand particles from becoming more compact under repeated loading. A higher density would cause higher propagation velocities and higher particle accelerations.

Other variables unique to the dry test were a smaller charge weight (6.22 kg), a more cylindrically elongated charge shape, and a high degree of grain crushing close to the explosive.

Comparison of the Poudre Valley sand regression data with the results obtained from centrifuge testing of Tyndall Beach and Ottawa 20-30 sands reveals that the Poudre Valley sand constant values are the lowest of the three sands. Poudre Valley sand slopes are similar to Tyndall Beach sand slopes and lower than Ottawa 20-30 sand slopes. Thus, scaled peak particle acceleration magnitudes are lower for Poudre Valley sand than for Tyndall Beach and Ottawa 20-30 sands, but attenuation rates are similar or lower (Figure C.10).

2. Prediction Equations for Peak Particle Velocity

In Table 5.2, R^2 values for regression data are all 0.95 or greater, placing a high degree of confidence in the prediction equations for peak particle velocity in Poudre Valley sand. Peak particle velocity has historically been the most reliable of the ground motion parameters in ground shock testing and is used most often for prediction and design purposes. Therefore, it is likely that peak particle velocity data is also the most indicative of the true dynamic behavior of the sands under comparison. The bulk of the conclusions then, will be drawn from comparison of the magnitudes and trends of peak particle velocity.

Constants for Poudre Valley sand range from 2.0 m/s to 2.6 m/s, significantly lower than the ranges for Tyndall Beach and Ottawa 20-30 sands reported by Walsh (1993) and for medium-dense moist sand reported by Drake and Little (1983). Slope values compare closely with Tyndall Beach sand slopes and are slightly lower than the ranges of slopes for Ottawa 20-30 sand and medium-dense moist sand.

The constant and slope values at the lower end of the ranges for Ottawa 20-30 sand are highly questionable since they are far lower than the average values for that sand, and have been omitted by Walsh in his analysis. Similar to the case for peak particle acceleration, magnitudes of peak particle velocity are lower for Poudre Valley sand, and attenuation rates are very close to those of Tyndall Beach and Dense Moist sand. If the questionable data points for Ottawa 20-30 sand are omitted, then both peak particle velocity magnitude and attenuation rates for Poudre Valley sand are lower than those for Ottawa 20-30 sand.

3. Predictive Equations for Peak Stress

In Table 5.3, R^2 values are acceptable for tests at 13 and 60 percent saturation, marginal for the dry test, and poor for the 20 percent test. Equations for prediction of peak stress in Poudre Valley sand at compactive saturations of 0, 13 and 60 percent have a medium to high degree of confidence associated with them. The validity of the prediction equation for 20 percent compactive saturation is questionable.

Peak stress data is widely used for prediction and design purposes. It's use in the present research is limited. The peak stress data obtained in this research is incomplete due to data acquisition errors, deficiency in data at large scaled ranges, and cross talk in the lines.

Cross talk occurred in tests conducted in the Fall of 1991 due to the use of a common power source for all gages. However, some stress data was salvaged by applying correction factors to superimposed signals caused by cross talk. Static calibration of gages with induced cross talk was performed to determine by what percentage the magnitudes of the superimposed signals should be increased or decreased.

Regression curves for peak stresses were constructed only from data from the large (6.22 and 7.0 kg) shots, since signals from the small (0.227 kg) shots were barely discernable from magnitudes of the TDR's digitizer output signals. With this deficiency in stress data at greater scaled ranges, regression analysis results were subject a greater degree of inaccuracy. A second series of small (0.227 kg) shots was implemented in the Spring of 1992 for the very purpose of establishing legitimate regression trends based on a wider data spread. Additionally, data acquisition problems led to the loss of stress data for the 40 percent test. In spite of the incompleteness of stress data, a limited amount of legitimate stress data is still available for comparison. Comparison of constants and slopes in Table 5.3 reveals that constants for Poudre Valley sand are lower than those for Tyndall Beach sand and medium-dense moist

sand, and comparable to those for Ottawa 20-30 sand. Values of slope compare closely to the values for Tyndall Beach sand and medium-dense moist sand, and are lower than slope values for Ottawa 20-30 sand.

Similar to the previous cases, peak stress magnitudes are generally lower for Poudre Valley sand while attenuation rates are comparable to or slightly lower than those of Tyndall Beach, Ottawa 20-30 and medium-dense moist sands.

4.   Summary

Comparison of regression data from Poudre Valley, Tyndall Beach, Ottawa 20-30 and medium-dense moist sands reveals the following: 1) scaled peak particle acceleration, peak particle velocity and peak stress magnitudes for Poudre Valley sand are generally lower than those for Tyndall Beach, Ottawa 20-30 and medium-dense moist sands; 2) attenuation rates for Poudre Valley sands are generally comparable or lesser than those of Tyndall Beach, Ottawa 20-30 and medium-dense moist sands.

Differences and similarities between the constants and slopes of the sands under comparison can be seen more clearly by comparing average values of the constants and slopes associated with each compactive saturation level, listed in Table 5.4. Predictive equations developed from average constants and slopes were used to plot peak parameter versus scaled range plots in Figures C.10 to C.12 for Poudre Valley, Tyndall Beach, Ottawa 20-30, dense, medium-dense and loose sands.

TABLE 5.1. PREDICTIVE EQUATIONS AND REGRESSION DATA FOR SCALED PEAK PARTICLE ACCELERATION IN POUDRE VALLEY SAND WITH COMPARISON TO WALSH'S (1993) AND DRAKE & LITTLE'S (1983) RESULTS.

Test saturation	Predictive equations for scaled peak particle acceleration in Poudre Valley sand, $g's \cdot kg^{1/3}$	Regression data		
		Constant, $g's \cdot kg^{1/3}$	Slope	R^2
0 %	$a_o \cdot W^{1/3} = 3040 \left(\dfrac{R}{W^{1/3}} \right)^{-4.70}$	3040*	-4.70	0.98
13 %	$a_o \cdot W^{1/3} = 1090 \left(\dfrac{R}{W^{1/3}} \right)^{-3.68}$	1090	-3.68	0.98
20 %	$a_o \cdot W^{1/3} = 1535 \left(\dfrac{R}{W^{1/3}} \right)^{-3.35}$	1535	-3.35	0.98
40 %	$a_o \cdot W^{1/3} = 1360 \left(\dfrac{R}{W^{1/3}} \right)^{-3.79}$	1360	-3.79	0.95
60 %	$a_o \cdot W^{1/3} = 1340 \left(\dfrac{R}{W^{1/3}} \right)^{-4.01}$	1340	-4.01	0.95
70 %	Not enough data points to run regression analysis			
S= 0 TO 70% Test Results Walsh, (1993)	Tyndall Beach sand	2800 to 5600	-3.16 to -4.27	> 0.91
	Ottawa 20-30 sand	300 to 5000	-1.39 to -5.00	----
Drake & Little (1983)-- Eq. (2.1)	Medium-dense moist sand	1100 to 2000	-3.5 to -3.75	----

* See text for discussion of possible reasons for high value.

83

TABLE 5.2. PREDICTIVE EQUATIONS AND REGRESSION DATA FOR PEAK PARTICLE VELOCITY IN POUDRE VALLEY SAND WITH COMPARISON TO WALSH'S (1993) AND DRAKE & LITTLE'S (1983) RESULTS.

Test Saturation	Predictive equations for peak particle velocity in Poudre Valley sand, m/s	Regression data		
		Constant, m/s	Slope	R^2
0 %	$V_o = 1.99\left(\dfrac{R}{W^{1/3}}\right)^{-2.41}$	1.99	-2.41	0.99
13 %	$V_o = 2.00\left(\dfrac{R}{W^{1/3}}\right)^{-2.25}$	2.00	-2.25	0.95
20 %	$V_o = 2.22\left(\dfrac{R}{W^{1/3}}\right)^{-2.21}$	2.22	-2.21	0.97
40 %	$V_o = 2.59\left(\dfrac{R}{W^{1/3}}\right)^{-2.21}$	2.59	-2.21	0.99
60 %	$V_o = 2.61\left(\dfrac{R}{W^{1/3}}\right)^{-2.34}$	2.61	-2.34	0.99
70 %	Not enough data points to run regression analysis			
S= 0 TO 70% Test Results, Walsh (1993)	Tyndall Beach sand	3.49 to 4.62	-2.03 to -2.53	> 0.99
	Ottawa 20-30 sand	0.67 to 6.97	-0.51 to -3.22	----
Drake & Little (1983)-- Eq. (2.2)	Medium-dense moist sand	3.84 to 4.84	-2.5 to -2.75	----

TABLE 5.3. PREDICTIVE EQUATIONS AND REGRESSION DATA FOR PEAK STRESS IN POUDRE VALLEY SAND WITH COMPARISON TO WALSH'S (1993) AND DRAKE & LITTLE'S (1983) RESULTS.

Test saturation	Predictive equations for peak stress in Poudre Valley sand, kPa	Regression data		
		Constant, kPa	Slope	R^2
0 %	$P_o = 1220\left(\dfrac{R}{W^{1/3}}\right)^{-2.07}$	1220	-2.07	0.87
13 %	$P_o = 1200\left(\dfrac{R}{W^{1/3}}\right)^{-1.97}$	1200	-1.97	0.96
20 %	$P_o = 1570\left(\dfrac{R}{W^{1/3}}\right)^{-1.98}$	1570	-1.98	0.29
40 %	No stress data available			
60 %	$P_o = 2010\left(\dfrac{R}{W^{1/3}}\right)^{-2.22}$	2010	-2.22	0.95
70 %	Not enough data points to run regression analysis			
S= 0 TO 70% Test Results, Walsh (1993)	Tyndall Beach sand	1820 to 2110	-2.30 to -2.62	> 0.94
	Ottawa 20-30 sand	1130 to 1840	-2.89 to -3.25	> 0.91
Drake & Little (1983)-- Eq. (2.3)	Medium-dense moist sand	1910 to 2730	-2.5 to -2.75	----

85

TABLE 5.4.   AVERAGE VALUES OF CONSTANTS AND SLOPES OF POUDRE VALLEY,
TYNDALL BEACH AND OTTAWA 20-30 SANDS.

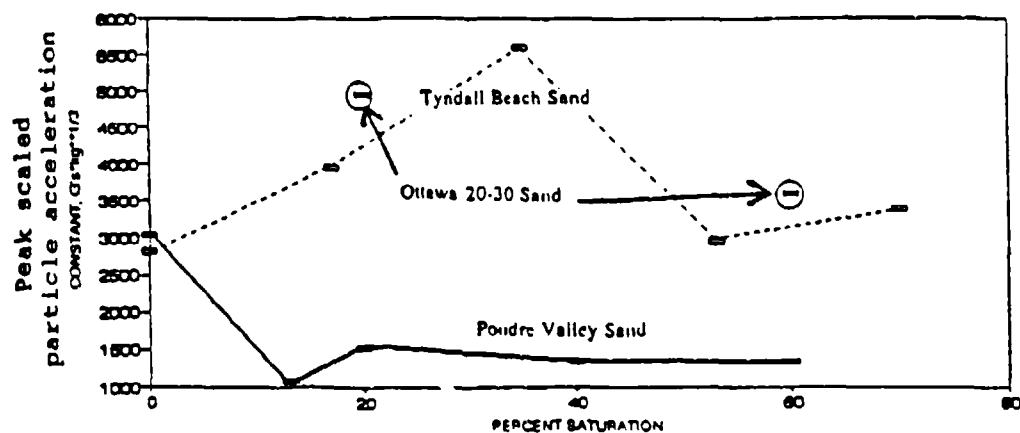|		Poudre Valley sand	Tyndall Beach sand	Ottawa 20-30 sand
Scaled peak particle acceleration	Constant $(g's \cdot kg^{1/3})$	1673	3749	4276
	Slope $(-n-1)$	-3.91	-3.55	-4.84
Peak particle velocity	Constant (m/s)	2.28	4.04	6.17
	Slope $(-n)$	-2.28	-2.27	-3.08
Peak stress	Constant (kPa)	1500	1996	1380
	Slope $(-n)$	-2.06	-2.43	-3.06

C. ANALYSIS OF REGRESSION DATA TRENDS

In this section the constants and slopes of the prediction equations and propagation velocity trends will be analyzed for trends over the range of saturations tested and compared with the trends for Tyndall Beach and Ottawa 20-30 sands reported by Walsh (1993). Stress transmission and propagation velocity trends will also be compared with trends reported by Ross (1989), Pierce (1989), Charlie et al. (1990a) and Veyera and Fitzpatrick (1990).

1. Analysis and Comparison of Trends of Constants

a. Analysis of Poudre Valley Sand Trends

Figure 5.1 shows constant values plotted over a range of compactive saturations. In Figure 5.1a the scaled peak particle acceleration constant for Poudre Valley sand decreases from 0 to 13 percent saturation, increases from 13 to 20 percent saturation, and then decreases from 20 to 60 percent saturation. In Figure 5.1b, peak particle velocity constants are even from 0 to 13 percent saturation, rise from 13 to 40 percent saturation, and level off from 40 to 60 percent saturations. In Figure 5.1c, peak stress constants decline slightly from 0 to 20 percent saturation, and rise from 20 to 60 percent saturation.

Higher constant values for a given saturation correspond with greater energy transmission through the sand. The highest transmission in Figures 5.1a and 5.1b occurs between 20 and 60 percent saturation, and also at 0 percent in Figure 5.1a. The highest stress transmission in Figure 5.1c occurs at 60 percent saturation. However, due to the deficiency in stress data at 20 and 40 percent saturations, it remains indeterminate at what range of compactive saturations stress transmission is greatest for Poudre Valley sand.
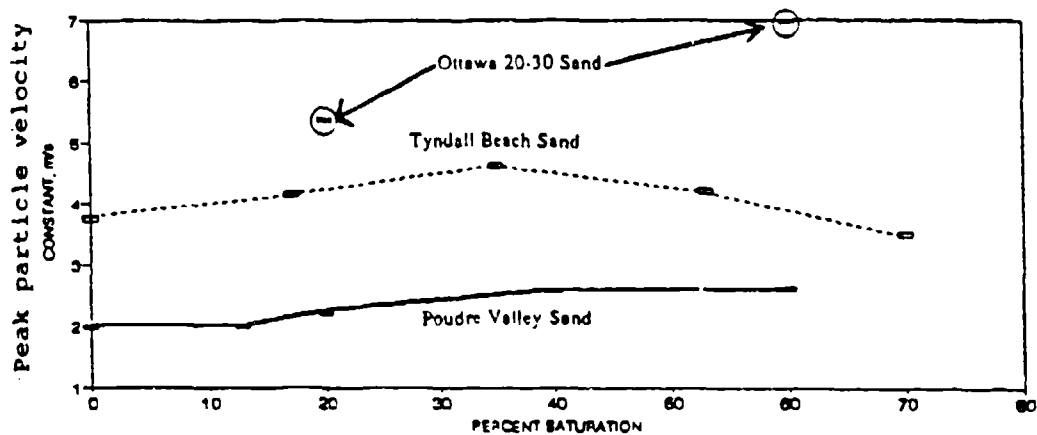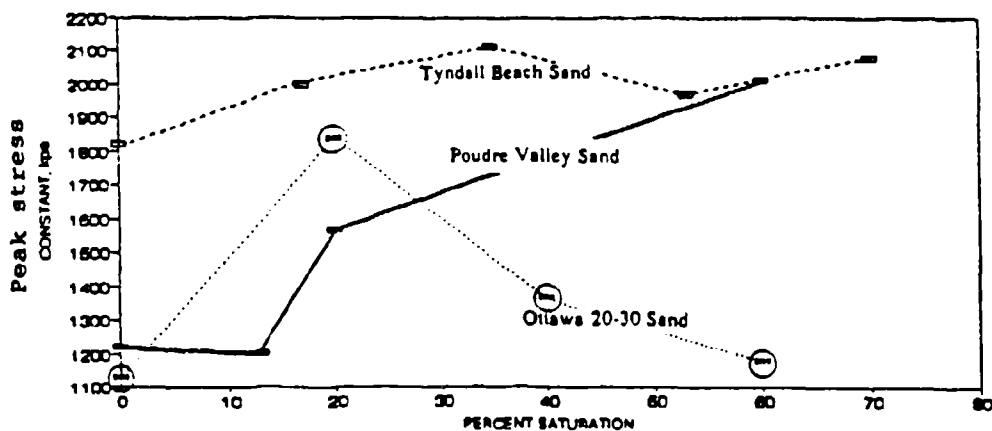
Figure 5.1   Constants (Y-Intercept at $R/W^{1/3}=1$) versus Percent Saturation
for Poudre Valley, Tyndall Beach and Ottawa 20-30 Sands. (a)
Scaled Peak Particle Acceleration. (b) Peak Particle Velocity.
(c) Peak Stress.

b.   Comparison of Trends

In Figure 5.1b, the trends for Poudre Valley sand and Tyndall Beach sand are strikingly similar, although the magnitudes of the particle velocity constants for the two sands are offset from each other. The trend for Poudre Valley sand in Figure 5.1a displays some resemblance to the trends in Figure 5.1b except for the high-scaled peak particle acceleration constant value at 0 percent saturation, which was discussed earlier.   Stress transmission comparison between peak stress constant trends for Poudre Valley sand, Tyndall Beach and Ottawa 20-30 sands in Figure 5.1c reveals similarities between 0 to 20 percent saturation but no similarities above 40 percent. Comparison with transmission ratio trends in Figure 2.5 (Charlie, et al., 1990a) and normalized transmission ratio trends in Figure 2.9 (Veyera and Fitzpatrick, 1990) also show no similarities above 40 percent saturation.   It appears that little comparison can be made due to deficiency in stress data.

However, peak particle velocity trends can be compared with peak stress trends since peak particle velocity and peak stress differ by a factor of ρc according to Equation (2.4). Peak particle velocity trends in Figure 5.1b show the same general shape as the stress transmission trends in Figures 2.5 and 2.9 except for the even trend from 40 to 60 percent saturations.

2.   Analysis and Comparison of Trends of Slopes

a.   Analysis of Poudre Valley Sand Trends

Figure 5.2 shows slope values plotted over a range of compactive saturations. Slope values for peak particle velocity and peak stress are equivalent to the negative attenuation coefficient $(-n)$ in Equations (2.2) and (2.3).   Slope values for scaled peak particle acceleration are equivalent to the negative attenuation coefficient minus 1 $(-n-1)$ in Equation (2.1).

89
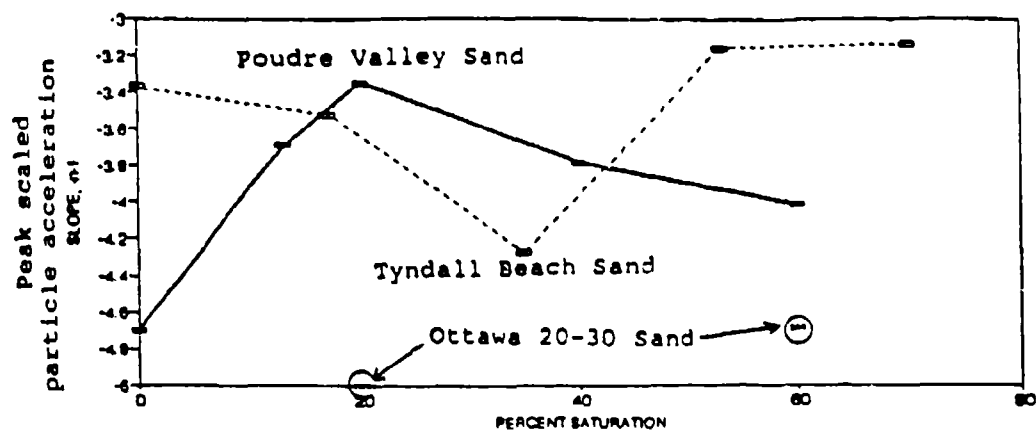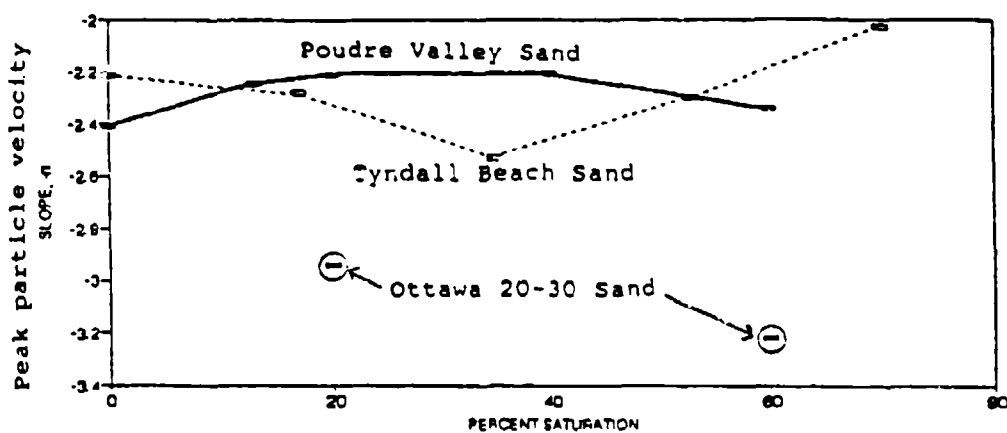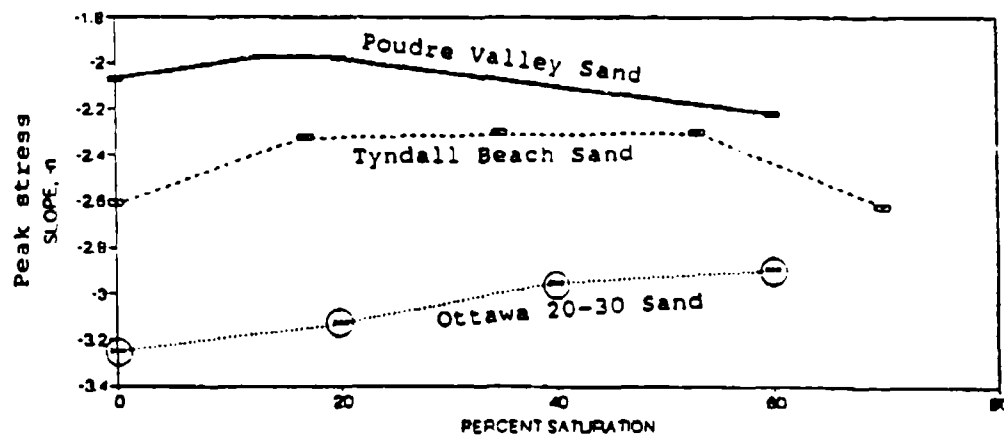
Figure 5.2   Slopes (-n-1 and -n) versus Percent Saturation for Poudre
              Valley, Tyndall Beach and Ottawa 20-30 Sands. (a) Scaled Peak
              Particle Acceleration.   (b) Peak Particle Velocity. (c) Peak
              Stress.

90
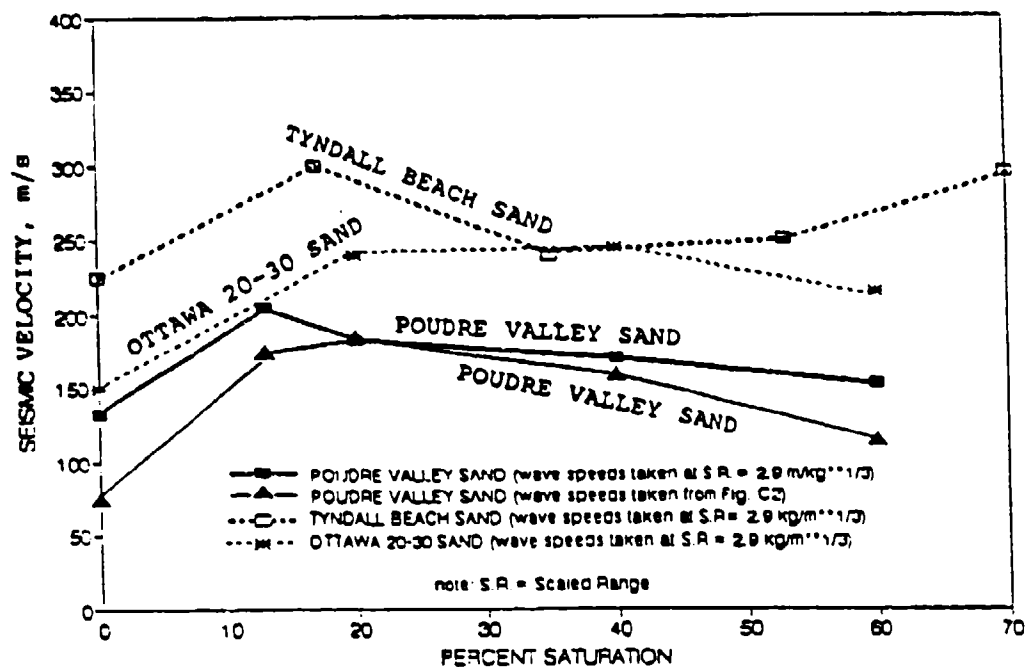
Figure 5.3   Seismic Velocity versus Percent Saturation for Poudre Valley,
             Tyndall Beach and Ottawa 20-30 Sands.
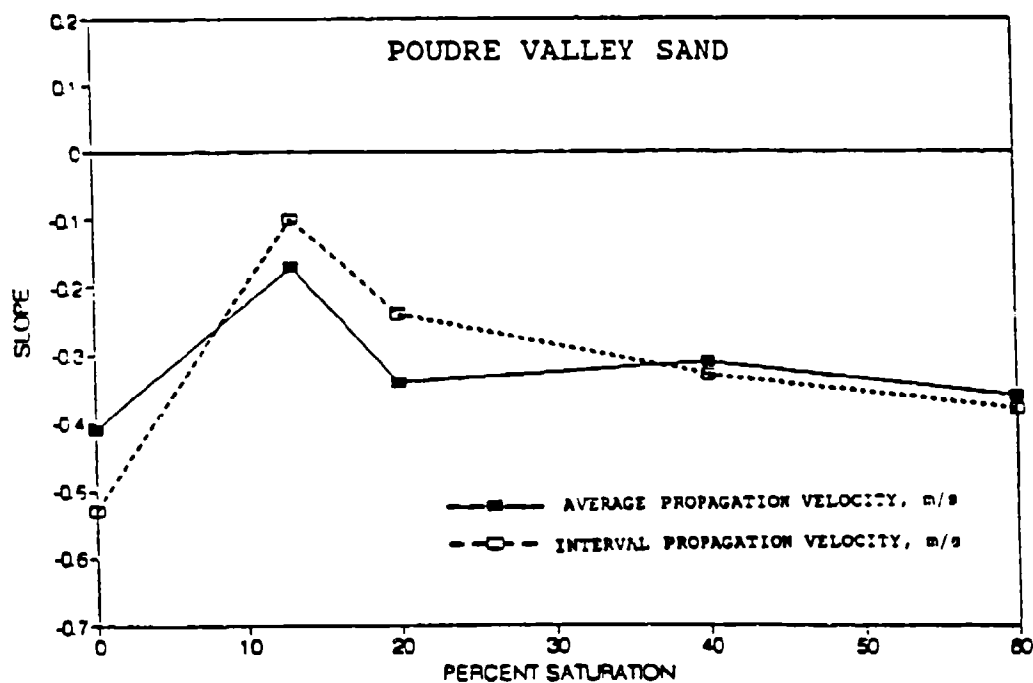
Figure 5.4   Slope versus Percent Saturation for Average and Interval
             Propagation Velocities of Poudre Valley Sand.

91

5. ANALYSIS OF ACOUSTIC IMPEDANCE AND PEAK STRESS VERSUS PEAK PARTICLE VELOCITY

Acoustic impedance, ρc, is a measure of a soil's ability to transmit stress waves. The acoustic impedance for Poudre Valley sand can be determined four ways. The first is by back calculating ρc using Equation (2.3),

$$\rho c = \frac{20.5 \cdot P_o}{f \cdot (2.52)^{-n} \left(\frac{R}{W^{1/3}}\right)^{-n}} . \tag{5.1}$$

The second is by using Equation (2.4) to calculate ρc as,

$$\rho c = \frac{P_o}{V_o} . \tag{5.2}$$

The third is by using the experimentally determined seismic velocity and measured total density. The fourth is by determining the slope from peak stress versus peak particle velocity in Figure 4.16.

Table 5.5 displays ρc values for Poudre Valley sand calculated from Equations (5.1) and (5.2), from multiplication of experimentally determined ρ and c values and slopes taken from Figure 4.16. Acoustic impedance values for Tyndall Beach sand, Ottawa 20-30 sand (Walsh 1993) and Dense Dry and Wet sands (Drake & Little, 1983) are included for comparison.

Peak stress P_o and peak particle velocity V_o values in Equations (5.1) and (5.2) are calculated at a scaled range of 2.9 $m/kg^{1/3}$ using the empirical equations developed in Tables 5.2 and 5.3. A scaled range of 2.9 $m/kg^{1/3}$ is also used in Equation (5.1). Acoustic impedance values from Figure 4.16 correspond with scaled range values up to 1 $m/kg^{1/3}$ ($R/W^{1/3}= 1$) since stress data were obtained only for the 6.22 kg and 7.0 kg shots.

TABLE 5.5. ACOUSTIC IMPEDANCE VALUES FOR POUDRE VALLEY, TYNDALL BEACH, OTTAWA 20-30 AND LOOSE & DENSE SANDS.

Saturation (%)	Acoustic impedance X 10³ (kg/m²-s)									
	P.V.S.[1]	P.V.S.[2]	P.V.S.[3]	P.V.S.[4]	P.V.S.[AVE]	T.B.S.[1]	T.B.S.[2]	O. 20-30[1]	O. 20-30[2]	L. & D. SAND
0	169	881	123	601	444	272	315	290	-----	-----
13	152	808	286	541	447	-----	-----	-----	-----	-----
17	-----	-----	-----	-----	-----	227	492	-----	-----	566[a]
20	201	903	305	720	532	-----	-----	447	283	262[b]
31	-----	-----	-----	-----	-----	-----	-----	-----	-----	-----
35	-----	-----	265	-----	-----	232	579	278	154	-----
40	-----	-----	-----	-----	-----	-----	-----	-----	-----	-----
53	-----	-----	-----	-----	-----	225	478	226	238	-----
60	321	875	205	785	547	285	345	-----	-----	-----
70	-----	-----	-----	772	-----	-----	-----	-----	-----	-----
74	-----	-----	-----	-----	-----	-----	-----	-----	-----	498[a]
76	-----	-----	-----	-----	-----	-----	-----	-----	-----	283 TO 339[b]

KEY
P.V.S.   Poudre Valley sand
T.B.S.   Tyndall Beach sand (Walsh, 1993)
O. 20-30   Ottawa 20-30 sand (Walsh, 1993)
L. & D.   Loose and dense sand (Drake & Little 1983)
[1]   Calculated from Equation (5.1)
[2]   Calculated from Equation (5.2)
[3]   Calculated from measured seismic velocity and total density
[4]   Determined from slope of peak stress versus peak particle velocity plots in Figure 4.16
[AVE] Average of ρc values using methods 1 to 4
[a]   Determined from dense poorly graded sand (Drake and Little, 1983)
[b]   Determined from loose poorly graded sand (Drake and Little, 1983)

Acoustic impedance values for Poudre Valley sand calculated using Equation (5.2) are significantly larger than ρc values for all other sands in Table 5.5. The large magnitudes of ρc values may be explained by the presence of large attenuation coefficients for the peak stress equations. According to Drake and Little (1983), attenuation coefficients for peak stress and peak particle velocity should be equal. Comparison of slope values in Tables 5.2 and 5.3 show attenuation coefficients for Poudre Valley sand are not equal.

This may be due to the lack of large scaled ranges in the peak stress regression data, which had the effect of decreasing slope values for peak particle acceleration and peak particle velocity regression curves. Stress data for the 0.227 kg shot was not discernable from the noise, precluding larger scaled ranges from being included in the regression analysis. Using attenuation coefficients from peak particle velocity equations in peak stress equations yields lower P_o values, resulting in lower ρc values ranging from 600,000 to 700,000 kg/m^2-s.

An average acoustic impedance value for Poudre Valley sand was determined by taking the average of acoustic impedance values obtained from the four different methods of determination. The average ρc value for Poudre Valley sand is roughly equal to or slightly greater than ρc values calculated for Tyndall Beach and Ottawa 20-30 sands (Walsh, 1993) and is comparable to ρc values for dense poorly graded sand (Drake and Little, 1983).

Peak stress is plotted as a function of peak particle velocity in Figure 5.5. Data from tests conducted at all compactive saturations are combined in the same plot for Tyndall Beach sand (Figure 5.5a) and for Poudre Valley sand (Figure 5.5b). The overall acoustic impedance value for Poudre Valley sand is 667,300 kg/m^2-s, which is higher than the ρc value reported by Walsh (1993) of 532,660 kg/m^2-s for Tyndall E ach sand. Table 5.6 shows the ranges of measured peak stress and peak particle velocity with corresponding scaled range values for both Poudre Valley and Tyndall Beach sand.

Figure 5.6 shows acoustic impedance plotted as a function of compactive saturation for Tyndall Beach sand (Figure 5.6a), Ottawa 20-30

sand (Figure 5.6b) and Poudre Valley sand (Figure 5.6c). Equations (5.1) and (5.2) are used to obtain the curves in Figures 5.6a and 5.6b for Tyndall Beach and Ottawa 20-30 sands (Walsh, 1993). All four methods of determining acoustic impedance for Poudre Valley sand listed in Table 5.5 are used to obtain the curves in Figure 5.6c. Attenuation trends of acoustic impedance values versus compactive saturation for Poudre Valley sand determined from the measured total dry density and seismi- velocities compare with trends seen in Figures 5.6a and 5.6b for Tyndall and Ottawa 20-30 sands. Attenuation trends of ρc values for Poudre Valley sand determined from the other three methods show little similarity with Tyndall Beach and Ottawa 20-30 acoustic impedance versus compactive saturation trends reported by Walsh (1993).
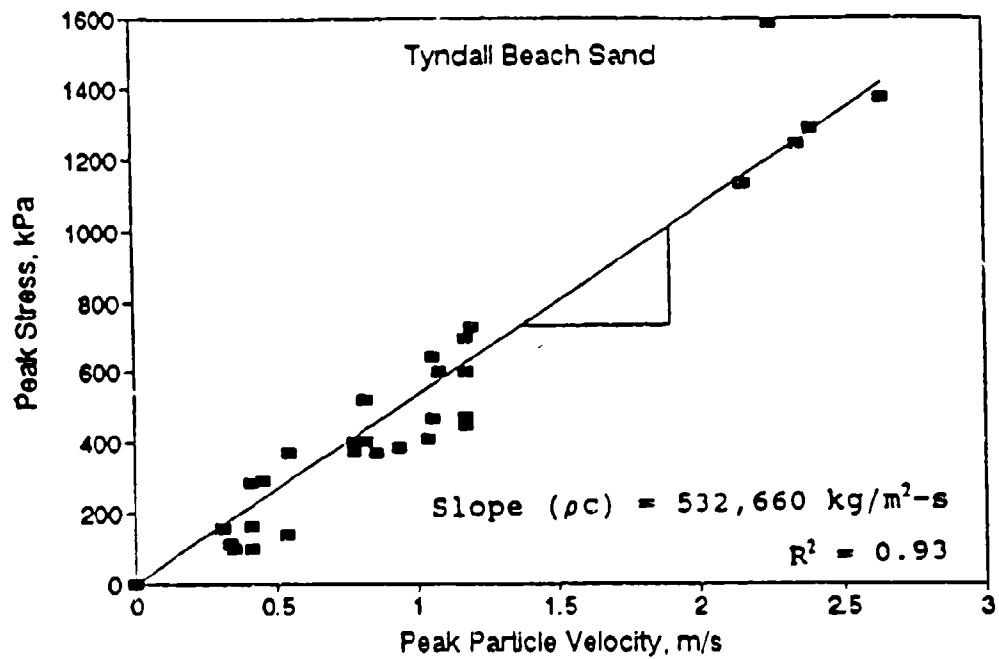
(a)
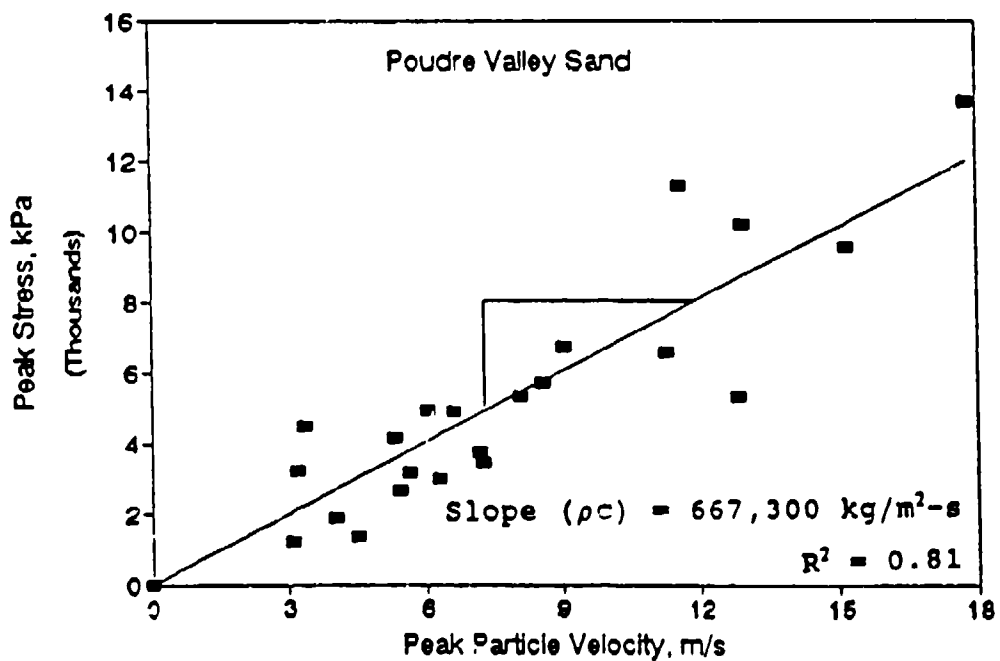
(b)

Figure 5.5   Peak Stress versus Peak Particle Velocity for All Compactive
Saturations Combined. (a) Tyndall Beach Sand (Replotted from
Walsh, 1993). (b) Poudre Valley Sand.

TABLE 5.6. RANGES OF MEASURED PEAK STRESS AND PEAK PARTICLE VELOCITY FOR EXPLOSIVE FIELD TESTING OF POUDRE VALLEY SAND AND EXPLOSIVE CENTRIFUGE TESTING OF TYNDALL BEACH SAND.

Test	Measured parameter	Range of measured values of peak stress and peak particle velocity from explosive field testing of Poudre Valley sand (present investigation) and explosive centrifuge testing of Tyndall Beach sand (Walsh, 1993)	Equations for average peak stress and peak particle velocity[3]
Explosive field testing of Poudre Valley sand[1]	Peak stress (kPa)	15,689 … 360	$P_s = 1500\left(\dfrac{R}{W^{1/3}}\right)^{-2.04}$
	Peak particle velocity (m/s)	31 … 1.37 … 0.11	$V_s = 2.28\left(\dfrac{R}{W^{1/3}}\right)^{-3.20}$
Scaled range (m/kg$^{1/3}$)		0.5 1.0 1.5 2.0 2.5 3.0 3.5 4.0	
Explosive centrifuge testing of Tyndall Beach sand[2]	Peak stress (kPa)	20,955 … 370	$P_s = 1996\left(\dfrac{R}{W^{1/3}}\right)^{-2.43}$
	Peak particle velocity (m/s)	2.43 … 0.84	$V_s = 4.04\left(\dfrac{R}{W^{1/3}}\right)^{-2.37}$

[1]Scaled range values for measured peak stress range from 0.32 m/kg$^{1/3}$ to 1.11 m/kg$^{1/3}$. Scaled range values for measured peak particle velocity range from 0.32 m/kg$^{1/3}$ to 3.8 m/kg$^{1/3}$.

[2]Scaled range values for measured peak stress range from 0.38 m/kg$^{1/3}$ to 2.0 m/kg$^{1/3}$. Scaled range values for measured peak particle velocity range from 1.25 m/kg$^{1/3}$ to 2.0 m/kg$^{1/3}$ (Walsh, 1993).

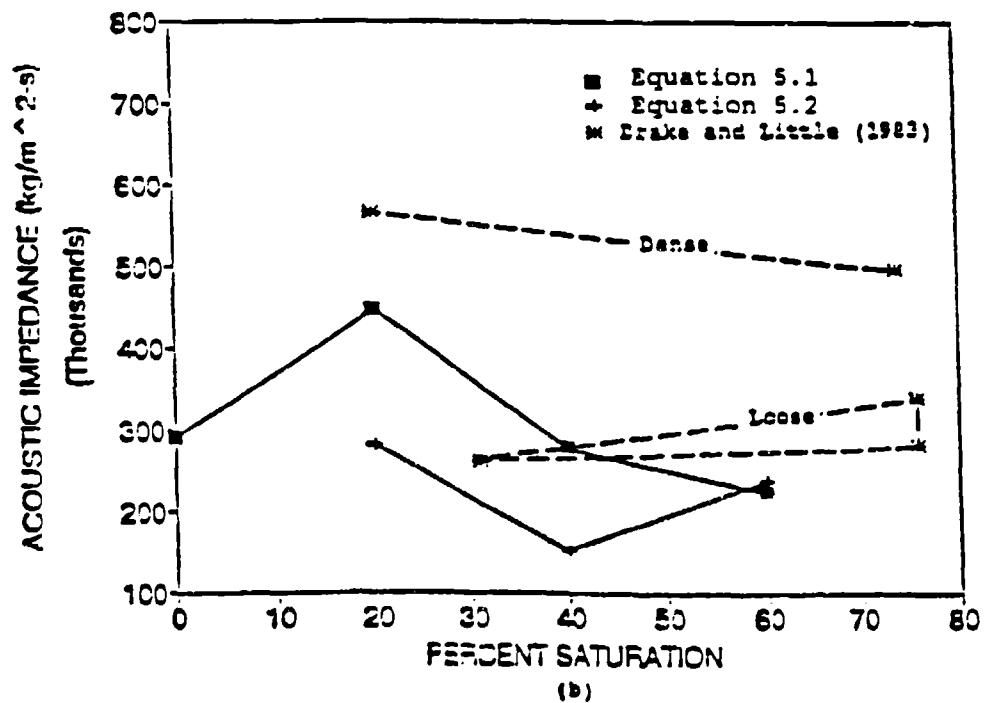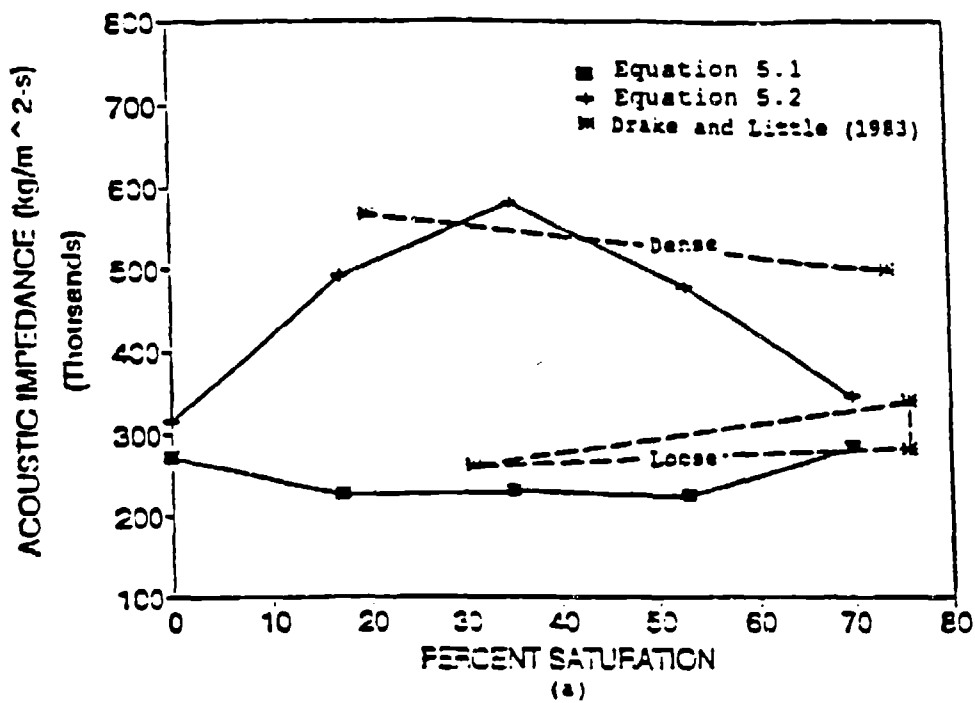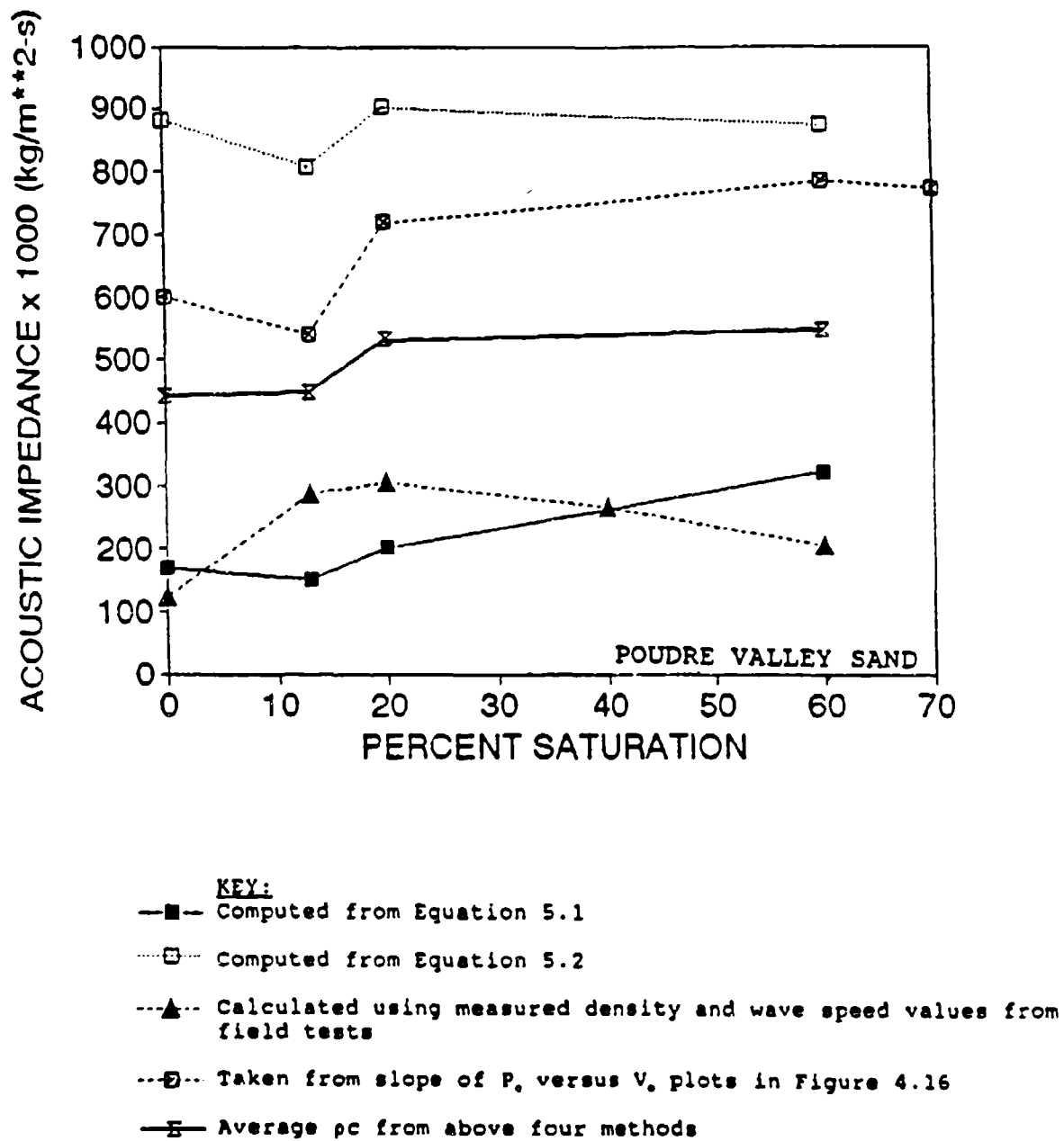[3]See Section V.B.4. for development of equations.

Figure 5.6   Acoustic Impedance (ρc) versus Percent Saturation Computed
from Equations 5.1 and 5.2. and Taken from Drake and Little
(1983). (a)   Tyndall Beach Sand   (b)   Ottawa 20-30 Sand
(Walsh, 1993).

98

KEY:

—■— Computed from Equation 5.1

···□··· Computed from Equation 5.2

···▲··· Calculated using measured density and wave speed values from field tests

···⊟··· Taken from slope of P_e versus V_e plots in Figure 4.16

—⊟— Average ρc from above four methods

(c)

Figure 5.6   (Continued) Acoustic Impedance (ρc) versus Percent Saturation
(c) Poudre Valley Sand.

F. ANALYSIS OF EFFECTIVE STRESS INCREASES DUE TO CAPILLARITY

Bishop and Blight (1963) observed that an increase in a soil's capillarity is associated with a corresponding increase in effective stress. They developed an empirical equation to predict the increase in effective stress as the product of the soil factor, χ, and matric suction $(u_a - u_w)$. Utilizing the water retention curve shown in Figure 4.4, the variation in increase of effective stress in Poudre Valley sand is plotted as a function of saturation in Figure 5.7, assuming that χ is equal to the soil's saturation, S. The greatest effective stress increase occurs at approximately 50 percent saturation. The effect of capillarity on effective stress diminishes for saturations larger and smaller than 50 percent. At 0 and 100 percent saturations, the increase in effective stress due to capillarity is zero. Comparison with Figure 4.3 reveals that the greatest increase in effective stress and the greatest compactive effort required to reach a constant dry density both occur between 40 and 50 percent saturations.
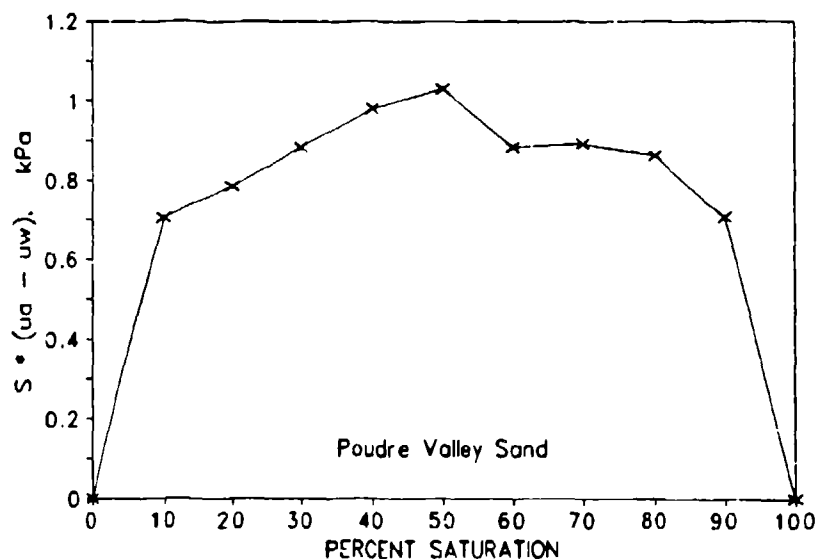

Figure 5.7 Increase in Effective Stress in Poudre Valley Sand due to Capillarity.

VI. SUMMARY, CONCLUSIONS AND RECOMMENDATIONS

A. SUMMARY

Proper design of buried structures against blast loading is dependent upon an accurate knowledge of the dynamic response to ground shock in the surrounding backfill material. The presence of moisture in sands during compaction has recently been found to influence blast-induced ground motion parameters and attenuation behavior, which form the basis for determination of soil-structure response to blast loading.

The objective of this research is to determine the influence that the degree of saturation during compaction of sand has on blast-induced scaled peak particle acceleration, peak particle velocity, peak stress and propagation velocity. This report presents the results of a series of explosive field tests in Poudre Valley sand at compactive saturations ranging from 0 to 70 percent at a constant dry density of 1635 kg/m³ (DR= 44 percent). Charge masses of 6.22 kg, 7.0 kg and 0.227 kg TNT equivalency were used, providing scaled range values ranging from 0.32 to 3.8 m/kg$^{1/3}$ for analysis.

Field procedure prior to explosive testing involved the placement, addition of water to, mixing and compaction of sand, instrumentation placement, . . ' .r. ration of the data acquisition system. Sand was compacted in .-..- .fts using a vibratory compactor. Compaction and moisture control procedures utilized nuclear density/moisture gage measurements. Instrumentation used to measure particle acceleration and soil stress were accelerometers and soil stress gages, which were placed at distances from the center of explosion ranging from .61 to 2.25-meters. The instruments and center of explosive were located 1.4 meters below ground surface.

Cube root scaling laws were used to construct peak ground motion parameter versus scaled range plots for each test saturation, from which attenuation trends over a range of compactive saturations could be determined. Predictive empirical equations were constructed from the regression data from these plots. The magnitudes and attenuation trends of ground motion parameters are analyzed and compared with those of Drake and Little (1983), Pierce (1989), Ross (1989), Charlie et al. (1990a), Veyera and Fitzpatrick (1990), and Walsh (1993).

B. CONCLUSIONS

Based on the results of this investigation and comparison of results with the aforementioned researchers, the following conclusions are drawn relative to the four major objectives stated in the Introduction.

1. Predictive Empirical Equations for Ground Motion and Stress

Predictive Equations for scaled peak particle acceleration, peak particle velocity and peak stress are given in Tables 5.1, 5.2 and 5.3, respectively. These equations are applicable for ground motion and stress prediction in sands with similar properties as Poudre Valley sand (refer to Section IV.B) under similar testing conditions (refer to Table 4.3). Confidence levels are high for scaled peak particle acceleration and peak particle velocity equations, and medium for peak stress equations. The developed predictive peak stress equations underpredict attenuation rates, evidenced by the low attenuation coefficients (n) in Figure 5.2c and the relatively flat attenuation curve in Figure C.12. The trends for peak ground motion and peak stress versus saturation follow the same trends for compactive effort versus saturation (Figure 4.3) and for increase in effective stress due to capillarity versus saturation (Figure 5.7).

102

2. Comparison with Split-Hopkinson Pressure Bar Results (Pierce, 1989; Ross, 1989; Charlie et al., 1990a; Veyera and Fitzpatrick, 1990)

Constant (Y-intercept at $R/W^{1/3} = 1$ m/kg$^{1/3}$) attenuation trends between 13 and 40 percent compactive saturations for Poudre Valley sand in Figures 5.1a and 5.1b are comparable with SHPB Transmission Ratio attenuation trends in Figures 2.5a, 2.6 and 2.9 for 50/80 silica and Ottawa 20-30 sands. Slope attenuation trends versus compactive saturation in Figure 5.2 (a,b,c) bear close resemblance to SHPB trends in Figures 2.5a, 2.6 and 2.9 for 50/80 silica and Ottawa 20-30 sands. Propagation velocity attenuation trends versus compactive saturation in Figures 5.3 and 5.4 for Poudre Valley sand are similar to SHPB trends for 50/80 silica and Ottawa sands in Figures 2.5b and 2.8.

3. Comparison with Centrifuge Modeling Results (Walsh, 1993)

Ground motion and stress constants for Poudre Valley sand are generally lower than those for Tyndall Beach and Ottawa 20-30 sands (see Tables 5.1 to 5.3 and Figure 5.1 for comparison). Peak particle velocity constant attenuation trends versus compactive saturation for Poudre Valley and Tyndall Beach sands are virtually identical, with the exception of the region from 40 to 60 percent. Scaled peak particle acceleration and peak stress constant attenuation trends are marginally similar.

Slope magnitudes compare closely with Tyndall Beach and Ottawa 20-30 sand (Tables 5.1 to 5.3 and Figure 5.2). Peak stress slope attenuation trends in Figure 5.2c are similar to that of Tyndall Beach sand and dissimilar to that for Ottawa sand. The trend for attenuation of peak particle velocity slopes for Poudre Valley sand is identical to the peak stress slope attenuation trend for Tyndall Beach sand.

103

The similarities and differences in stress wave propagation characteristics among Poudre Valley, Tyndall Beach and Ottawa 20-30 sands are clearly seen in Figures C.10 to C.12. In these Figures, peak parameter versus scaled range curves for all three sand types are within or very close to the envelope suggested by Drake and Little (1983) for dense, medium-dense and loose sands. Ottawa 20-30 sand has sharp attenuation rates in all three Figures, very similar to that of loose sand. This may be related to the fact that a 118 kg TNT equivalent explosion at a scaled depth of burial of 3.63 m was modeled in Ottawa 20-30 sand, whereas only 7.3 and 7.8 kg TNT equivalent explosions were modeled in Tyndall Beach sand, roughly equivalent to the 7.0 kg charge mass at a depth of 1.4 m used in field explosive tests in Poudre Valley sand.

Comparison of seismic velocity magnitudes and trends versus compactive saturation in Figure 5.3 reveals that seismic velocity values for Poudre Valley sand are lower than those for Tyndall Beach and Ottawa 20-30 sands, and that attenuation trends versus compactive saturation are similar for all three sands, with the exception of a deviation from 40 to 70 percent saturation for Tyndall Beach sand.

Based upon the foregoing comparison and discussion, centrifuge modeling is judged to be an accurate, viable method of predicting stress wave propagation characteristics in sand.

4.   Comparison with Empirical Equations (Drake and Little, 1983)

Constants for moist Poudre Valley sand are lower than the range suggested by Drake and Little (1983) for medium-dense moist sands for peak particle velocity and peak stress, and are similar for peak particle acceleration (Tables 5.1 to 5.3).

Slope values for scaled peak particle acceleration (-n-1), peak particle velocity (-n) and peak stress (-n) for Poudre Valley sand compare equally to slightly lower than those for medium-dense moist sands given by Drake and Little (Tables 5.1 to 5.3).

The overall wave propagation behavior of Poudre Valley sand shown in the peak parameter versus scaled range plots in Figures C.10 to C.12 is comparable to the envelope suggested by Drake and Little (1983) for dense, medium-dense and loose sands.

C.   RECOMMENDATIONS ANALYSIS AND DESIGN

The following factors are possible influences of stress wave propagation behavior and may enter into the analysis and design process for backfill material surrounding buried structures:

1.   Sand compactive saturation level
2.   Type of modeling: full scale, centrifuge
3.   Physical properties of the sand
     • grain shape
     • grain size
     • grain size distribution
     • physical composition
     • capillarity
4.   Sand placement density
     • dry density
     • relative density
5.   Explosives
     • energy yield
     • confinement or non-confinement
     • depth of burial
     • shape

Several design recommendations can be made based upon analysis and comparison of wave propagation behavior among the sand types and test conditions discussed in the present investigation.

1.   The greatest stress wave transmission occurred between 20 and 60 percent compactive saturations for the sands analyzed and compared in this research. Depending upon the compactive saturation, magnitudes of peak parameter constants and slopes and propagation velocities in the present research varied by an

average factor of 1.4 and sometimes varied by as much as a factor of 2. If possible and feasible, the contractor should compact sands at saturation levels outside of the range of greatest stress transmission. If this can not be accomplished, the compactive saturation associated with the lowest stress transmission characteristics should be determined and used which is within the range feasible compactive saturations for the contractor.

2. The empirical predictive equations and suggested design coefficients developed by Drake and Little (1983) for scaled peak particle acceleration, peak particle velocity and peak stress (Equations (2.1) to (2.3)) should be used for soil conditions where the effect of the degree of saturation at the time of compaction is unknown or indeterminate as a general estimate of wave propagation behavior. Predictive equations developed in the present research, given in Tables 5.1 to 5.3, should be used when the degree of saturation at the time of compaction is known, to predict peak ground motion parameters in compacted sand backfills similar to those analyzed in this report.

3. Centrifuge testing should be used to determine stress wave transmission and attenuation characteristics of backfill materials for proposed underground structures. Care must be taken to best simulate the actual loading conditions in the field.

4. A greater depth of burial of explosive is associated with higher confinement pressures and hence greater magnitudes of peak particle stress and propagation velocities. The depth of the buried structure should be no greater than that absolutely necessary for strategic purposes.

106

5. Sands with angular grain shapes appear to have the greatest attenuation characteristics. Sands with rounded grain shapes appear to have the lowest attenuation characteristics. Wherever possible, avoid using sands with rounder grain shapes as backfill material.

D. RECOMMENDATIONS FOR FUTURE RESEARCH

1. Perform fully-instrumented full-scale weapon tests (100 to 200 kg explosive mass) in sand compacted at a representative saturation level to verify ground motion and stress wave propagation results obtained from the 0.227 kg to 7.0 kg explosive tests reported in this paper.

2. Evaluate past ground shock data and conduct additional centrifuge and field testing to quantitatively determine the effects of explosive confinement on peak ground motion parameter and peak stress magnitudes at varying compactive saturations.

3. Conduct a series of explosive tests at fixed compactive saturations, varying the sand's relative density to quantitatively assess its effects on peak ground motion and peak stress magnitudes.

4. Continue research at the microscopic level to determine the mechanism(s) by which capillary forces influence particle arrangement and orientation during compaction. Eventually develop analytical tools to predict particle arrangement and orientation and their effects upon stress transmission.

5. Conduct explosive testing on sands with diverse grain sizes, shapes and mineral composition to quantitatively determine the

107

probable ranges of peak ground motion and peak stress magnitudes for each sand type.

6. Develop a comprehensive, definitive data base of suggested design coefficients for varying sand types, compactive saturations, dry densities and explosive types.

REFERENCES

Ambraseys, N. R. and Hendron, A. J., (1968), "Dynamic Behavior of Rock Masses," _Rock Mechanics in Engineering Practice_, (K. G. Stagg and O. C. Zienkiewicz, Eds.), John Wiley & Sons, Inc., London, pp. 203-227.

ASTM (1987). Annual Book of ASTM Standards. American Society for Testing and Materials, Philadelphia, PA

Bishop, A. W. and Blight, G. E., (1963), "Some Aspects of Effective Stress in Saturated and Partly Saturated Soils," _Geotechnique_, Vol. 13, No. 3, Sept., pp. 177-197.

Bradley, D. M., Townsend, F. C., Fagundo, F. E. and Davidson, J. L., _Centrifugal Scaling Laws for Ground Launch Cruise Missile Shelter_, ESL-TR-84-07, Air Force Engineering and Services Center (RDCS), Tyndall Air Force Base, FL, April 1984, 90 pp., UNCLASSIFIED

Bretz, T. E., (1989), "Soil Liquefaction Resulting from Blast-Induced Spherical Stress Waves," Ph.D Dissertation, Department of Civil Engineering, Colorado State University, Fort Collins, CO, Fall, pp. 74,79,80.

Brownell, K. C., (1992a), "Centrifuge Modeling of Explosion-Induced Craters in Unsaturated Sand," M.S. Thesis, Department of Civil Engineering, Colorado State University, Fort Collins, CO, Fall, 218 pp.

Brownell, K. C. and Ross, C. A., (1992b), Personal Communication, Air Force Civil Engineering Support Center, Structural Research Branch, Tyndall Air Force Base, Panama City, FL

Buckingham, E., (1915), "Model Experiments and the Forms of Empirical Equations," _Transactions_, ASME, Vol. 37, June, pp. 551.

Charlie, W. A., Hassen, H., Doehring, D. and Hubert, M. (1987), "Microcomputers in Shock Testing of Water Saturated Sands," _The Shock and Vibration Bulletin_, No. 57, The Shock and Vibration Information Center, Naval Research Laboratory, Washington, DC, January, pp. 157-159.

Charlie, W. A., Ross, C. A. and Pierce, S. J., (1990a), "Split-Hopkinson Pressure Bar Testing of Unsaturated Sand," _Geotechnical Testing Journal_, ASTM, Vol. 13, No. 4, Dec., pp. 291-300.

Charlie, W. A., Walsh, A. J. and Brownell, K. C., (1990b), "Standard Operation Procedures to Enhance Scientific Research at the Colorado State University Engineering Research Center," Department of Civil Engineering, Colorado State University, Fort Collins, CO, Sept.

Cole, R. H., (1948), "_Underwater Explosions_," Princeton University Press, Princeton, NJ

Dowden, N. A., (1993), "Centrifuge Modeling of Stress Wave Attenuation in Poudre Valley Sand," M.S. Thesis, Department of Civil Engineering, Fort Collins, CO, Spring.

Dowding, C. H., (1985), _Blast Vibration Monitoring and Control_, Prentice-Hall, Inc., Englewood Cliffs, NJ, 297 pp.

Drake, J. D. and Little, C. D., (1983), "Ground Shock from Penetrating Conventional Weapons," Symposium Proceedings from The Interaction of Non-Nuclear Munitions with Structures, U.S. Air Force Academy, CO, May, pp. 1-6.

Editors, (1984), Military Explosives, TM 9-1300-214, HQ Department of the Army, Washington, DC, September, pp. 8-72,76,111.

Ensign-Bickford Company, (1984), Primacord® Handbook, Simsburg, CT, 500 pp.

Felice, C. W., (1986), The Response of Soil to Impulse Loads using the Split-Hopkinson Pressure Bar Technique, AFWL-TR-85-92, Air Force Weapons Laboratory, Air Force Systems Command, Kirtland Air Force Base, NM, May, UNCLASSIFIED.

Fredlund, D. G., (1985), "Soil Mechanics Principles That Embrace Unsaturated Soils," Eleventh International Conference of Soil Mechanics and Foundation Engineering, ISSMSM, Saskatoon, Saskatchewan, Canada, Vol. 2, pp. 465-471.

Hassan, H., (1993), "Saturated Sand Response and Liquefaction Under Planar Explosive Loading," M.S. Thesis, Department of Civil Engineering, Fort Collins, CO, Spring.

Holtz, R. D. and Kovacs, W. D., An Introduction to Geotechnical Engineering, Prentice-Hall, Englewood Cliffs, NJ, 1981, pp. 665-680.

Pierce, S. J., (1989), "High Intensity Compressive Stress wave Propagation Through Unsaturated Sands," M.S. Thesis, Department of Civil Engineering, Colorado State University, Fort Collins. CO, Spring, 127 pp.

Richart, F. E. Jr., Hall, J. R. Jr. and Woods, R. D., (1970), Vibrations of Soils and Foundations, Prentice-Hall, Inc., Englewood Cliffs, NJ, pp. 60-92.

Ross, C. A. (1989), Split-Hopkinson Pressure Bar Tests, Report No. ESL-TR-88-2, Air Force Engineering and Services Center (RDCM), Tyndall Air Force Base, FL, 80 pp.

Schure, L. A. (1990), "Porewater Pressure Increases Resulting from Blast-Induced Spherical Stress Waves," M.S. Thesis, Department of Civil Engineering, Fort collins, CO, Summer, 211 pp.

Veyera, G. E. and Fitzpatrick, B. J., (1990), Stress Transmission and Microstructure in Compacted Moist Sand, Contract No. F49620-88-C-0053/SB5881-0387, Air force Engineering and Services Center, Tyndall Air Force Base, FL, Dec., 56 pp., UNCLASSIFIED.

Veyera, G. E., (1992), Uniaxial Stress-Strain Behavior of Unsaturated Soils at High Strain Rates, Final Report, AFCESA/RACS, Tyndall Air Force Base, FL, 20 pp.

Walsh, A. J., (1993), "Centrifuge Modeling of Stress Wave Propagation in Unsaturated Sands," M.S. Thesis, Department of Civil Engineering, Colorado State University, Fort Collins, CO, Spring, 130 pp.

APPENDIX A

INSTRUMENTATION SPECIFICATIONS AND CALIBRATION DATA

ENDEVCO® SERIES 7270A
PIEZORESISTIVE ACCELEROMETERS

High g   High Resonant Frequency

The Model 7270A Series of Piezoresistive Accelerometers are rugged undamped units designed for shock measurements. ENDEVCO chemically sculptures the sensing system of the 7270A from a single piece of silicon. This etched silicon chip includes the inertial mass and strain gages arranged in an active four-arm Wheatstone bridge circuit complete with a novel on-chip zero balance network. The low mass, extremely small size and unique construction of the element blends an exceptionally high resonant frequency with characteristics such as low impedance, high overrange, and zero damping for no phase shift. The high resonant frequency of these sensors permits their survival in the presence of these high frequency components in a shock pulse that could shatter the seismic system of accelerometers having lower resonance. High resonance frequencies and zero damping allow the accelerometers to respond accurately to fast rise time, short duration shock motion. With a frequency response extending down to dc or steady state accelerations, these transducers are ideal for measurement of long duration transients.

(All values are typical at +75°F (+24°C) with 10 volts excitation applied unless otherwise specified.)

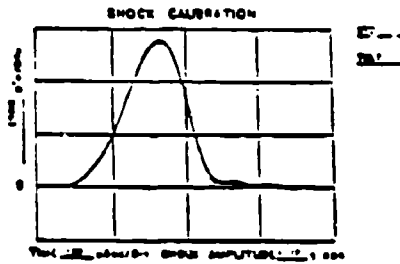|	MODEL 7270A-6K	MODEL 7270A-20K
PERFORMANCE		
RANGE g	6000	20 000
SENSITIVITY		
(at 10 Vdc excitation, ref 100 Hz)		
Minimum/Maximum µV/g	18/50	8/15
NON-LINEARITY & HYSTERESIS		
(% of reading, max to full range) %	±1	±2
FREQUENCY RESPONSE[1]		
(±5% max, ref 100 Hz) kHz	20	50
MOUNTED RESONANT FREQ kHz	180	350
TRANSVERSE SENSITIVITY (max) %	5	5
THERMAL SENSITIVITY SHIFT		
(ref +75°F (+24°C)) %/°F	−.06	−.06
%/°C	−.12	−.12
ZERO MEASURAND OUTPUT (max) mV	±100	±100
THERMAL ZERO SHIFT (max)[2] mV	±30	±30
BASE STRAIN SENSITIVITY		
(at 250 µstrain) mV	<5	<5
OVERRANGE LIMITS g	16 000	60 000
ELECTRICAL		
EXCITATION[3][4] Vdc	10.0	10.0
INPUT RESISTANCE[5] Ω	850	850
OUTPUT RESISTANCE[5] Ω	850	850
INSULATION RESISTANCE		
(minimum at 100 Vdc) MΩ	100 between sensors, cable shield or case.	
GROUNDING	Cable shield isolated from sensors and case.	
	Case isolated from sensors.	
PHYSICAL		
WEIGHT (excluding cable) oz (gm)	0.05 (1.5)	
CASE MATERIAL	17-4 ph CRES	
ELECTRICAL CONNECTIONS	Integral 4-conductor shielded cable, 4 ft (1.2 m), minimum.	
MOUNTING/TORQUE[6]	Two holes for 4-40 high strength screws and #4 washers.	
ENVIRONMENTAL		
TEMPERATURE		
Operating °F (°C)	−20 to +150 (−18 to +66)	
Non-Operating °F (°C)	−65 to +250 (−54 to +121)	
HUMIDITY	Sealed by epoxy	

Figure A.1   ENDEVCO Model 7270A 6,000 g and 20,000 g Accelerometer Specifications.

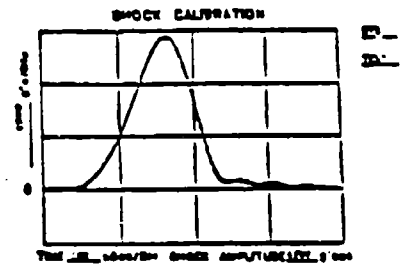**TABLE A.1. ENDEVCO MODEL 7270A ACCELEROMETER CALIBRATION DATA.**

Instrument #	Range, g's	Sensitivity, µV/g
EN20F	6,000	29.134
EN23F	6,000	30.269
EN25F	6,000	30.260
EN27F	20,000	8.470
EN35F	6,000	28.554
EN37F	6,000	30.447
EN39F	20,000	7.871
EN43F	20,000	9.242
EN44F	20,000	9.218
EN47F	20,000	11.087
EN52F	20,000	10.010
EM60F	6,000	30.094
EN61F	6,000	32.068
EN65F	6,000	31.591

Calibration data supplied by Endevco Co,
Calibrations are traceable to N.B.S.
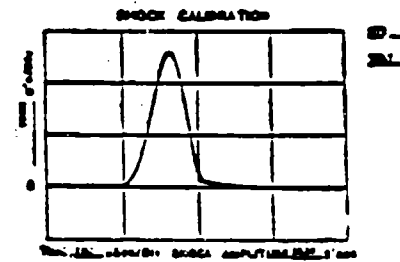
Figure A.2 Endevco Model 7270A 6,000 g Accelerometer Calibration Curves.

114
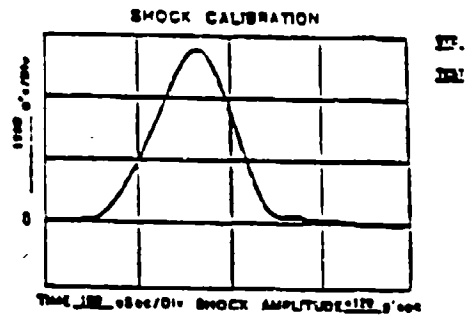
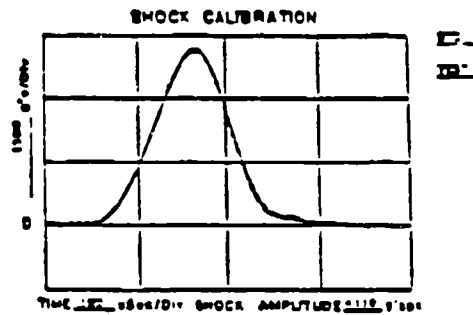Figure A.3   Endevco Model 7270A 20,000 g Accelerometer Calibration Curves.

TABLE A.2.   ENDEVCO UNIVERSAL SIGNAL CONDITIONING SYSTEM SERIES 4470 WITH
              4476.1A MODE CARD (REPRINTED FROM BRETZ, 1989).

Specifications

Input Characteristics

Transducers	2 or 4 arm resistive elements
Input Impedance	1 megaohm maximum
Source Resistance	2000 ohms maximum
Overload Recovery Time	50 microseconds
Common Mode Rejection	80 dB minimum at 60 Hz
	70 dB minimum at 1000 Hz
Common Mode Voltage	5 V peak, maximum

Output Characteristics

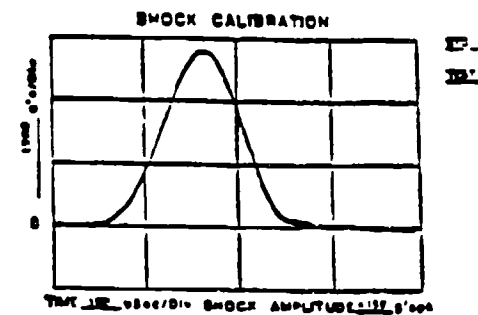|	
Output Voltage	
Full Scale	± 2.5 V peak
Overvoltage	± 7.5 V peak maximum
Linear Output Current	± 10 mA peak maximum
Output Impedance	less than 20 ohms
Noise and Ripple	2 mV rms, maximum
Capacitive Load Effect	stable to 10 microfarads
Zero Stability and	
Temperature Coefficient	0.2% of FS for 24 hours plus
	0.02% per degree F

Transducer Excitation Regulator

|	
Output Voltage	Adjustable 9.5 to 10.5 VDC
Output Current	0 to 50 mA DC
Line and Load Regulation	Less than 0.2% change for line voltage change 95 to 135 VAC and load change 2000 to 300 ohms
Temperature Stability	Less than 0.005% per degree C over temperature range (-12° C to + 65° C)
Time Stability	Less than 0.03% for 48 hours

Transfer Characteristics

Gain Ranges	Full Scale Output (FSO) for 20, 40, 60, 80, or 100% of full range acceleration
Accuracy	± 1.5% of full scale
Frequency Response	± 5% DC to 20,000 hz
Gain Stability	less than ± 0.1% for 24 hours plus ± 0.009% per degree C
DC Linearity	less than ± 2.5 mV
Balance Limiting	40.2 kiloohm resistor

KULITE

LQ-080U

SOIL STRESS GAGE
Designed and developed in cooperation with the
U.S. Army Corp of Engineer Waterways Experiment
Station, Vicksburg, Mississippi.
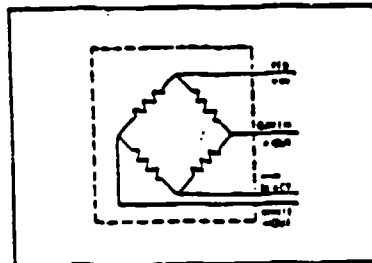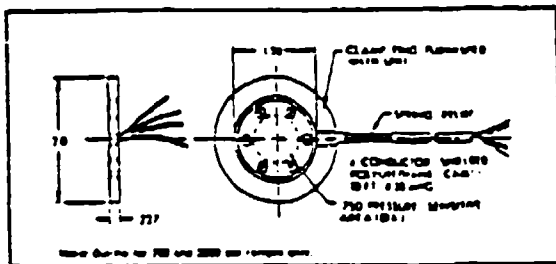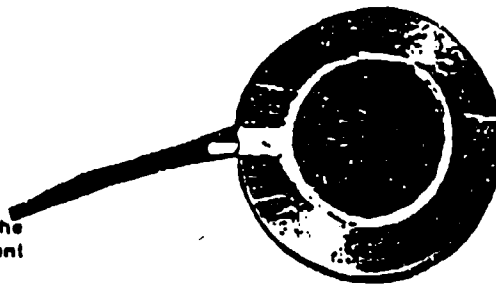
The LQ-080U series of soil stress gages are designed to meet the requirements of the civil engineering field to make accurate measurements of blast induced soil reactions.

Inclusion of a gage in soil disrupts the stress field and induces either stress concentrations or reliefs depending on gage thickness. This stress-transfer phenomenon can seriously affect gage accuracy. To overcome this erection, the LQ-080U employs a pair of extremely stiff diaphragms with a diameter-to-thickness ratio of greater than 5 and a diameter-to-deflection ratio of greater than 2000. This design together with good gage-medium matching ensures accuracy and repeatability of readings.

The DC energized sensing element of the LQ-080U comprises 4 active semiconductor strain gages directly bonded to the measuring diaphragms. The output may be conveniently monitored on most conventional instrument systems. During assembly, the entire unit is given a conformal coating to prevent any ingress of moisture after final on-site installation.

The LQ-080U Series is available calibrated or uncalibrated, with or without mounting ring.

SPECIFICATIONS

Figure A.4   Kulite LQ-080U Soil Stress Gage Specifications.

117

TABLE A.3.   SOIL STRESS GAGE CALIBRATION DATA.

Instrument #	Mounting ring	Range, psi	Sensitivity, psi/V*
SN 8426885	YES	3000	3600
SN 5418885	YES	3000	3600
SN 7422185	YES	3000	3600
SN 8426085	YES	3000	3600
SN 115550187	YES	3000	3600
SN 095513191	NO	6000	12,358
SN 095513291	NO	6000	12,204
SN 095513391	NO	6000	11,893
SN 095513491	NO	6000	11,936
SN 095513591	NO	6000	11,862
SN 095512791	NO	6000	13,387
SN 095513891	NO	6000	12,337

* Input voltage= 12 V

Note: Static laboratory calibration at Colorado State University
established that soil stress gages without a mounting ring yielded output
stresses an average of 2.4 times greater than soil stress gages with a
mounting ring. Gages without mounting rings yielded output stresses very
close to the manufacturer's fluid calibration data.

APPENDIX B

FIELD TEST RESULTS

The following tables present raw field data for explosive tests conducted in Poudre Valley sand at 0, 13, 20, 40, 60 and 70 percent compactive saturations utilizing 6.22, 7.0 kg and 0.227 kg charge masses.

Accelerometers are abbreviated with an "A" and soil stress gages are abbreviated with a "T". Instrument numbers are succeeded by either an "S" or an "F", denoting that the test was conducted either in the Spring of 1992 or the Fall of 1991. Duplicate distances arise from more than one instrument being placed at the same distance.

Data cells with no numerical entry indicate that data was not provided by particular instrument or that data was not available due to noise interference or some other factor. For example, stress data for the 0.227 kg shot was not discernible from the magnitude of the noise originating from the TDR's digitizer.

INSTRUMENT #	DISTANCE (m)	DISTANCE (m)	SCALED DISTANCE (m/kg^1/3)	PEAK PARTICLE ACCELERATION (g's)	PEAK SCALED PARTICLE ACCELERATION (g's·kg^1/3)	PEAK PARTICLE VELOCITY (m/s)	PEAK SOIL STRESS (kpa)	ARRIVAL TIME (s)	RISE TIME (s)	INTERVAL WAVE SPEED (m/s)
0.2 kg TEST										
A1-S	3.17	0.9892	0.9254	13074	25778	8.12	—	0.000128	0.000040	208.88
A2-S	3.07	1.1188	0.9893	6530	16318	5.87	—	0.000328	0.000068	201.00
A3-S	4.07	1.4234	0.7740	5670	10847	3.23	—	0.000528	0.000128	204.80
A4-S	5.07	1.7282	0.9300	3000	7450	3.00	—	0.005020	0.000170	224.46
A5-S	6.11	1.9806	1.0228	3728	7132	2.71	—	0.005620	0.000100	217.71
A6-S	3.17	0.9892	0.9254	20040	34780	8.12	—	0.000128	0.000100	208.88
A7-S	3.07	1.1188	0.9893	13578	25973	5.46	—	0.003626	0.000110	204.60
A8-S	4.07	1.4234	0.7740	6228	15742	4.03	—	0.004928	0.000110	254.00
A9-S	5.07	1.7282	0.9300	7810	14941	2.81	—	0.008320	0.000080	203.00
T1-S	3.17	0.9892	0.9254	—	—	—	5304.00	0.000128	—	—
T2-S	3.07	1.1188	0.9893	—	—	—	3208.00	0.003128	—	—
T3-S	4.07	1.4234	0.7740	—	—	—	3254.00	0.004428	—	—
T4-S	5.07	1.7282	0.9300	—	—	—	1227.00	0.008078	0.000110	—
T5-S	6.01	2.0138	1.1055	—	—	—	1172.00	—	—	—
T6-S	3.17	0.9892	0.9254	—	—	—	—	—	—	—
T7-S	4.07	1.4234	0.7740	—	—	—	1986.00	0.004728	0.000080	—
0.227 kg TEST										
A1-S	4.08	1.4295	2.3435	67	83	0.26	—	0.000208	0.000028	174.18
A2-S	5.17	1.5758	2.5833	47	28	0.25	—	0.000630	0.000110	202.64
A3-S	6.13	1.8145	3.0130	20	12	0.14	—	0.001330	0.001820	121.46
A4-S	7.12	2.1702	3.5577	14	9	0.08	—	0.014000	0.002100	142.83
A5-S	7.01	2.3105	3.8025	10	6	0.08	—	0.014000	0.002620	99.57
A6-S	4.08	1.3411	2.1886	77	47	0.26	—	0.007400	0.000878	181.23
A7-S	4.07	1.4844	2.3334	61	37	0.20	—	0.008490	0.001060	111.22
A8-S	5.01	1.7708	2.8031	30	18	0.18	—	0.011330	0.001950	106.45
A9-S	6.78	2.0685	3.3078	10	10	0.08	—	0.014000	0.001860	110.73
T1-S	4.08	1.4295	2.3435	—	—	—	—	—	—	—
T2-S	5.17	1.5758	2.5833	—	—	—	—	—	—	—
T3-S	6.13	1.8145	3.0130	—	—	—	—	—	—	—
T4-S	7.12	2.1702	3.5577	—	—	—	—	—	—	—
T5-S	7.01	2.3105	3.8023	—	—	—	—	—	—	—
T6-S	4.08	1.4295	2.3435	—	—	—	—	—	—	—
T7-S	6.15	1.8745	3.0130	—	—	—	—	—	—	—

TABLE B.2. RESULTS OF FIELD TEST CONDUCTED AT 13 PERCENT COMPACTIVE SATURATION.

122

TABLE B.3. RESULTS OF FIELD TEST CONDUCTED AT 20 PERCENT COMPACTIVE SATURATION.

TABLE B.4. RESULTS OF FIELD TEST CONDUCTED AT 40 PERCENT COMPACTIVE SATURATION.

INSTRUMENT #	DISTANCE (m)	DISTANCE (m)	SCALED DISTANCE (m/kg**1/3)	PEAK PARTICLE ACCELERATION (g's)	PEAK SCALED PARTICLE ACCELERATION (g's*kg**1/3)	PEAK PARTICLE VELOCITY (m/s)	PEAK SOIL STRESS (kpa)	ARRIVAL TIME (s)	RISE TIME (s)	INTERVAL WAVE SPEED (m/s)
7.0 kg TEST										
A1-F	3.00	0.8146	0.4780	3079	7421	12.16	—	0.002720	0.000940	338.18
A2-F	3.50	1.0668	0.5577	4404	8425	8.98	—	0.003248	0.000740	293.04
A3-F	4.50	1.3718	0.7170	3898	7453	5.63	—	0.004429	0.000980	258.25
A4-F	6.50	1.9812	1.0357	2745	5251	2.78	—	0.007000	0.000820	237.11
T1-F	3.00	0.8146	0.4780	—	—	—	—	—	—	—
T2-F	3.50	1.0668	0.5577	—	—	—	—	—	—	—
T3-F	4.50	1.3718	0.7170	—	—	—	—	—	—	—
T4-F	6.50	1.9812	1.0357	—	—	—	—	—	—	—
0.227 kg TEST										
A1-S	3.58	1.0912	1.7898	164	100	0.78	—	0.005148	0.001920	211.98
A2-S	4.71	1.4358	2.3535	77	47	0.40	—	0.007128	0.001994	173.95
A3-S	5.87	1.7282	2.8331	39	24	0.17	—	0.009708	0.001312	113.11
A4-S	6.63	2.0193	3.3103	27	18	0.20	—	0.010364	0.002496	195.00
A5-S	7.58	2.3104	3.7875	10	6	0.18	—	0.011600	0.004096	195.00
T1-S	3.58	1.0912	1.7898	—	—	—	—	—	—	—
T2-S	4.71	1.4358	2.3535	—	—	—	—	—	—	—
T3-S	5.87	1.7282	2.8331	—	—	—	—	—	—	—
T4-S	6.63	2.0193	3.3103	—	—	—	—	—	—	—
T5-S	7.58	2.3104	3.7875	—	—	—	—	—	—	—

TABLE B.5. RESULTS OF FIELD TEST CONDUCTED AT 60 PERCENT COMPACTIVE SATURATION.

INSTRUMENT #	DISTANCE (ft)	DISTANCE (m)	SCALED DISTANCE (m/kg^1/3)	PEAK PARTICLE ACCELERATION (g's)	PEAK SCALED PARTICLE ACCELERATION (g's*kg^1/3)	PEAK PARTICLE VELOCITY (m/s)	PEAK SOIL STRESS (kpa)	ARRIVAL TIME (s)	RISE TIME (s)	INTERVAL WAVE SPEED (m/s)
7.0 kg TEST										
A1-F	3.00	0.9144	0.4780	3781	7233	11.78	—	0.002900	0.000700	351.69
A2-F	3.50	1.0668	0.5577	8314	15804	11.50	—	0.003100	0.000440	390.00
A3-F	4.50	1.3716	0.7170	4925	8517	5.32	—	0.004600	0.000500	204.29
A4-F	6.50	1.9812	1.0357	2072	3581	3.38	—	0.007879	0.000800	187.99
T1-F	3.00	0.9144	0.4780	—	—	—	12913	0.002900	—	315.31
T2-F	3.50	1.0668	0.5577	—	—	—	6840	0.003750	—	179.29
T3-F	4.50	1.3716	0.7170	—	—	—	3404	0.004750	—	304.80
T4-F	4.50	1.3716	0.7170	—	—	—	3127	0.004750	—	304.80
0.227 kg TEST										
A6-S	3.58	1.0912	1.7808	100	110	0.67	—	0.005120	0.000440	213.12
A7-S	4.71	1.4356	2.3535	73	45	0.32	—	0.007128	0.000620	171.53
A8-S	5.87	1.7282	2.8331	25	15	0.14	—	0.009128	0.001580	148.30
A9-S	8.63	2.6208	3.3128	14	8	0.18	—	—	—	—
T8-S	4.71	1.4356	2.3535	—	—	—	—	—	—	—
T7-S	8.63	2.6193	3.3163	—	—	—	—	—	—	—

TABLE B.6.   RESULTS OF FIELD TEST CONDUCTED AT 70 PERCENT COMPACTIVE SATURATION.

INSTRUMENT #	DISTANCE (m)	DISTANCE (m)	SCALED DISTANCE (m/kg**1/3)	PEAK PARTICLE ACCELERATION (g's)	PEAK SCALED PARTICLE ACCELERATION (g's*kg**1/3)	PEAK PARTICLE VELOCITY (m/s)	PEAK SOIL STRESS (kpa)	ARRIVAL TIME (s)	RISE TIME (s)	INTERVAL WAVE SPEED (m/s)
70 kg TEST										
A1-F	3.00	0.9144	0.4780	11258	21538	10.60	—	0.002850	0.000160	320.84
A2-F	3.50	1.0668	0.5577	6048	11571	9.04	—	0.003400	0.000180	277.09
A3-F	4.50	1.3716	0.7170	5305	10148	8.06	—	0.004760	0.000240	224.12
A4-F	6.50	1.9812	1.0357	2838	5429	2.01	—	0.007900	0.000240	184.14
T1-F	3.00	0.9144	0.4780	—	—	—	—	—	—	—
T2-F	3.50	1.0668	0.5577	—	—	—	16267	0.003320	—	321.00
T3-F	4.50	1.3716	0.7170	—	—	—	11947	0.004400	—	282.00
T4-F	6.50	1.9812	1.0357	—	—	—	—	—	—	—

126

APPENDIX C

SUPPLEMENTAL PLOTS OF RESULTS

Analysis of Propagation Velocity Plots

Figures C.1 and C.2 show interval propagation velocity variation with distance for the 6.22 kg, 7.0 kg and 0.227 kg shots. In both figures, interval propagation velocity begins to level off with increasing distance from the center of explosion. The plots for 0 and 60 percent saturation show a moderately sharper rate of decrease in propagation velocity over distance than the plots for 13, 20 and 40 percent saturations. This correlates with the attenuation trends for propagation velocity in Figures 5.3 and 5.4.

Figures C.3 and C.4 show the interrelationship between interval propagation velocity and peak particle velocity for the 6.22 kg, 7.0 kg and 0.227 kg shot. One interesting feature that stands out in Figure C.3 (7.0 kg shot) is that the lowest propagation velocities associated with a given peak particle velocity occur in the 13 percent test. The opposite is true in Figure C.4 (0.227 kg shot)-- the highest propagation velocities associated with a given peak particle velocity occur in the 13 percent test. Although propagation velocities are lower at smaller scaled ranges for the 13 percent test, low attenuation rates result in higher propagation velocities at greater scaled ranges.

These characteristics match trends seen in Figures 5.1 and 5.2. The lowest values for peak particle acceleration, peak particle velocity and peak particle stress in Figure 5.1 and some of the highest slope values in Figure 5.2 occur at 13 percent saturation. Similar trends are noticed in Figures 2.5a and 2.6.

In Figure C.5, propagation velocity attenuation characteristics similar to those in Figure C.3 and C.4 are noticed in the 13 percent and 20 percent test.

Figures C.8 and C.9 show plots of pulse rise time versus arrival time. Drake and Little (1983) approximate that rise time should be one-tenth the arrival time according to Equation (2.5). Values of t_r/t_a for the 6.22 kg, 7.0 kg and 0.227 kg shots compare fairly closely to .10.

128

Figures C.10, C.11 and C.12 show scaled peak particle acceleration, peak particle velocity and peak stress plotted as a function of scaled range for Poudre Valley (present investigation), Tyndall, Ottawa (Walsh, 1993) and sands of varying density (Drake and Little, 1983) for comparison.

Figure C.1 Interval Propagation Velocity versus Distance for Tests Conducted at 0, 13, 20, 40, 60 and 70 Percent Saturations in Poudre Valley Sand using 6.22 kg and 7.0 kg Charge Masses.

130

Figure C.2 Interval Propagation Velocity versus Distance for Tests Conducted at 0, 13, 20, 40, 60 and 70 Percent Saturations in Poudre Valley Sand using a 0.227 kg Charge Mass.

131

Figure C.3   Interval Propagation Velocity versus Peak Particle Velocity
             for Tests Conducted at 0, 13, 20, 40, 60 and 70 Percent
             Saturations in Poudre Valley Sand using 6.22 kg and 7.0 kg
             Charge Masses.

Figure C.4 Interval Propagation Velocity versus Peak Particle Velocity
for Tests Conducted at 0, 13, 20, 40, and 60 Percent
Saturations in Poudre Valley Sand using a 0.227 kg Charge
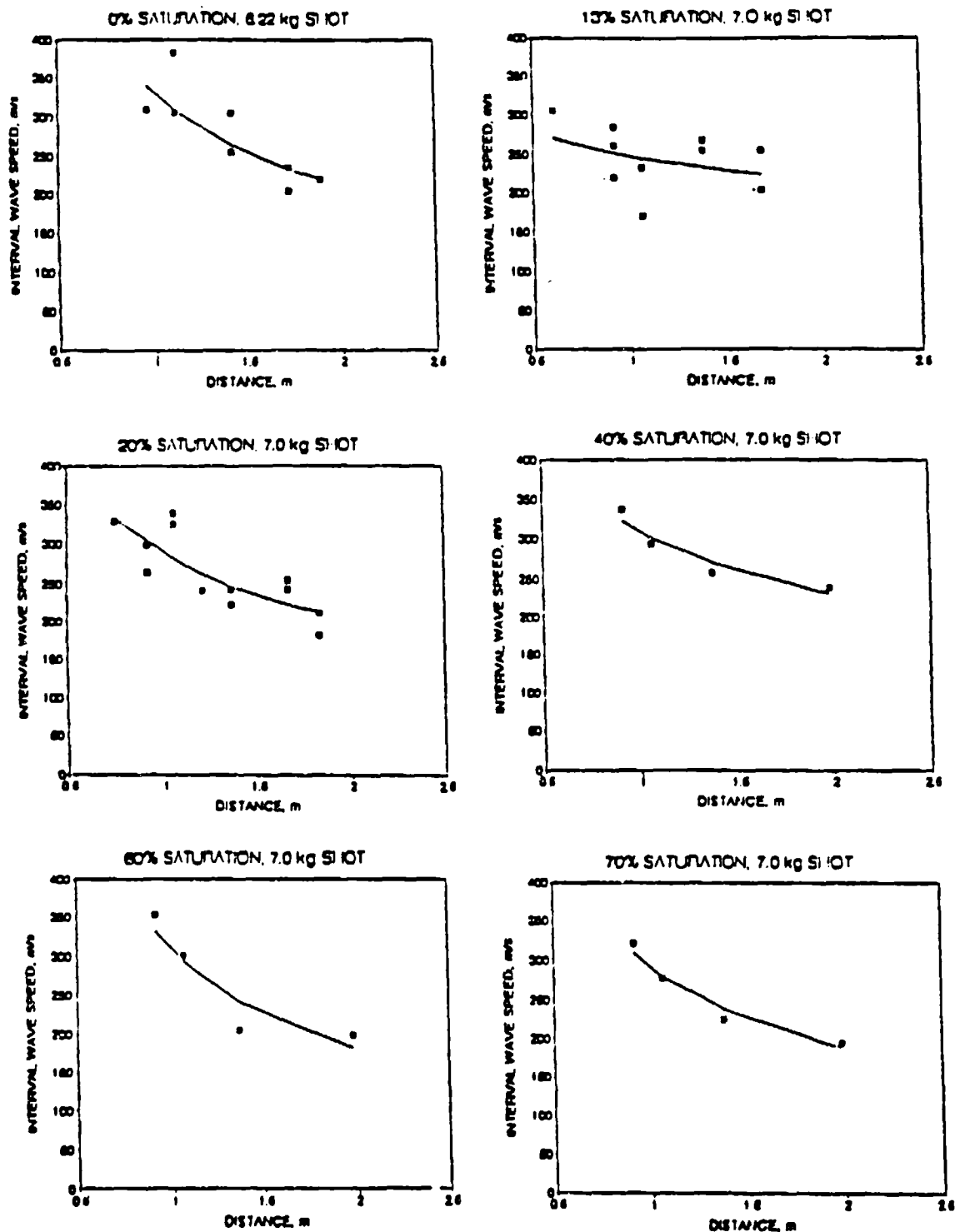Mass.

133
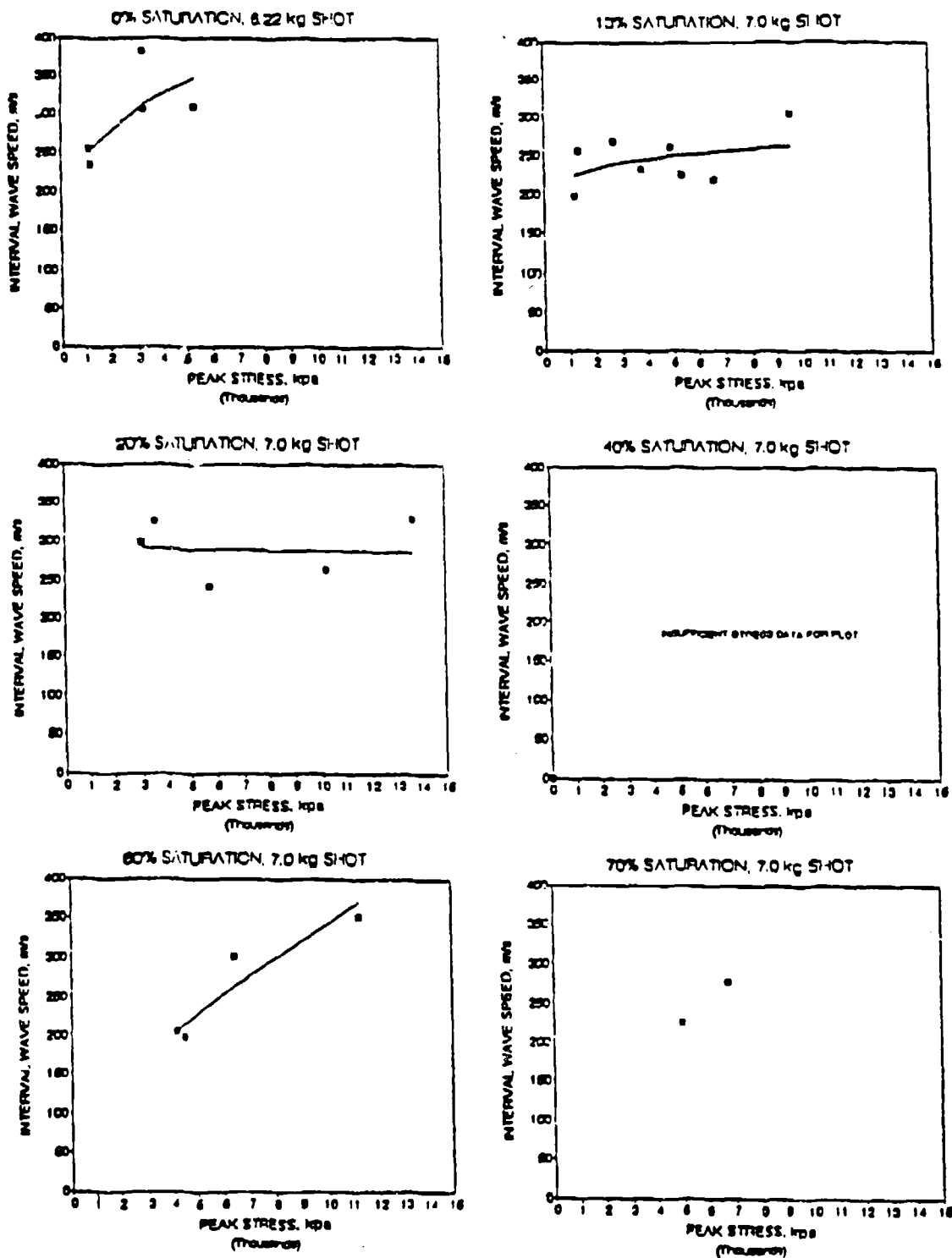
Figure C.5 Interval Propagation Velocity versus Peak Stress for Tests Conducted at 0, 13, 20, 40, 60 and 70 Percent Saturations in Poudre Valley Sand using 6.22 kg and 7.0 kg Charge Masses.
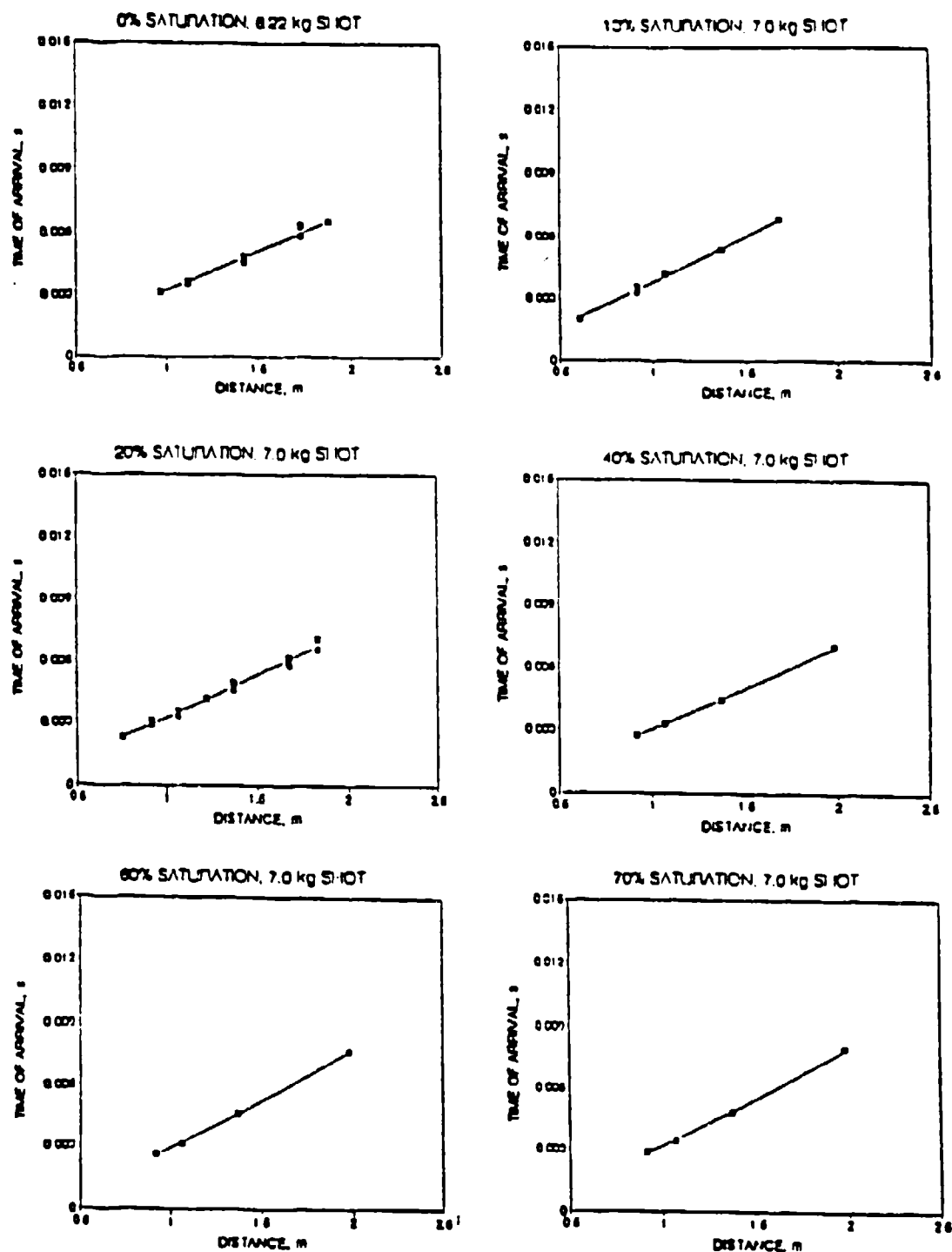
Figure C.6   Pulse Time of Arrival versus Distance for Tests Conducted at
0, 13, 20, 40, 60 and 70 Percent Saturations in Poudre Valley
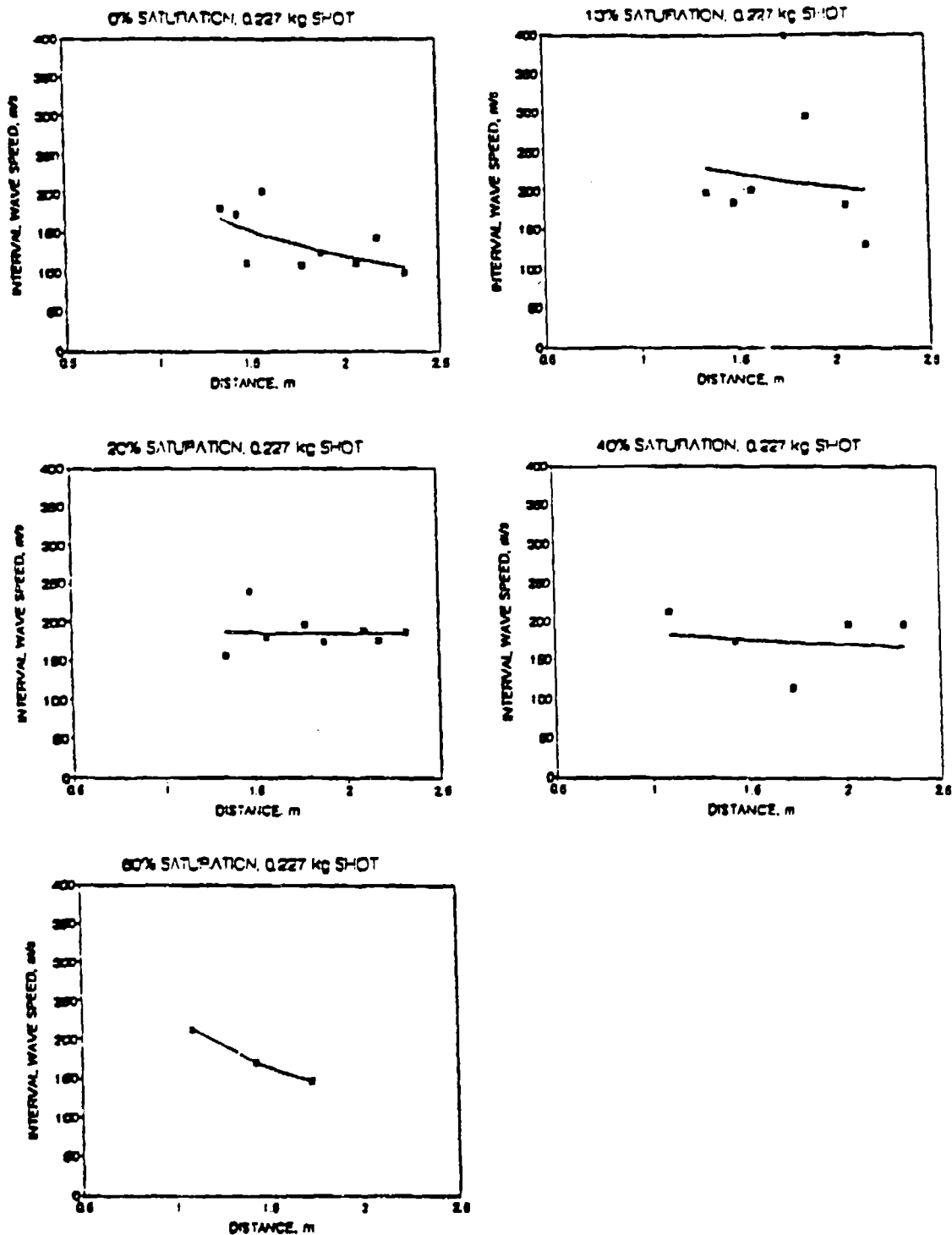Sand using 6.22 kg and 7.0 kg Charge Masses.

135
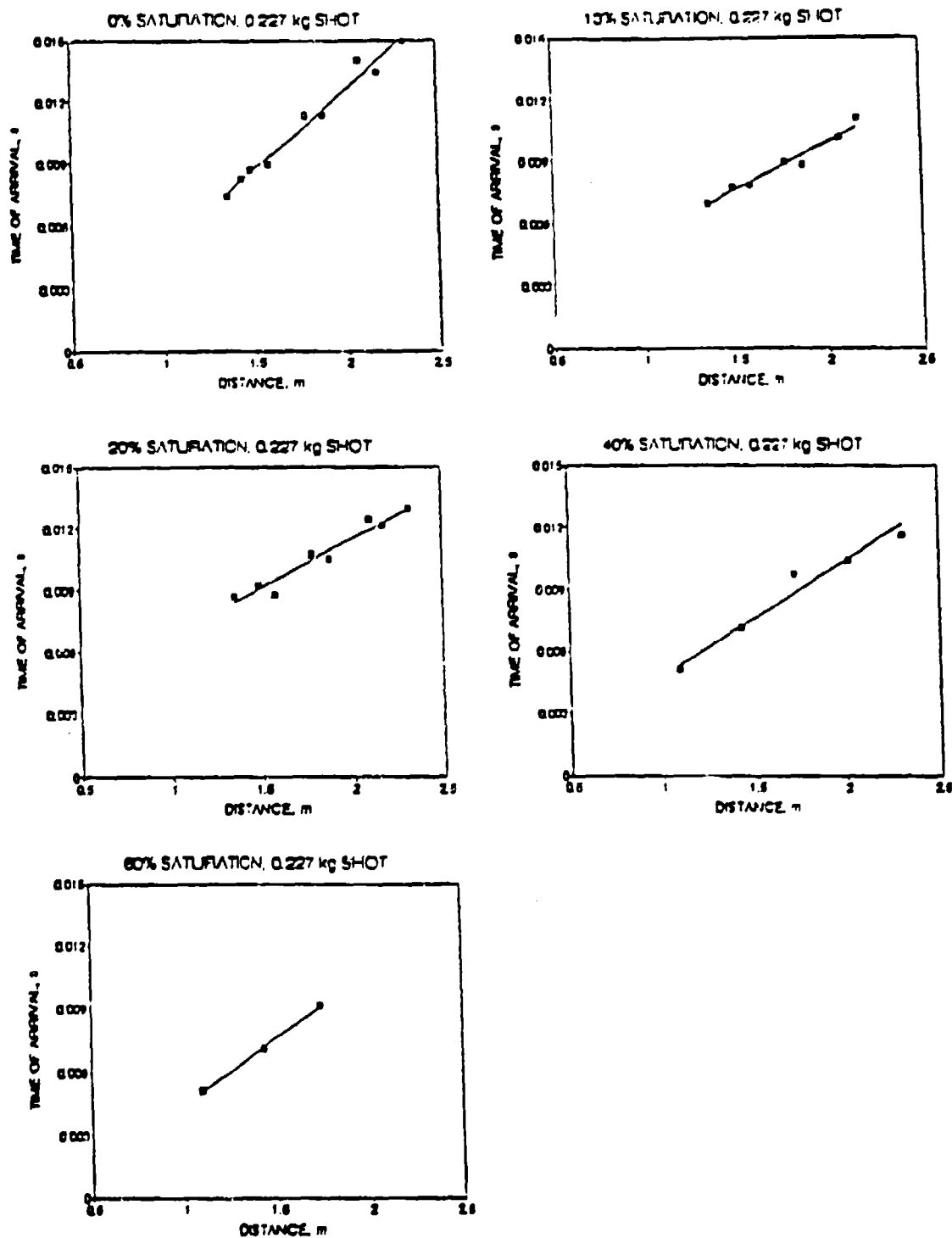
Figure C.7   Pulse Time of Arrival versus Distance for Tests Conducted at
0, 13, 20, 40, 60 and 70 Percent Saturations in Poudre Valley
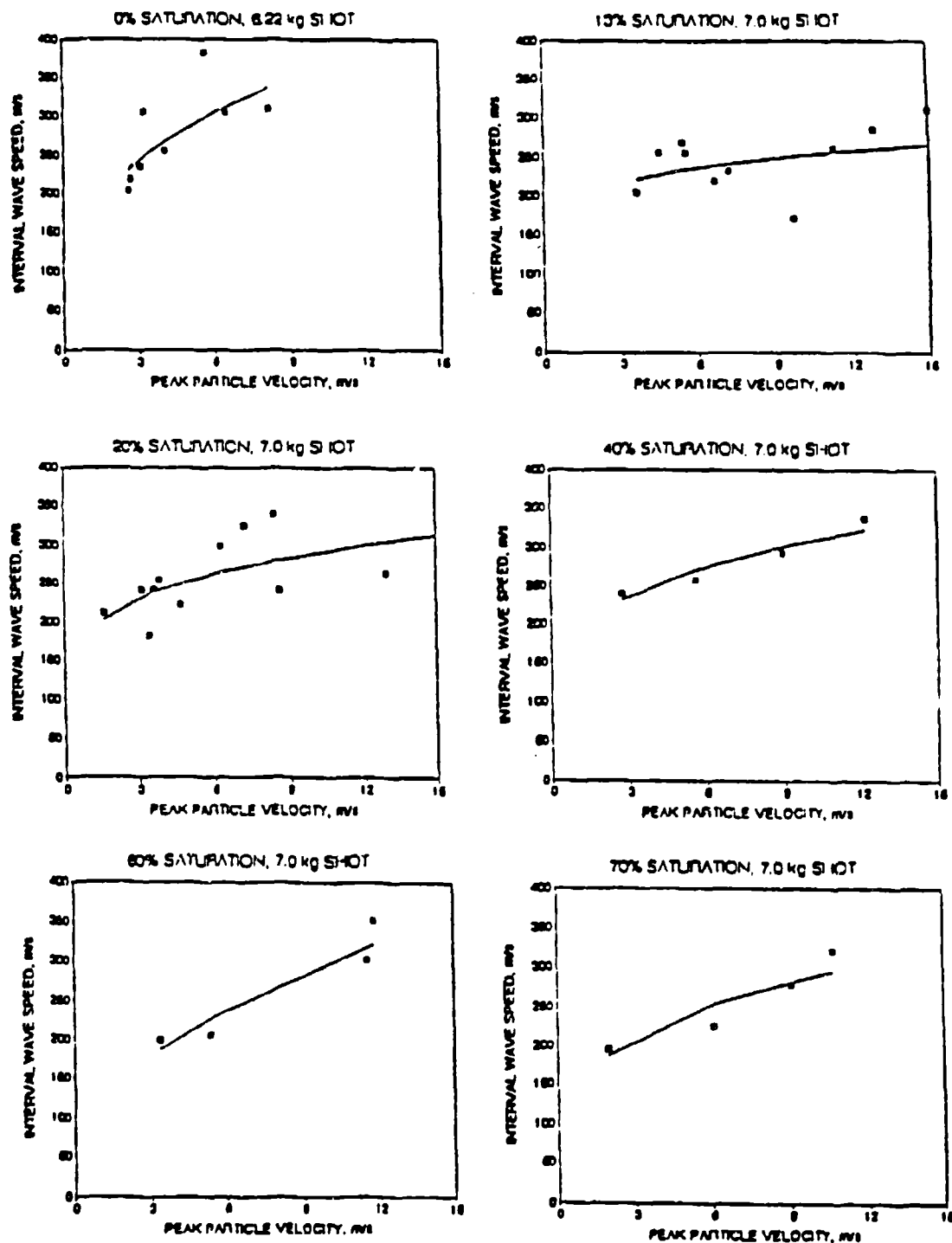Sand using a 0.227 kg Charge Mass.

136
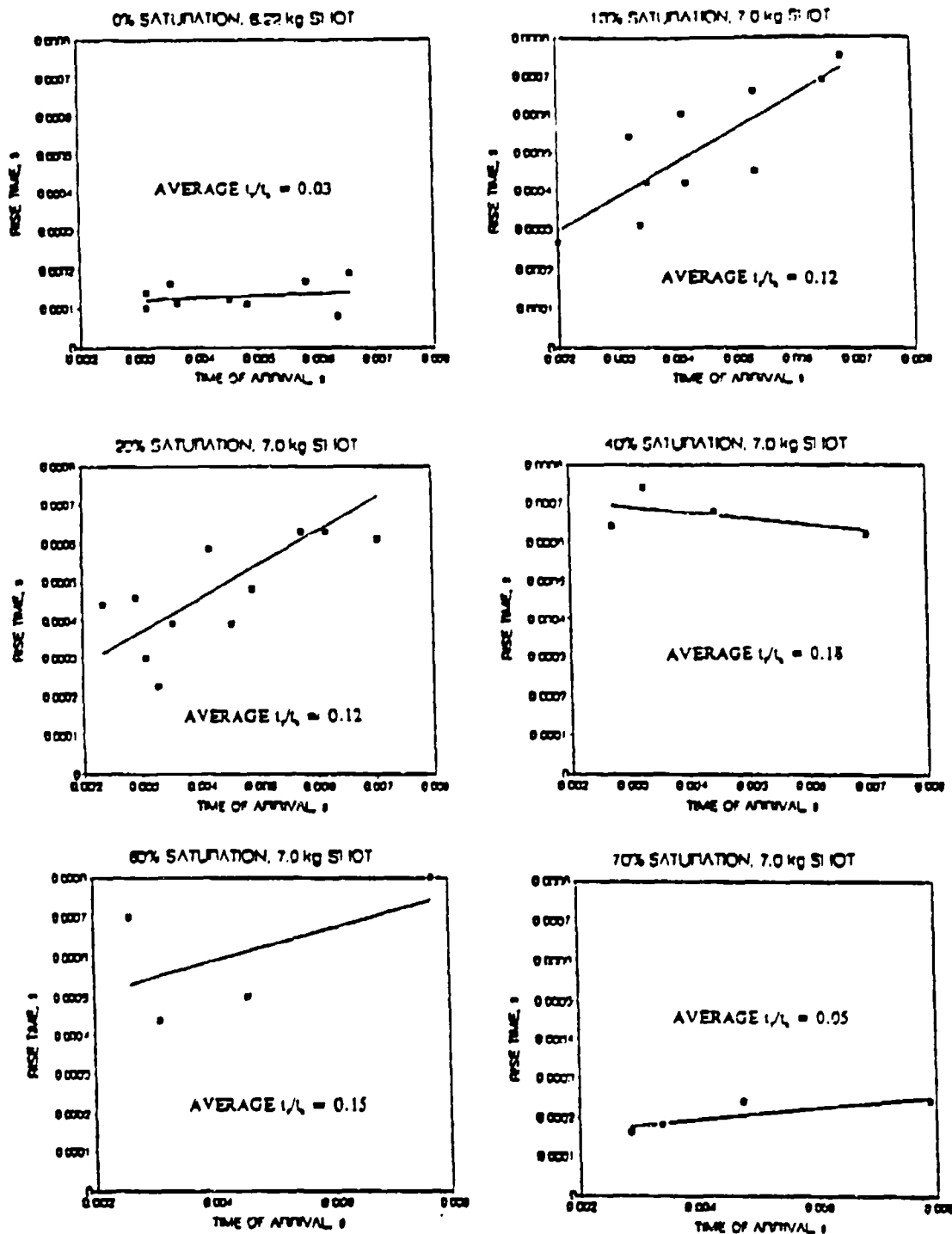
Figure C.8   Pulse Rise Time versus Time of Arrival for Tests Conducted at 0, 13, 20, 40, 60 and 70 Percent Saturations in Poudre Valley Sand using 6.22 and 7.0 kg Charge Masses.

137
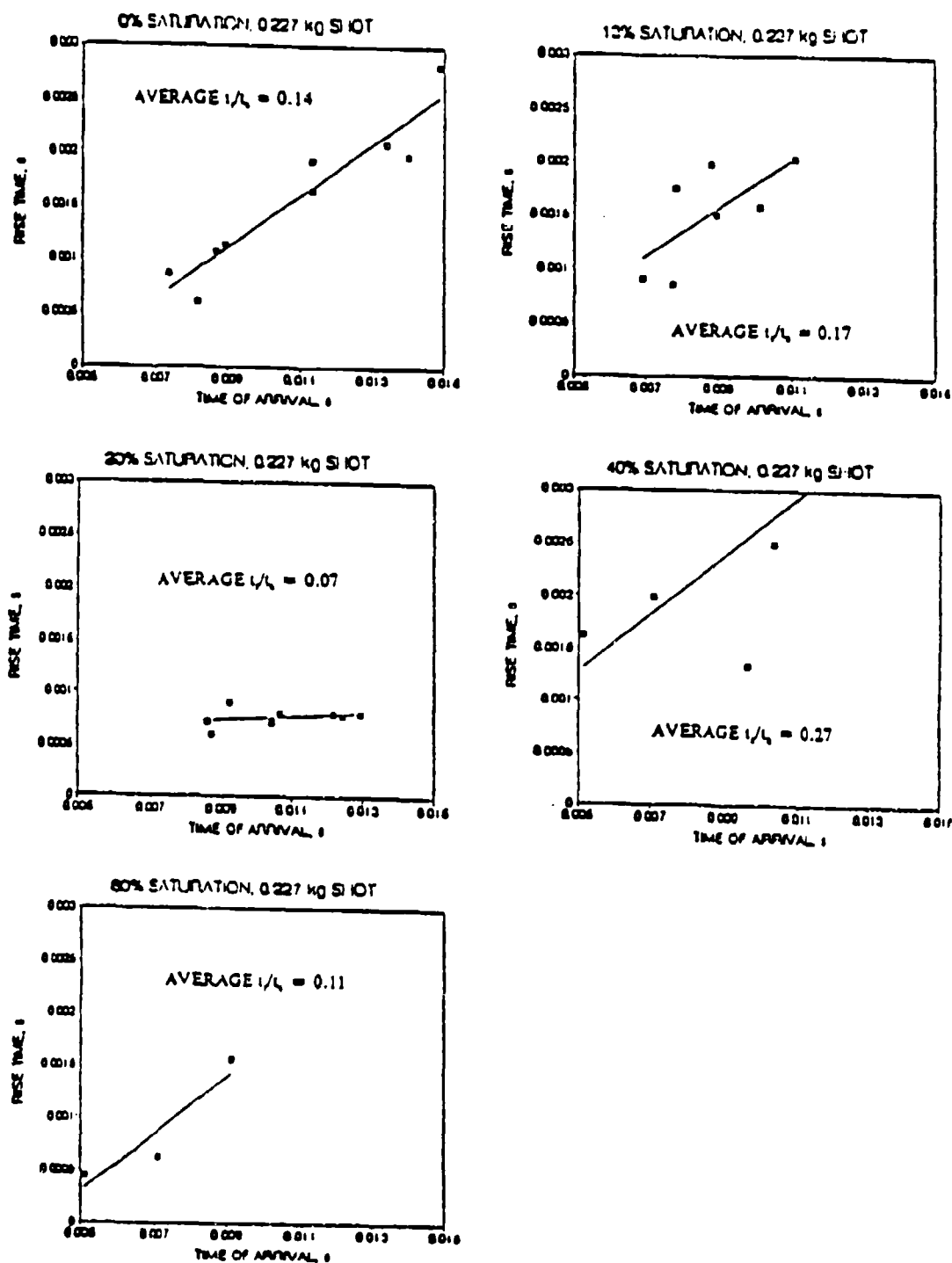
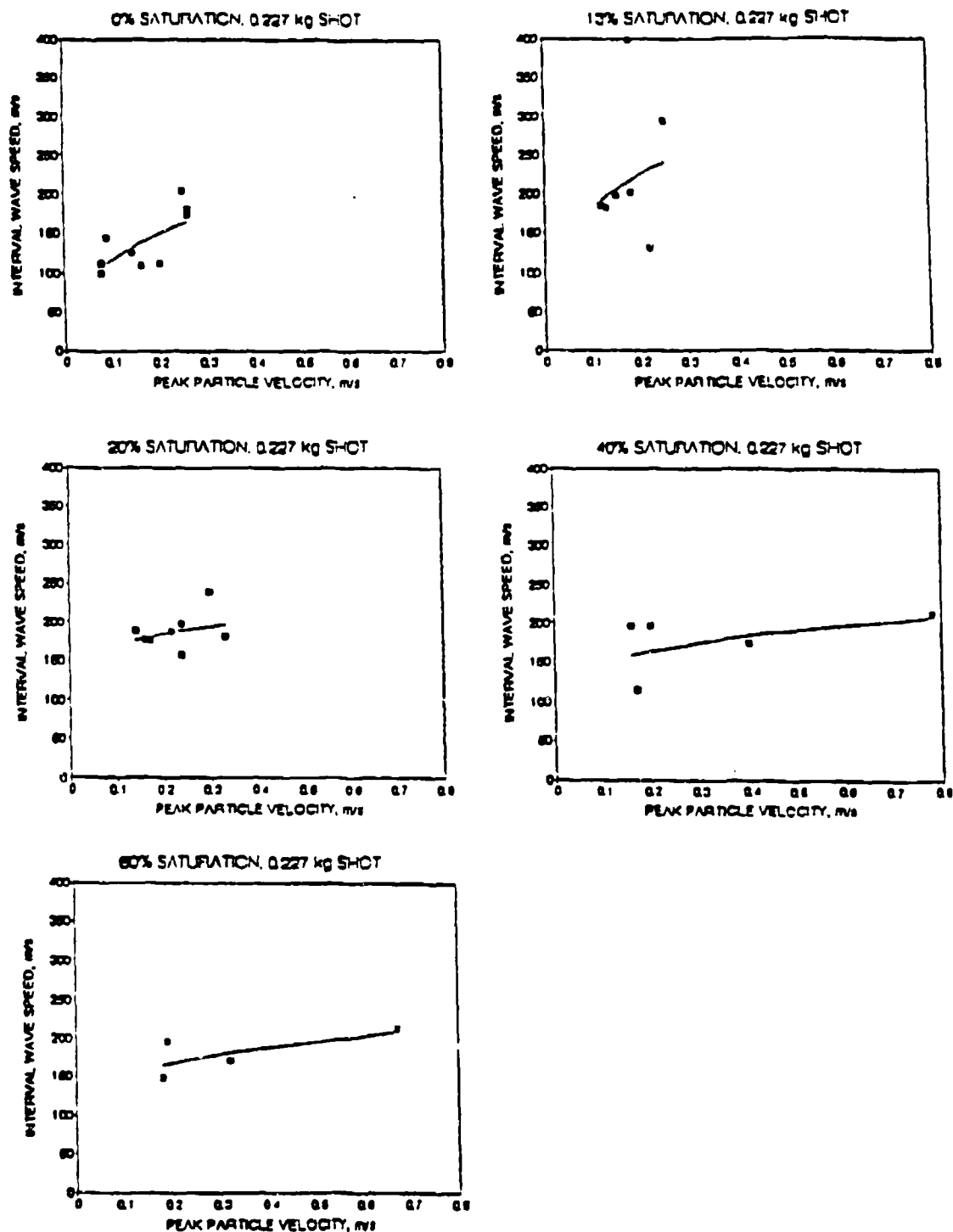**Figure C.9** Pulse Rise Time versus Time of Arrival for Tests Conducted at 0, 13, 20, 40 and 60 Percent Saturations in Poudre Valley Sand using a 0.227 kg Charge Mass.

138
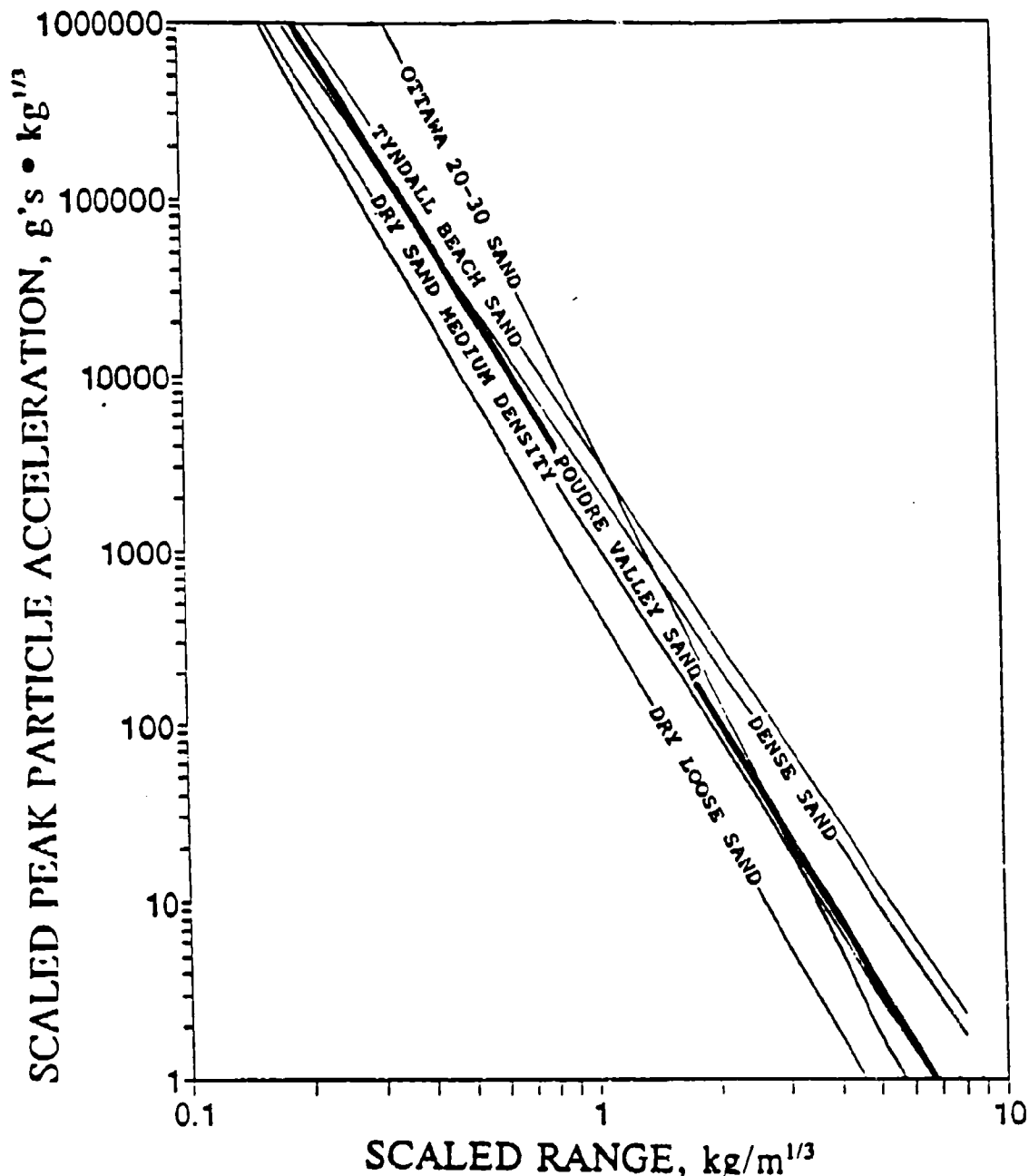
note: equations for average scaled peak particle acceleration are
          used to plot curves for Poudre Valley, Tyndall Beach and
          Ottawa 20-30 sands (see Section V.B.4 for development of
          equations).

Figure C.10 Scaled Peak Particle Acceleration versus Scaled Range from
             Explosive Field Testing in Poudre Valley Sand, Explosive
             Centrifuge Testing in Tyndall Beach and Ottawa 20-30 Sands
             (Walsh 1993), and Explosive Data for Varying Sand Densities
             Replotted from Figure 2.2 (Drake and Little 1983).

139
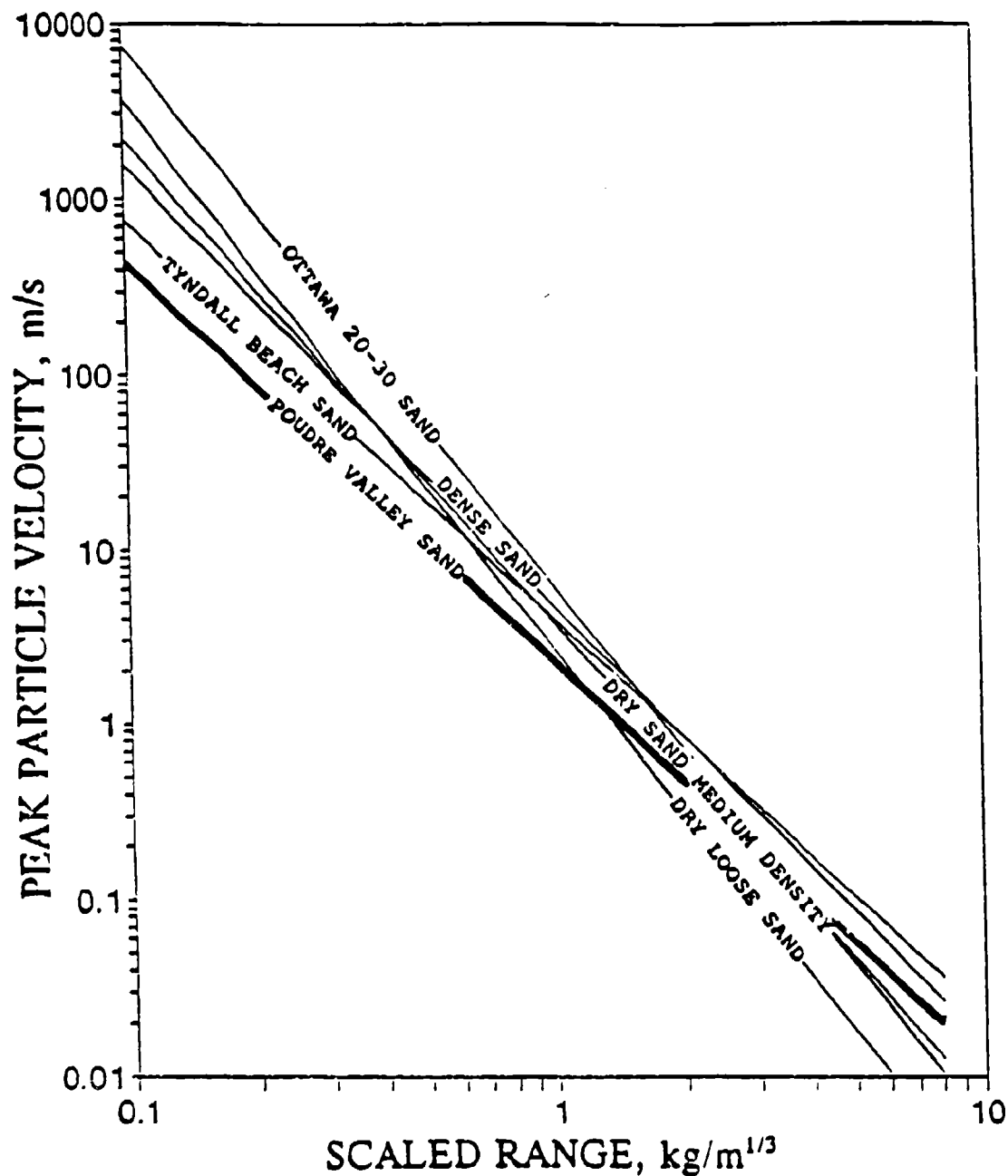
note: equations for average peak particle velocity are used to plot
              curves for Poudre Valley, Tyndall Beach and Ottawa 20-30 Sands
              (see Section V.B.4 for development of equations).

Figure C.11 Peak particle velocity versus scaled range from explosive
             field testing in Poudre Valley Sand, explosive centrifuge
             testing in Tyndall Beach and Ottawa 20-30 Sands (Walsh 1993),
             and explosive data for varying sand densities replotted from
             Figure 2.2 (Drake and Little 1983).

Axis labels: PEAK STRESS, kpa (vertical) and SCALED RANGE, kg/m$^{1/3}$ (horizontal)

Curve labels: DENSE SAND, DRY SAND MEDIUM DENSITY, POUDRE VALLEY SAND, TYNDALL BEACH SAND, OTTAWA 20-30 SAND, DRY LOOSE SAND
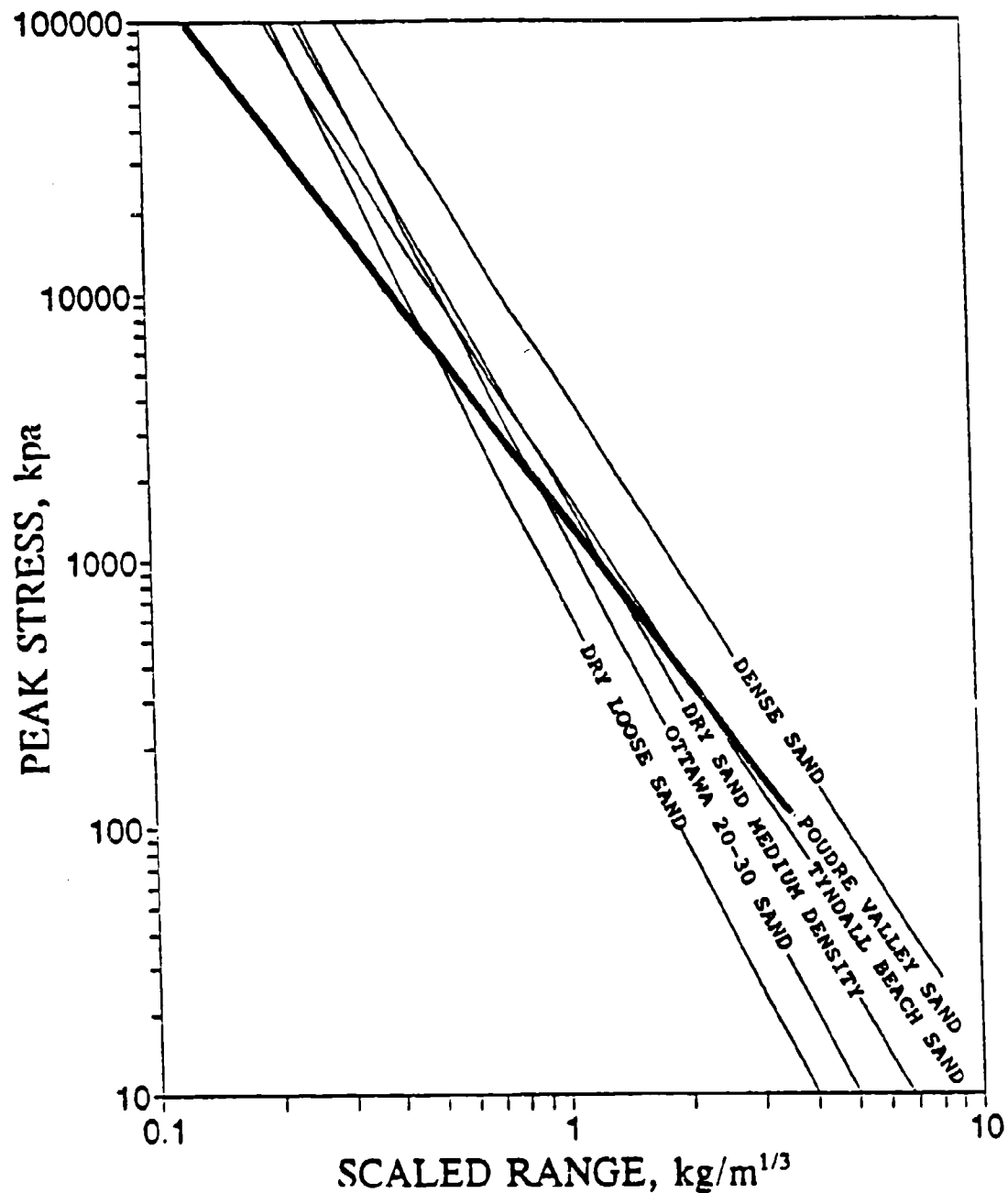
note: equations for average peak stress are used to plot curves for
            Poudre Valley, Tyndall Beach and Ottawa 20-30 sands (see
            Section V.B.4 for development of equations).

Figure C.12 Peak Stress versus Scaled Range from Explosive Field Testing
             in Poudre Valley Sand, Explosive Centrifuge Testing in Tyndall
             Beach and Ottawa 20-30 Sands (Walsh 1993), and Explosive Data
             for Varying Sand Densities Replotted from Figure 2.2 (Drake
             and Little 1983).

(The reverse of this page is blank.)

APPENDIX D

GRADATION REPORTS OF POUDRE VALLEY SAND FROM WESTERN MOBILE INC.

AND

GRAIN SIZE DISTRIBUTION CURVES FOR 50/80 SILICA, OTTAWA 20-30, EGLIN,
TYNDALL BEACH AND POUDRE VALLEY SANDS.

Western Mobile Inc.

GRADATION REPORT

(form — Project 4373, WASHPLANT, Concrete Sand, sample date 05-11-91; prepared by Rhonda Nixon, date 5-11-91; Fineness Modulus 2.74)

Western Mobile Inc.

GRADATION REPORT

(form — Project 4373, WASHPLANT, Stockpile under belt, Concrete Sand, sample date 12-13-91; prepared by Rhonda Nixon, date 12-13-91; Fineness Modulus 2.73)

Figure D.1 Gradation Reports on Poudre Valley Sand from Western Mobile Inc. (a) Fall 1991 Batch. (b) Spring 1992 Batch.
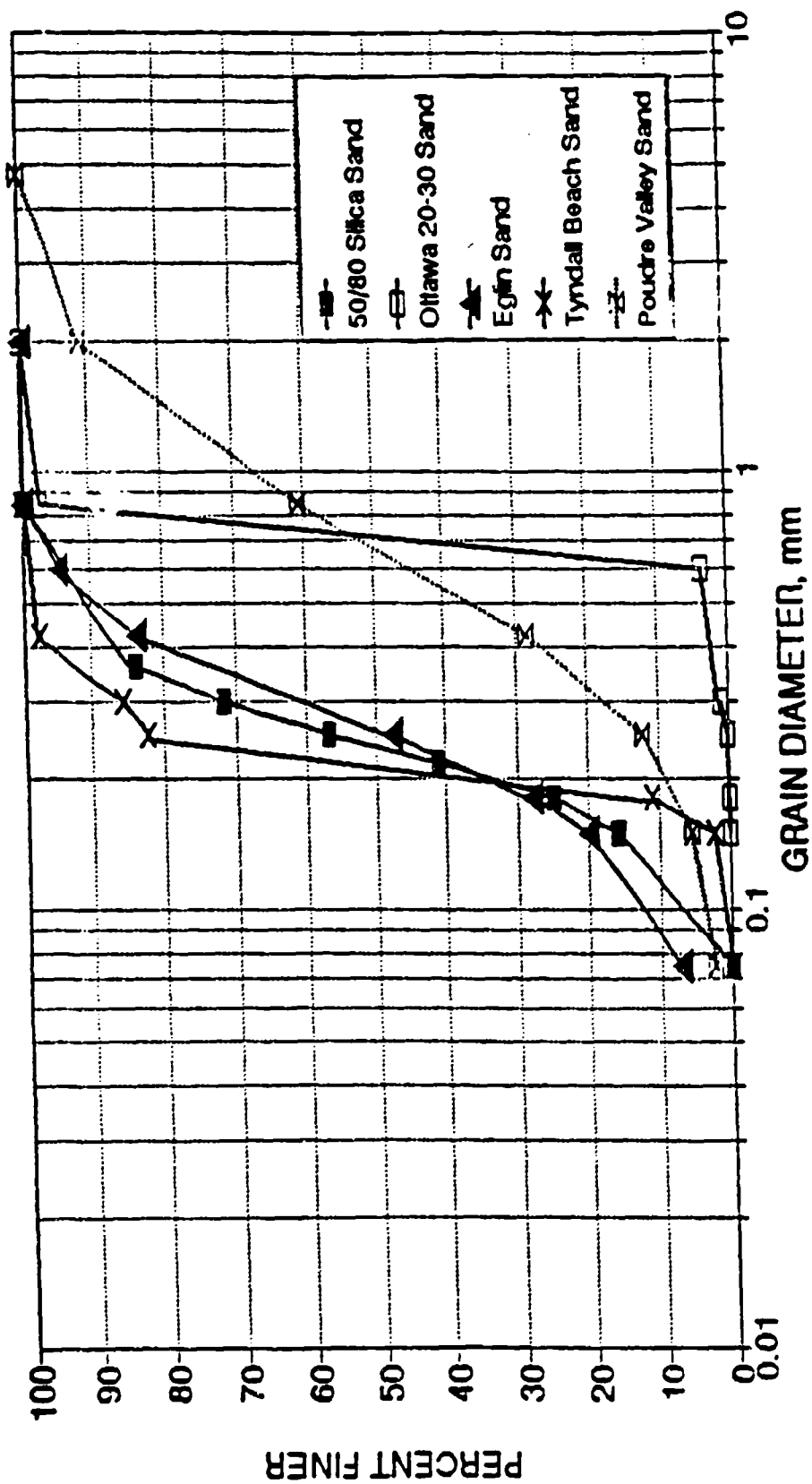
Figure D.2   Comparison of Grain Size Distribution Curves for 50/80 silica, Ottawa 20-30, Eglin, Tyndall Beach and Poudre Valley Sands.

145
(The reverse of this page is blank.)

APPENDIX E

FIELD NUCLEAR DENSITY/MOISTURE GAUGE RESULTS

TABLE E.1. FIELD NUCLEAR DENSITY/MOISTURE GAUGE RESULTS

Test 1 - 13% Compactive Saturation (Fall 1991)

Layer Depth (m)	(ft)	Dry Density (kg/m³)	(pcf)	Saturation (S) (%)	Water Content (w), (%)
2.13-2.44	7-8	1629	101.7	13.1	3.09
1.83-2.13	6-7	1634	102.0	14.7	3.45
1.52-1.83	5-6	1613	100.7	14.8	3.59
1.22-1.52	4-5	1619	101.1	15.2	3.64
0.91-1.22	3-4	1605	100.2	13.4	3.29
0.61-0.91	2-3	1583	98.8	13.6	3.45
0.30-0.61	1-2	1510	100.5	14.1	3.44
0-0.30	0-1	1624	101.4	15.4	3.66
	Mean	1615	100.8	14.3	3.45

Test 2 - 20% Compactive Saturation (Fall 1991)

Layer Depth (m)	(ft)	Dry Density (kg/m³)	(pcf)	Saturation (S) (%)	Water Content (w), (%)
2.13-2.44	7-8				
1.83-2.13	6-7	1608	100.4	26.1	6.37
1.52-1.83	5-6	1608	100.4	25.5	6.22
1.22-1.52	4-5	1616	100.9	18.8	4.53
0.91-1.22	3-4	1629	101.7	19.1	4.50
0.61-0.91	2-3	1610	100.5	17.9	4.35
0.30-0.61	1-2	1626	101.5	24.3	5.78
0-0.30	0-1	1600	99.9	16.7	4.12
	Mean	1615	100.8	21.2	5.12

Test 3 - 40% Compactive Saturation (Fall 1991)

Layer Depth (m)	(ft)	Dry Density (kg/m³)	(pcf)	Saturation (S) (%)	Water Content (w) (%)
2.13-2.44	7-8				
1.83-2.13	6-7	1603	100.1	33	8.12
1.52-1.83	5-6	1627	101.6	42.6	10.09
1.22-1.52	4-5	1616	100.9	47.7	11.51
0.91-1.22	3-4	1639	102.3	38.7	9.00
0.61-0.91	2-3	1639	102.3	41.0	9.54
0.30-0.61	1-2	missing in field notes			
0-0.30	0-1	missing in field notes			
	Mean	1624	101.4	40.6	9.65

Test 4 - 60% Compactive Saturation (Fall 1991)

Layer Depth (m)	(ft)	Dry Density (kg/m³)	(pcf)	Saturation (S) (%)	Water Content (w), (%)
2.13-2.44	7-8				
1.83-2.13	6-7	1677	104.7	59.4	12.99
1.52-1.83	5-6	1632	101.9	52.9	12.44
1.22-1.52	4-5	1623	101.3	54.8	13.08
0.91-1.22	3-4	1631	101.8	60.3	14.21
0.61-0.91	2-3	1600	99.9	44.9	11.1
0.30-0.61	1-2	1611	100.6	55.7	13.53
0-0.30	0-1	1656	103.4	44.9	10.16*
	Mean	1632	101.9	53.3	12.50

*Note: Less water (lower w) added because of excessive drainage into lower layers.

Test 5 - 70% Compactive Saturation (Fall 1991)

| Layer (Depth) | | Dry Density | | Saturation (S) | Water Content (w), |
(m)	(ft)	(kg/m^3)	(pcf)	(%)	(%)
2.13-2.44	7-8				
1.83-2.13	6-7	1666	104.0	74.0	16.55
1.52-1.83	5-6	1658	103.5	81.0	18.32
1.22-1.52	4-5	1663	103.8	78.0	17.46
0.91-1.22	3-4	1722	107.5	63.8	14.76
0.61-0.91	2-3	1655	103.3	64.8	14.68
0.30-0.61	1-2	1639	102.3	44.4	10.32*
0-0.30	0-1	1647	102.8	49.4	11.35*
	Mean	1653	103.2	65.1	14.78

*Note: Top two layers compacted dryer due to excessive drainage into lower layers.

Test 6 - 0% Compactive Saturation (Spring 1992)

| Layer Depth | | Dry Density | | Saturation (S) | Water Content (w), |
(m)	(ft)	(kg/m^3)	(pcf)	(%)	(%)**
2.13-2.44	7-8	1632	101.9	7.3	1.72
1.83-2.13	6-7	1671	104.3	4.3	0.96
1.52-1.83	5-6	1661	103.7	3.6	0.80
1.22-1.52	4-5	1618	101.0	3.8	0.92
0.91-1.22	3-4	1643	102.6	5.8	1.35
0.61-0.91	2-3	1671	104.3	3.8	0.83
0-0.30	1-2*	1664	103.9	3.1	0.70
	Mean	1651	103.1	4.6	1.04

Notes:
*Last two layers placed all at once.

**Sand particles were completely dry on the surface. The nuclear density/moisture gauge was probably measuring hydration water within the particle structure.

Test 7 - 13% Compactive Saturation (Spring 1992)

Layer Depth (m)	(ft)	Dry Density (kg/m³)	(pcf)	Saturation (S) (%)	Water Content (w), (%)
2.13-2.44	6-7	1645	102.7	13.1	3.02
1.83-2.13	5-6	1629	101.7	11.3	2.67
1.52-1.83	4-5	1643	102.6	9.5	2.20
1.22-1.52	3-4	1605	101.2	8.7	2.07
0.91-1.22	2-3	1634	102.0	9.4	2.20
0.61-0.91	1-2	1615	100.8	12.5	3.03
0.30-0.61	0-1	1643	102.6	10.9	2.51
0-0.30	Mean	1632	101.9	10.8	2.53

Test 8 - 20% Compactive Saturation (Spring 1992)

Layer Depth (m)	(ft)	Dry Density (m/kg³)	(pcf)	Saturation (S) (%)	Water Content (w), (%)
2.13-2.44	6-7	1639	102.3	23.1	5.37
1.83-2.13	5-6	1623	101.3	18.1	4.31
1.52-1.83	4-5	1648	102.9	19.6	4.49
1.22-1.52	3-4	1642	102.5	23.6	5.45
0.91-1.22	2-3	1624	101.4	20.8	4.95
0.61-0.91	1-2	1639	102.3	18.8	4.38
0.30-0.61	0-1	1607	100.3	16.4	4.01
	Mean	1632	101.9	20.1	4.71

Test 9 - 40% Compactive Saturation (Spring 1992)

Layer Depth (m)	(ft)	Dry Density (m/kg³)	(pcf)	Saturation (S) (%)	Water Content (w), (%)
2.13-2.44	6-7	1659	103.6	43.1	9.69
1.83-2.13	5-6	1603	100.1	41.9	10.30
1.52-1.83	4-5	1666	104.0	42.9	9.55
1.22-1.52	3-4	1656	103.4	41.0	9.27
0.91-1.22	2-3	1647	102.8	44.6	10.25
0.61-0.91	1-2	1596	99.6	46.0	11.44
0.30-0.61	0-1	1645	102.7	39.2	9.02
	Mean	1639	102.3	42.7	9.93

Test 10 - 60% Compactive Saturation (Spring 1992)

Layer Depth (m)	(ft)	Dry Density (kg/m³)	(pcf)	Saturation (S) (%)	Water Content (w), (%)
2.13-2.44	6-7	1661	103.7	54.2	12.17
1.83-2.13	5-6	1709	106.7	56.5	11.72
1.52-1.83	4-5	1644	102.6	46.0	10.61
1.22-1.52	3-4	1719	107.3	68.3	13.94
0.91-1.22	2-3	1611	100.6	41.2	10.00
0.61-0.91	1-2	1590	99.3	42.8	10.74
0.30-0.61	0-1	1645	102.7	39.2	9.02
	Mean	1655	103.3	49.7	11.17

Notes:

1. Readings were taken at 3 to 5 locations for each lift at depths of 4", 8" and backscatter (surface). The numbers listed are averages of those values.

2. Density and moisture content were very difficult to control at 40 and 60 percent compactive saturations due to the following reasons:

   - Compactor "sinks" into sand (liquefaction effect);

   - Compactor "bogs" down in areas, overcompacting the sand; or

   - Excessive drainage into lower lifts.

3. Test 9 and 10 were conducted simultaneously, Test 9 (40% c.s.) in the east half, and Test 10 (60% c.s.) in the west half of the tank. The top layer was compacted at the same water content for both the east half and west half of the tank. The water content was decreased for this lift due to excessive drainage into lower layers.

(The reverse of this page is blank.)